ABSTRACT

Title of dissertation: FEW-BODY UNIVERSALITY IN WAVEGUIDE QUANTUM ELECTRODYNAMICS

Yidan Wang
Doctor of Philosophy, 2021

Dissertation directed by: Professor Alexey V. Gorshkov
Department of Physics

Professor Michael J. Gullans
Department of Physics

Photons are elementary particles of light, and their interactions in vacuum are extremely weak. The seclusion of photons makes them perfect carriers of classical and quantum information, but also poses difficulties for employing them in quantum information technologies. Recent years have seen tremendous experimental progress in the development of synthetic quantum systems where strong and controllable coupling between single photons is achieved. In a variety of solid-state and optical platforms, propagating photons are coupled with local emitters such as atoms, quantum dots, NV centers, or superconducting qubits. Despite the different nature of the platforms, many of these systems can be described using the same theoretical framework called waveguide quantum electrodynamics (WQED).

Dissipation is an inevitable ingredient of many synthetic quantum systems and is a source of error in quantum information applications. Despite its important role

in experimental systems, the implications of dissipation in scattering theory have not been fully explored. Chapter 2 discusses our discovery of the dissipation-induced bound states in WQED systems. The appearance of these bound states is in a one-to-one correspondence with zeros in the single-photon transmission. We also formulate a dissipative version of Levinson's theorem by looking at the relation between the number of bound states and the winding number of the transmission phases.

In Chapter 3, we study three-body loss in Rydberg polaritons. Despite past theoretical and experimental studies of the regime with dispersive interaction, the dissipative regime is still mostly unexplored. Using a renormalization group technique to solve the quantum three-body problem, we show how the shape and strength of dissipative three-body forces can be universally enhanced for Rydberg polaritons. We demonstrate how these interactions relate to the transmission through a single-mode cavity, which can be used as a probe of the three-body physics in current experiments.

The high level of control of the synthetic quantum systems behind WQED offers many inspirations for theoretical studies. In Chapter 4 of this dissertation, we explore a new direction of scattering theory motivated by the controllability of dispersion relations in synthetic quantum systems. We study single-particle scattering in one dimension when the dispersion relation is $\epsilon(k) = \pm|d|k^m$, where $m \geq 2$ is an integer. For a large class of interactions, we discover that the S-matrix evaluated at an energy $E \to 0$ converges to a universal limit that is only dependent on m. We also give a generalization of Levinson's theorem for these more general dispersion relations in WQED systems.

FEW-BODY UNIVERSALITY IN WAVEGUIDE QUANTUM ELECTRODYNAMICS

by

Yidan Wang

Dissertation submitted to the Faculty of the Graduate School of the
University of Maryland, College Park in partial fulfillment
of the requirements for the degree of
Doctor of Philosophy
2021

Advisory Committee:
Professor Victor Galitski, Chair
Professor Alexey V. Gorshkov, Advisor
Professor Michael J. Gullans, Co-Advisor
Professor Alicia J. Kollár
Professor Andrew M. Childs (Dean's Representative)

Acknowledgments

I would first like to thank my advisor Alexey Gorshkov, who has supported me throughout the long years with his patience and encouragement. Alexey has given me a lot of freedom to explore research topics in my taste and at my own pace. I am grateful that you have always been able to find value in whatever new results I got. This validation from you had helped me go through the tough beginning years of graduate studies when I doubted my research capabilities.

I am also very grateful to Michael J. Gullans, who has gradually become my second advisor during our many years of collaboration. You offered me tremendous help in all my major projects and have rescued me many times when I got stuck in calculations. The wisdom I learned from you on scattering theory laid the foundation for many discoveries in this dissertation.

I want to thank Darrick E. Chang. You have taught me many things as an advisor whenever we got a chance to meet during conferences or visits. You have also offered me great help during my job applications.

Many professors at JQI and QuiCs have also offered me tremendous help in research, including Jake Taylor, Andrew Childs, Alicia Kollár, Trey Porto, Ian Spielman, Mohammad Hafezi, Victor Galitski, and Steve Rolston.

During my Ph.D. studies, I have collaborated and learned from many postdocs in the group, including Seth Whitsitt, Przemek Bienias, Igor Boettcher, Jim Garrison, Zhexuan Gong, Rex Lundgren, and Mohammad Maghrebi. Many of you have become professors elsewhere or found good positions in the industry. I want to offer special thanks to Ran Qi; you were the one who provided me many intuitions in scattering theory when I first started my research at JQI.

I want to thank many graduate students at JQI who has collaborated with me or offered me a lot of help in research: Marcin Kalinowski, Ron Belyansky, Shangjie

Guo, Dalia Ornelas Huerta, Fangli Liu, and Jeremy Young. In particular, Marcin Kalinowski was a visiting student at JQI who co-first authored the work presented in Chapter 3.

I want to thank my friends in the physics department: Abhinav Deshpande, Leonard J. Campanello, Swarnav Banik, Ming Song, Qin Liu, Chunxiao Liu, Aniruddha Bapat, Xunnong Xu, Bo Miao, Wanting Liao, Chiao-Hsuan Wang, Bin Cao, Houquan Fan, and Jeremy Young (again) for the fun times we enjoyed together. Many of you are my comrades who went through similar struggles together and supported me throughout the years. I want to thank Zackaria Chacko. You have been both a great friend and mentor to me.

I want to thank many friends outside the physics department: David Osorio Herrera, Lanfei Shi, Nguyen Thi Phuk Tan, Xiaolu Zeng, Yu Zang, Na Li, Tianxing Jiang, Luanjiao Hu, and Min Zhou. I have many happy memories of working with you in the library and coffee shops, visiting places and cooking together or chatting for hours on the phone. I want to thank Xuesen Na, who is both my friend and my math collaborator on the work presented in Chapter 4.

At last, I would like to thank my parents and partner for their love, patience, and support. You are the ones who made it possible for me to pursue whatever I want in life.

Citations to Previously Published Work

Much of the work presented in this dissertation has appeared in previously published papers. We also list the work by the author that relates to the present thesis but is not covered in the thesis in detail.

- Chapter 2: "Single-photon bound states in atomic ensembles," **Yidan Wang**, Michael J. Gullans, Antoine Browaeys, J. V. Porto, Darrick E. Chang, Alexey V. Gorshkov, arXiv:1809.01147

  Work related to Chapter 2 is also reported in

  - "Beyond spontaneous emission: Giant atom bounded in the continuum," Shangjie Guo, **Yidan Wang**, Thomas Purdy, and Jacob Taylor, Physical Review A, 102, 033706(2020)

- Chapter 3: "Resonant enhancement of three-body loss between strongly interacting photons," Marcin Kalinowski, **Yidan Wang [co-first author]**, Przemyslaw Bienias, Michael J. Gullans, Dalia P. Ornelas-Huerta, Alexander N. Craddock, Steven L. Rolston, J. V. Porto, Hans Peter Büchler and Alexey V. Gorshkov, arXiv:2010.09772

  Work related to Chapter 3 is also reported in

  - "Effective Field Theory for Rydberg Polaritons," Michael J. Gullans, Jeff D. Thompson, **Yidan Wang**, Qi-Yu Liang, Vladan Vuletic, Mikhail D. Lukin, Alexey V. Gorshkov, Physical Review Letters, 117, 113601(2016)
  - D. P. Ornelas-Huerta, A. N. Craddock, E. A. Goldschmidt, A. J. Hachtel, **Yidan Wang**, P. Bienias, A. V. Gorshkov, S. L. Rolston, and J. V. Porto, "On-demand indistinguishable single photons from an efficient and pure source based on a Rydberg ensemble", Optica 7, 813-819 (2020)

- Chapter 4: "Universality in one-dimensional scattering with general dispersion relations," **Yidan Wang**, Michael J. Gullans, Xuesen Na, Alexey V. Gorshkov, arXiv:2103.09830

  We are preparing the following manuscript related to the work in Chapter 4:

  - "Classification of universal scattering in one dimension with general dispersion relations", **Yidan Wang**, Michael J. Gullans, Alexey V. Gorshkov, in preparation

Table of Contents

Acknowledgements ii

Citations to Previously Published Work iv

1 Introduction 1
- 1.1 Background . . . 1
- 1.2 Outline of dissertation . . . 3
- 1.3 Waveguide quantum electrodynamics (WQED) . . . 5
  - 1.3.1 Rydberg ensembles . . . 6
- 1.4 Introduction to scattering theory . . . 7
  - 1.4.1 S-matrix . . . 9
- 1.5 Universality in few-body scattering . . . 11
  - 1.5.1 Low-energy universality . . . 12
  - 1.5.2 Effective field theory . . . 12
  - 1.5.3 Divergent scattering length and the emergence of bound states 13
  - 1.5.4 Dimensionality and zero-energy scattering . . . 14

2 Single-photon bound states in atomic ensembles 18
- 2.1 Introduction . . . 18
- 2.2 The system . . . 20
- 2.3 Dissipative bound states . . . 22
  - 2.3.1 Derivation of spin model M . . . 24
  - 2.3.2 Bound states and their wavefunction normalization . . . 26
  - 2.3.3 Single-atom example . . . 28
- 2.4 Transmission coefficient . . . 29
  - 2.4.1 Overview of results . . . 29
  - 2.4.2 The proof . . . 30
- 2.5 Second-order photon-photon correlation function for a weak coherent pulse . . . 33
  - 2.5.1 Single atom example . . . 36
- 2.6 Levinson's theorem . . . 37

2.7 Energy exchange processes associated with the spin models 39
2.8 Outlook 41

3 Resonant enhancement of three-body loss between strongly interacting photons 42
3.1 Introduction 42
3.2 System 45
3.2.1 Running-wave cavity Hamiltonian 47
3.2.2 Qualitative picture 50
3.3 Two-body problem 50
3.4 Three-body problem 53
3.4.1 Main results 53
3.4.2 Details of the three-body calculation 58
3.5 Experimental probing 62
3.5.1 Transmission calculations 63
3.6 Outlook 67

4 Universal scattering with general dispersion relations 69
4.1 Introduction 69
4.2 Emitter scattering 71
4.3 Universal scattering 73
4.3.1 Overview of results 73
4.3.2 Calculation of $L(\omega)$ 79
4.3.3 Bright zero-energy eigenstates 80
4.3.4 The proof 82
4.4 Levinson's theorem 86
4.4.1 Overview of results 86
4.4.2 The proof 89
4.5 Outlook 98

Bibliography 100

List of Figures

2.1 An illustration of N atoms coupled to a 1D photon channel, with V_i corresponding to the amplitude of the coupling of the photons to atom i. In addition to this specific photonic channel of interest, the atoms can also interact via additional photonic channels, which results in an effective dipole-dipole interaction K'. 20

2.2 (Color online) Schematic of the eigenvalues of (a) M and (b) M^{tot} for $N = 7$. $\Gamma \sim \frac{V_i^2}{2}$ is the scale of the single-atom decay rate to the 1D channel. The eigenvalues of M in the lower half plane (shaded region) give valid bound states (yellow). There is no eigenvalue of M^{tot} above the real line. 26

(a) Eigenvalues of M 26

(b) Eigenvalues of M^{tot} 26

2.3 (Color online) $\log(g^{(2)}(\tau))$ as a function of the ratio $\Gamma/\Gamma^{\text{tot}}$ and $\tau = r$. At $\Gamma/\Gamma^{\text{tot}} = 0.5$, $t_{k=w_{eg}} = 0$ and $g^{(2)}(\tau)$ diverges for all τ. 37

2.4 (Color online) $\mathrm{Im}[t_k]$ vs. $\mathrm{Re}[t_k]$ as k varies from $-\infty$ to $+\infty$ for (a) $N = 1$ and (b) $N = 2$. The trajectories start from $(1, 0)$, go in the counter-clockwise direction, and end at $(1, 0)$. The origins are marked as stars in the center of the figures. The number of times the trajectories enclose $(0, 0)$ is equal to $N - N_B$, where N_B is the number of dissipative bound states. 39
(a) $N = 1$ 39
(b) $N = 2$ 39
2.5 The energy flow digrams associated with (a) the eigenvectors of M^{tot}, (b) the single-photon bound states and (c) the scattering states. $M^{\mathrm{tot}} = w_{eg}\mathbb{1} + K + K'$ and $M = w_{eg}\mathbb{1} + K^\dagger + K'$. 40
(a) $M^{\mathrm{tot}}|\tilde{e}_\alpha\rangle = \tilde{e}_\alpha|\tilde{e}_\alpha\rangle$ 40
(b) $M|e_\alpha\rangle = e_\alpha|e_\alpha\rangle$ 40
(c) $(k\mathbb{1} - M^{\mathrm{tot}})|e_k\rangle = |v_k\rangle$ 40

3.1 (a) Gas of neutral atoms is suspended in an optical cavity. Each atom is a three-level system with the ground state $|g\rangle$, intermediate lossy state $|p\rangle$ with half-width γ, and a high-lying Rydberg state $|s\rangle$, which experiences strong interactions. Classical control field with Rabi frequency Ω and detuning δ couples states $|p\rangle$ and $|s\rangle$. Quantum photon field with collective coupling g drives the $|g\rangle - |p\rangle$ transition and is tuned to the two-photon resonance. (b) Energy of the upper (blue) and lower (green) branches of spin waves as a function of the single-photon detuning. At $\delta = \Omega/\sqrt{2}$ scattering of three DSPs (black) into spin waves (dotted purple) is on resonance. 44

3.2 (a) Diagrammatic representation (see inset for legend) of the Lippmann-Schwinger equation for the scattering of two dark-state polaritons. Processes with only one spin wave are forbidden by momentum conservation. (b) Schematic representation of Faddeev equations for the three-body T-matrix $T_3^{12}(\omega)$, where particles 1 and 2 interact first. (c) Truncation of the three-body equations (b) to second order in r_b/L allows us to express the spin-wave contribution using an effective three-body potential U_3 between DSPs. 55

3.3 (a) Ratio of imaginary parts of $E_3^{(2)}$ and $E_3^{(1)}$ at $\gamma/\Omega = 0.01$. Near $\delta/\Omega = 1/\sqrt{2}$, we observe enhancement caused by a three-body resonance. $\delta = \Omega$ is a singular point where $r_b \to 0$. (b) Real and imaginary parts of $E_3^{(2)}$ as a function of γ/Ω at $\delta/\Omega = 1/\sqrt{2}$. (inset) Our numerical results (blue) agree with analytical scaling arguments (dashed red) suggesting that the ratio $\mathrm{Im}(E_3^{(2)})/\mathrm{Re}(E_3^{(2)})$ diverges as Ω/γ in the limit $\gamma/\Omega \to 0$. 56

3.4 (a-b) Three-body loss parameter r_3 in units of Γ^{-2} as a function of real and imaginary part of u_3/Γ for the case of $u_2 = 0$, which corresponds to negligible two-body correlations in the microscopic model. The five curves in (b) correspond to the five values of $\mathrm{Im}(u_3)$ indicated by the horizontal lines in (a). 57

4.1 Illustration of 1D scattering (z is a spatial coordinate) near zero energy for dispersion relation $\epsilon(E) = \sigma|d|k^m$ with $\sigma = \pm 1$. Panel (a) is for odd m, where the scattering matrix is a single transmission coefficient dependent on m and the sign of energy is $E = 0^{\pm}$. Panel (b) is for even m, where the scattering matrix is a 2×2 matrix. The eigenstates of the scattering matrix are the symmetric and antisymmetric incoming states, with eigenphases $\exp(2\pi i\sigma/m)$ and 1, respectively. 77

(a) odd m 77

(b) even m 77

4.2 Illustrations of the trajectories of $\det[\boldsymbol{S}(E)]$ of a dissipative system in the complex plane when E is increased from E_{min} to E_{max} for (a) $\epsilon(k) = \pm|d|k$, where the trajectory starts and ends at 1. (b) $\epsilon = |d|k^2$, where the trajectory starts at -1 and ends at 1. (c) $\epsilon = |d|k^6$, where the trajectory starts at $\exp(i\pi/3)$ and ends at 1. (d) $\epsilon = \pm|d|k^5$, where the trajectory for $E \in (-\infty, 0)$ (solid yellow) starts at 1 and ends at $S(0^-) = \exp(i\pi/5)$, while the trajectory for $E \in (0, +\infty)$ (solid blue) starts at $S(0^+) = \exp(i\pi/5)$ and ends at 1. 87

(a) $\epsilon = \pm|d|k$ 87

(b) $\epsilon = |d|k^2$ 87

(c) $\epsilon = |d|k^6$ 87

(d) $\epsilon = \pm|d|k^5$ 87

4.3 Illustration of the integration contours for the calculation of the winding phase of $\det[\boldsymbol{S}(E)]$. (a) Contours for a dispersion relation $\epsilon(k) = |d|k^m$ with odd m. (b) Contours for a dispersion relation $\epsilon(k) = |d|k^m$ with even m. The density of states diverges at the origin $E = 0$, marked by the red dot. The blue lines represent the continuum spectrum, while the yellow stars represent bound-state energies. The dashed lines with arrows are the integration paths for the evaluation of the winding number of $\det[\boldsymbol{S}(E)]$. The semicircles (circles) are added to form closed integration contours so that the residue theorem can be invoked. The red semicircles (circle) go around the origin with an infinitesimal radius, while the black semicircles (circle) have an infinite radius. 93

(a) $\epsilon(k) = |d|k^m$, odd m 93

(b) $\epsilon(k) = |d|k^m$, even m 93

List of Tables

4.1 The set A and the value of $\kappa_m = \sum_{j \in A} (-\mu)^{2j}$ for both odd and even m. 80

Chapter 1: Introduction

1.1 Background

Quantum mechanics is a set of physical laws that govern the world of very small particles at very low energies. It portrays a fundamentally probabilistic world, where a single object can be in two places at once—superposition—and where two objects in remote locations can have classically unattainable correlations—entanglement. Photons, which are elementary particles of light, have been a prototypical system for the discovery and testing of quantum mechanics. Early experiments on the photoelectric effect and double-slit interference helped establish the concept of wave-particle duality in quantum mechanics. In the early 70s and 80s [5, 57], quantum entanglement was first tested experimentally using photons generated from atomic cascades.

The development of quantum mechanics has brought about revolutionary ideas to upgrade our computation and communication methods, which are today based on classical mechanics. By replacing the classical machines with quantum tools, certain information processing tasks are moderately or exponentially improved, the most notable of which is Shor's algorithm for factoring [137]. The easily accessible quantum characteristics have made photons a key player in the development of quantum technologies, including sensing, imaging, communications, simulation, and computation. The extremely weak interactions between photons make them perfect carriers of classical and quantum information. And single-qubit operations on photons can be easily

performed with incredibly high fidelity. Many of the cornerstone protocols of quantum information science were first realized optically, including teleportation [23, 164] and cryptography [16, 85, 158, 163]. The generation and manipulation of non-classical light has enabled single-photon switches and transistors [7, 35, 155], quantum circulators [132], isolators [131], and long-distance quantum state transfer [161, 172]. On one hand, it is possible in principle to design all-photonic quantum computers using measurements and linear operations [23, 26, 118, 119]. On the other hand, photons are used as the "flying qubits" to connect quantum computers at different locations and enable distributed processing [128, 138].

Despite the advantages, there are still a few difficulties when employing photons for quantum information technologies. In communication networks, quantum information carried by the "messenger" photons needs to be transferred to stationary qubits for computation and storage, but existing conversion methods used for classical signals are inefficient at the few-photon level. The extremely weak interactions of free photons are an advantage for information transmission, but also make the construction of deterministic two-photon gates difficult, and pose an obstacle to building a practical universal all-photonic quantum computer [150]. These difficulties have motivated scientists in the fields of quantum optics, condensed-matter physics, and atomic physics to build systems where photons are strongly coupled to local emitters. In this setup, quantum information can be transferred from the flying photons to the emitters acting as stationary qubits in a quantum computer; and multi-qubit gates between photons become possible as nonlinearities of the emitters induce nonlinearities between single photons.

Examples of such systems include photonic-crystal waveguides coupled to atoms [3, 62, 63, 76, 80] and solid-state emitters [75, 103, 139], free-space photons propagating through dense Rydberg atomic clouds [54, 122], optical nanofibers coupled to

atoms [39, 61, 131, 132, 140, 141, 144], transmission lines coupled to superconducting qubits [44, 160], and metallic nanowires coupled to NV centers [78] and quantum dots [2]. Despite the different nature of the platforms, many of these systems can be described using the same theoretical framework called waveguide quantum electrodynamics (WQED). The high level of control in experimental WQED systems makes them both a toolbox for quantum technologies and a playground for studies of other less controllable or accessible quantum systems.

In the next section, we provide an overview of the results presented in this dissertation.

1.2 Outline of dissertation

In this dissertation, we theoretically explore a few directions of scattering theory motivated by the features and capabilities of experimental WQED systems. We focus on illustrating universal scattering properties independent of the details of the WQED system, or even applicable to general scattering systems beyond WQED.

In Chapters 2 and 3, we explore the role of dissipation in scattering theory. Dissipation is an inevitable ingredient of many synthetic quantum systems and is a source of error in quantum information applications. Despite its important role in experimental systems, the implications of dissipation in scattering theory have not been fully explored. In Chapter 2, we discuss our discovery of the dissipation-induced bound states in a WQED system where propagating photons interact with N two-level atoms. These bound states can be calculated from an effective spin model, and their existence relies on dissipation in the system. The appearance of these bound states is in a one-to-one correspondence with zeros in the single-photon transmission and with divergent bunching in the second-order photon-photon correlation function.

We also formulate a dissipative version of a key index theorem in quantum scattering theory known as Levinson's theorem—which relates the scattering phases to the number of bound states. This theorem allows a direct experimental measurement of the number of bound states using the measured transmission phases.

In Chapter 3, we continue our discussion of dissipation in the three-body scattering of Rydberg polaritons. Rydberg polaritons provide an example of a rare type of system where three-body interactions can be as strong as or even stronger than two-body interactions. The three-body interactions can be either dispersive or dissipative, with both types possibly giving rise to exotic, strongly-interacting, and topological phases of matter. Despite past theoretical and experimental studies of the regime with dispersive interaction, the dissipative regime is still mostly unexplored. Using a renormalization group technique to solve the quantum three-body problem, we show how the shape and strength of dissipative three-body forces can be universally enhanced for Rydberg polaritons. We demonstrate how these interactions relate to the transmission through a single-mode cavity, which can be used as a probe of the three-body physics in current experiments.

The high level of control of synthetic quantum systems behind WQED offers many inspirations for theoretical studies. In Chapter 4, we explore single-particle scattering in one dimension when the dispersion relation is $\epsilon(k) = \pm|d|k^m$, where $m \geq 2$ is an integer. We study WQED scattering problems in which a single-particle in a one-dimensional waveguide scatters off of an inhomogeneous, discrete set of sites locally coupled to the waveguide. For a large class of these problems, we rigorously prove that, when there are no bright zero-energy eigenstates, the S-matrix evaluated at energy $E \to 0$ converges to a universal limit that is only dependent on m. We also give a generalization of Levinson's theorem to scattering off emitters for these more general dispersion relations.

In the remaining sections of Chapter 1, we review a few topics to better clarify the context and motivations of the problems studied in the later chapters. In Sec. 1.3, we give a brief discussion of the enhancement of photon-emitter interactions in WQED systems. In Sec. 1.4, we provide a formal introduction to scattering theory. In Sec. 1.5, we discuss universality in traditional scattering theory, a concept that motivates our studies of WQED systems in the later chapters.

1.3 Waveguide quantum electrodynamics (WQED)

In this section, we provide a brief and heuristic explanation of the principles behind strong photon-emitter couplings and single-photon nonlinearities in typical WQED systems. The goal of the experiment is to coerce a single mode of the electromagnetic field and a quantum emitter (or an ensemble of emitters) to preferentially exchange an excitation. For a single emitter, the figure of merit is given by the optical depth [141]:

$$OD = \frac{A_{\text{emitter}}}{A_{\text{mode}}} \sim \frac{\Gamma}{\Gamma^{tot}}, \tag{1.1}$$

where A_{emitter} is the "area" of the emitter representing its resonant scattering cross-section. A_{mode} is the waist area of the photon mode of interest and measures how tightly confined the photon mode is in the transverse direction. The optical depth can also be understood as the ratio between the decay rate of the emitter to the desired photon mode Γ and all photon modes Γ^{tot}.

The value of OD measures the strength of the coupling between the photon and a single emitter. A large OD can be achieved by either increasing A_{emitter} or reducing A_{mode}. To increase the size of the atoms, one can use large "artificial atoms" such

as superconducting qubits. A_{mode} can be reduced by tight confinement of the photon mode of interest. For example, optical photons can be focused to a narrow beam waist by a lens with a large numerical aperture, or by being sent through a narrow-width optical nanofiber [141]. Once a strong coupling is achieved between a single photon and a single emitter, photon-photon nonlinearities can be induced from the nonlinearity of the emitter.

1.3.1 Rydberg ensembles

Another approach to achieving strong photon-emitter coupling is to use an atomic ensemble, which in some cases can be effectively seen as a giant atom. Assuming that the photon field is uniform across a dense atomic cloud with a size much smaller than the resonant wavelength, the optical depth is enhanced by the number of atoms N:

$$OD = \frac{A_{\text{emitter}}}{A_{\text{mode}}} N. \tag{1.2}$$

In this case, because the single-atom coupling to light is still weak, a single-atom nonlinearity cannot induce strong nonlinear interactions between photons. The way to achieve strong photon-photon interactions is to couple light to high-lying atomic states (Rydberg levels) using a second, stronger laser field. Because of the strong long-range interactions between atoms in the Rydberg level, no more than a single Rydberg excitation can be present in the atomic cloud, which leads to a strong effective nonlinear interaction between the incoming photons. In Chapter 3, we study dissipative three-photon nonlinearities in such systems.

1.4 Introduction to scattering theory

In this section, we follow Ref. [152] and review some basic concepts in scattering theory. Even though the results presented in this thesis focus on waveguide QED systems in 1D, in this section we will discuss scattering in 1D, 2D, and 3D. The reason is that we want to prepare for a discussion that involves different dimensions in a later section. Specifically, in Sec. 1.5, we will use the different universal scattering behaviors in different dimensions to motivate the work presented in Chapter 4.

The discussion in this chapter focuses on potential scattering with a quadratic dispersion relation, but the formal definitions can be generalized to other types of interactions and dispersion relations. For simplicity, we set $\hbar = 1$ and the mass of the particle to be $1/2$. The state vector $|\psi(t)\rangle$ satisfies the time-dependent Schrödinger equation:

$$i\frac{d}{dt}|\psi(t)\rangle = H|\psi(t)\rangle\,. \tag{1.3}$$

The Hamiltonian H has the form $H = H^0 + V$, where H^0 is the kinetic energy of a free particle, and V represents some local potential.

The energy eigenstates of H_0 are given by the momentum eigenstates $|\boldsymbol{k}\rangle$. Define $U(t) \equiv \exp(-iHt)$ and $U_0(t) \equiv \exp(-iH_0t)$. Every $|\boldsymbol{k}\rangle$ corresponds to the eigenstates of the full Hamiltonian H with energy $E = |\boldsymbol{k}|^2$ through the Møller wave operators $\Omega_\pm$:

$$|\psi_{\boldsymbol{k}}^{\pm}\rangle = \Omega_\pm|\boldsymbol{k}\rangle\,, \tag{1.4}$$

$$\Omega_\pm \equiv \lim_{t\to\mp\infty} U(t)^\dagger U^0(t). \tag{1.5}$$

The Møller operators are isometric and satisfy

$$\Omega_{\pm}^{\dagger}\Omega_{\pm} = 1. \tag{1.6}$$

The sign $\pm$ in $|\psi_{\boldsymbol{k}}^{\pm}\rangle$ represents the specific boundary condition of the scattering state: far away from the interaction region in the incoming/outgoing direction, $|\psi_{\boldsymbol{k}}^{\pm}\rangle$ is identical to a free particle with momentum $\boldsymbol{k}$. $|\psi_{\boldsymbol{k}}^{\pm}\rangle$ are called scattering states and they satisfy the following orthogonality relations:

$$\langle\psi_{\boldsymbol{k}}^{\pm}|\,\psi_{\boldsymbol{k'}}^{\pm}\rangle = \delta(\boldsymbol{k}-\boldsymbol{k'}). \tag{1.7}$$

In general, there may exist eigenstates $|\psi_i\rangle$ of H that are not connected to any momentum state $|\boldsymbol{k}\rangle$ through the Møller operators. Here, $i = 1, 2, \ldots N_B$ is the label of the bound states and N_B is the total number of bound states. The wavefunctions of bound states are localized around the region of interaction and their energies form a discrete spectrum of H that is generically below 0, i.e. below the scattering threshold. The orthogonality relations between the bound states and scattering states are given by

$$\langle\psi_{\boldsymbol{k}}^{\pm}|\,\psi_i\rangle = 0, \quad \langle\psi_i|\,\psi_j\rangle = \delta_{ij}. \tag{1.8}$$

The bound states together with the scattering states $\{\psi_{\boldsymbol{k}}^{+}\}(\{\psi_{\boldsymbol{k}}^{-}\})$ form a complete eigenbasis of H:

$$H = \int_{-\infty}^{+\infty} d\boldsymbol{k}\ |\boldsymbol{k}|^2\,|\psi_{\boldsymbol{k}}^{\pm}\rangle\,\langle\psi_{\boldsymbol{k}}^{\pm}| + \sum_{i=1}^{N_B} E_i\,|\psi_i\rangle\,\langle\psi_i|\,. \tag{1.9}$$

1.4.1 S-matrix

In scattering theory, we are often interested in the transition amplitudes between the incoming and outgoing free particles instead of the shapes of the scattering eigenstates in the interaction region. To calculate these transition amplitudes, let us illustrate the relation between an incoming/outgoing wavefunction prepared far away from the scattering center and the actual solution of the time-dependent Schrödinger equation given by Eq. (1.3).

The general solution of Eq. (1.3) has the form $|\psi(t)\rangle = U(t)\,|\psi\rangle$, where $U(t)$ is the time evolution operator and $|\psi\rangle$ is any normalized wavefunction. Define a normalized wave packet $|\phi_{in}\rangle$ centered around momentum $\boldsymbol{k}_{in}$ and $|\psi^+_{in}\rangle \equiv \Omega_+\,|\phi_{in}\rangle$. Using Eq. (1.5), we have

$$U(t)\,|\psi^+_{in}\rangle - U^0(t)\,|\phi_{in}\rangle \xrightarrow[t\to-\infty]{} 0, \tag{1.10}$$

which means that the wave packet $U(t)\,|\psi^+_{in}\rangle$ looks identical to the freely propagating state $U^0(t)\,|\phi_{in}\rangle$ when $t \to -\infty$. Similarly, if $|\phi_{out}\rangle$ is a normalized wave packet centered around momentum $\boldsymbol{k}_{out}$, then the wave packet $U(t)\,|\psi^-_{out}\rangle \equiv \Omega_-\,|\phi_{out}\rangle$ would look identical to $U^0(t)\,|\phi_{out}\rangle$ when $t \to +\infty$: $U(t)\,|\psi^-_{out}\rangle - U^0(t)\,|\phi_{out}\rangle \xrightarrow[t\to+\infty]{} 0$.

The transition amplitude between an incoming state that takes the shape of $U_0(t)\,|\phi_{in}\rangle$ at time $t \to -\infty$ to an outgoing state that takes the shape of $U_0(t)\,|\phi_{out}\rangle$ at time $t \to +\infty$ would simply be given by

$$\langle\psi^-_{out}|\,\psi^+_{in}\rangle \equiv \langle\phi_{out}|\,\mathcal{S}\,|\phi_{in}\rangle\,, \tag{1.11}$$

where the scattering operator $\mathcal{S}$ is defined as

$$\mathcal{S} = \Omega_-^\dagger \Omega_+. \tag{1.12}$$

Because energy is a conserved quantity, if the incoming state has a well-defined energy E, the outgoing state must also have the same energy E. We can define the scattering matrix $S(E)$ for $E > 0$ as the projection of the scattering operator $\mathcal{S}$ onto the subspace of eigenstates with energy E. In the following, we discuss the representation of the S-matrix in different dimensions and define the S-wave scattering phases. The purpose of introducing these quantities is to prepare for the discussion of the universal limits of the S-matrix in Sec. 1.5.4, which serves as the motivation to the work in Sec. 4.

Let us assume that the particle mass is still given by $1/2$. In 1D, any energy $E > 0$ would correspond to two degenerate momenta $k = \sqrt{E}, k = -\sqrt{E}$. In the momentum basis $\{|k = \sqrt{E}\rangle, |k = -\sqrt{E}\rangle\}$, $S(E)$ can be written as a 2×2 matrix. We can also represent the S-matrix in the symmetric and antisymmetric basis $\{\frac{1}{\sqrt{2}}(|k = \sqrt{E}\rangle \pm |k = -\sqrt{E}\rangle)\}$, which are labelled by $l = 0$ and $l = 1$, respectively.

In 2D and higher dimensions, it is inconvenient to use the momentum eigenstates as the basis states for the S-matrix because there are uncountably many momentum eigenstates at the same energy $E > 0$. It is more convenient to choose the discrete eigenstates of the angular momentum operator as the basis states. In 2D and 3D, the angular momentum eigenbasis can be labelled by two integers: l and m_l, where $l = 0, 1, 2, \ldots$ is called the angular momentum quantum number and m_l the magnetic quantum number. In both 2D and 3D, $l = 0$ represents states that do not have any angular dependence, i.e. non-rotating; and $m_l = 0$ when $l = 0$. When $l \geq 1$, the magnetic quantum number $m_l = \pm 1$ describes the direction of rotation in 2D and

$m_l = -l, -l+1, \ldots l-1, l$ describes the orbital orientation in space. The S-matrix $S(E)$ in both 2D and 3D can be written as an infinite dimensional matrix linking the transmission and refection coefficients between states at energy E with different angular momentum and magnetic quantum numbers. For all three dimensions, we refer to the $l = 0$ eigenstates as S-wave.

For simplicity of discussion, we assume that in 1D (2D/3D), the interaction is (rotationally/spherically) symmetric. States with different angular momentum or magnetic quantum numbers would decouple from each other in the scattering process, and the S-matrix projected to each of the angular momentum channels is represented by a single complex number. Let $S_D^0(E)$ denote the scattering matrix for the S-wave ($l = 0$) channel in dimension $D = 1, 2, 3$. We can define the S-wave scattering phase $\delta_D(E)$ in dimension $D = 1, 2, 3$ via $S_D^0(E) \equiv \exp(2i\delta_D(E))$.

1.5 Universality in few-body scattering

After the introduction to scattering theory in the last section, we are ready to review some universal relations in few-body scattering that motivate the studies in later chapters of this dissertation. We assume that particles have quadratic dispersion relations and their interactions are short-range.

Universality describes the phenomenon when a large class of systems has the same properties independent of the details of each system, and quantitative features of certain physical observables can be deduced from a finite number of parameters common to the definition of the systems. In a narrower definition, universality in the studies of low-energy scattering theory, statistical mechanics, and condensed matter physics often refers to situations when systems very different at short distances have identical long-distance behavior.

1.5.1 Low-energy universality

One of the most important universal phenomena in scattering theory is that the low-energy scattering properties are primarily decided by a—the scattering length [15, 24, 25]. By low-energy, we mean that the de Broglie wavelength of the particle is much larger than the range of interactions. a plays an important role both in few-body and many-body systems. It determines the properties of a many-body system if the constituents of the system have not only sufficiently low energies but also separations that are large compared to the range of interaction. A classic example is the interaction energy per particle in the ground state of a sufficiently dilute homogeneous Bose-Einstein condensate:

$$\mathcal{E}/n \approx \frac{2\pi}{m} an, \tag{1.13}$$

where m is the mass of a single boson, $\mathcal{E}$ and n are the energy density and number density, respectively. The dilute Bose-Einstein condensate is a perfect illustration of universality: the constituents may have completely different internal structures and interactions, but the many-body systems will have the same microscopic behavior if their scattering lengths are the same.

1.5.2 Effective field theory

Generically, the scattering length a is comparable to the range of the interaction: $|a| \sim r_s$; and universality is a perturbative weak-coupling phenomenon where a plays the role of a coupling constant. Universal properties can be calculated as expansions in the dimensionless combination $a\kappa$, where κ is an appropriate wave number variable. To describe the scattering process of more than two particles, or to a precision that is

higher-order in $a\kappa$, additional parameters may be needed to characterize the scattering process. Nevertheless, the low-energy scattering to any given precision in orders of $a\kappa$ can be captured by a certain number of constant parameters, irrespective of the details of the finite-range interactions. This suggests that we can write down an effective theory with only contact interactions characterized by a few constants to reproduce the scattering process in the original system to any precision we want. This is the idea of effective field theory. At sufficiently low energies, the most general Lagrangian in 3D with contact interactions may be written as [74]

$$\mathcal{L} = \psi^\dagger \left(i\partial_t + \frac{\nabla^2}{2m} \right) \psi - \frac{C_0}{2}(\psi^\dagger \psi)^2 - \frac{D_0}{6}(\psi^\dagger \psi)^2 + \dots, \tag{1.14}$$

where the dots represent higher-order-derivative terms that are suppressed at low energies. The strength of the two-body interaction C_0 is determined from the scattering length a, while D_0 depends on three-body scattering. In Chapter 3, we apply the idea of effective field theory to Rydberg polaritons and derive dissipative two-body and three-body interaction parameters. These parameters are fed into an effective single-cavity transmission model, which can be used to probe the dissipative three-body physics of the Rydberg polariton system.

1.5.3 Divergent scattering length and the emergence of bound states

In exceptional cases, the scattering length a can be much larger in magnitude than the range of the interaction: $|a| \gg r_s$. During a continuous tuning of parameters, this happens when a new bound state is about to appear from the scattering threshold, or when there exists a shallow bound state. If it is the latter case, the energy of the shallow bound state is $-\frac{1}{ma^2}$, where m is the mass of the particle and $\hbar = 1$. The nonperturbative dependence of the bound-state energy on a reflects the fact that

universality in the case of large scattering length is a nonperturbative strong-coupling phenomenon. We comment that the phenomenon that the bound states generically emerge from the scattering threshold is a consequence of the Hermitian nature of the Hamiltonian. In Chapter 4, we illustrate that, in dissipative systems, new bound states may emerge from the continuum spectrum instead of from the scattering threshold. And instead of corresponding to a divergent scattering length, the appearance of a dissipative bound state in the system corresponds to zero transmission at the energy of the emerging bound state.

In the three-body sector, a remarkable nonperturbative universal phenomenon in the resonant limit $a \to \pm\infty$ is the Efimov effect [25, 49]. For three identical bosons interacting in 3D, there are infinitely many arbitrarily-shallow three-body bound states with binding energies $E_T^{(n)}$ that have an accumulation point at $E = 0$. As the threshold is approached, the ratio of the binding energies of successive states approaches a universal constant:

$$E_T^{(n+1)}/E_T^{(n)} \to 1/515.03 \quad \text{as} \quad n \to \infty \quad \text{with} \quad a = \pm\infty. \tag{1.15}$$

The universal ratio in this equation is independent of the details of the short-range interactions between the particles.

1.5.4 Dimensionality and zero-energy scattering

The inspiration that motivated Chapter 4 is an implicit assumption behind the construction of low-energy universality—the scattering phase goes to a universal limit when $E \to 0$. As we illustrate soon, the scattering length a corresponds to the coefficient of the first-order Taylor expansion of the scattering phase $\delta_D(k^2)$ in $k = \sqrt{E}$ around $z = 0$. Without the fact that $\delta_D(k^2)$ goes to a limit independent of the details

of the interaction at zero energy, the low-energy scattering theory would not be written as a perturbative expansion in k.

To illustrate this point, let us provide the definitions of the scattering length a and the effective range r_s in different dimensions. For simplicity, in 1D, we consider symmetric interactions, while in 2D and 3D, we consider rotationally/spherically symmetric interactions. In the center-of-mass coordinates, let $\boldsymbol{r} = \boldsymbol{r}_1 - \boldsymbol{r}_2$ represent the relative coordinates of the two particles at $\boldsymbol{r}_1, \boldsymbol{r}_2$. The relative motion of the two particles with interaction $V(\boldsymbol{r}_1 - \boldsymbol{r}_2)$ can be mapped to single-particle scattering with potential $V(\boldsymbol{r})$. In Section 1.4.1, we have defined the S-wave scattering phase $\delta_D(E)$ in potential scattering in dimensions $D = 1, 2, 3$. The energy E in the potential scattering model corresponds to the kinetic energy of the two particles in a co-moving frame where the total momentum is 0. We assume that in the model of single-particle potential scattering, the mass of the particle is $1/2$, hence the kinetic energy is $E = \boldsymbol{k}^2$, where $\boldsymbol{k}$ is a momentum vector in dimension D.

Defining $k = \sqrt{E}$, in 2D and 3D ($D = 2, 3$), the scattering length a and the effective range r_s are defined via

$$k \cot \delta_D(k^2) = -\frac{1}{a} + \frac{1}{2} r_s k^2 + O(k^4) + \dots . \tag{1.16}$$

On the other hand, in 1D [10][1],

$$k \tan \delta_1(k^2) = \frac{1}{a} - \frac{1}{2} r_s k^2 + O(k^4) + \dots . \tag{1.17}$$

Why is the definition of a different in 1D compared to higher dimensions? The reason

[1] In our definition, the effective range r_s has the opposite sign compared to the definition in Ref. [10] for a better comparison to higher dimensions.

that the zero-energy limits of the scattering phase are different in different dimensions:

$$\delta_D(0^+) \equiv \lim_{E\to 0^+} \delta_D(E) = \begin{cases} 0 & D = 2, 3 \\ \frac{\pi}{2} & D = 1 \end{cases}. \tag{1.18}$$

Using Eq. (1.18), Eqs. (1.16) and (1.17) can be written in the same form:

$$k \cot(\delta_D(k^2) - \delta_D(0^+)) = -\frac{1}{a} + \frac{1}{2} r_s k^2 + O(k^4) + \ldots. \tag{1.19}$$

Using the Taylor expansion of the cotangent function and keeping the lowest-order term in k, we obtain

$$\delta_D(k^2) - \delta_D(0^+) = -ak + o(k^2), \tag{1.20}$$

which demonstrates that $-a$ corresponds to the lowest-order Taylor expansion of $\delta_D(k^2)$ in k around zero energy.

Eq. (1.20) illustrates the origin of the existence of low-energy universality. If we accept the premise that $\delta_D(k^2)$ is a well-behaved function of the wavevector k, then as long as $\delta_D(k^2)$ has a fixed point independent of the details of the system, i.e. a universal limit at a certain energy, Taylor expansion can be naturally computed around that fixed point. It is guaranteed that, when energy is close enough to the fixed point, the scattering properties are primarily dependent on the first-order Taylor coefficient, i.e. the scattering length.

Why is the universal zero-energy limit of the scattering phase different in different dimensions? This difference is associated with the behavior of the density of states at zero energy: when $E \to 0$, the density of states diverges $\sim E^{-1/2}$ in 1D, goes to a constant in 2D, and vanishes in 3D. This observation motivates us to ask the

following question: what happens to the zero-energy limit of the S-matrix if the density of states diverges in 1D even faster than with a quadratic dispersion relation? In Chapter 4, we provide an answer to this question. The high level of control in WQED systems allows dispersion relations to be tuned, providing a way to test our theory experimentally.

Chapter 2: Single-photon bound states in atomic ensembles

Work in this chapter was published in Ref. [165].

2.1 Introduction

Systems of strongly interacting photons are important for scaling up quantum computers and networks [102]. The generation and manipulation of non-classical light enable single-photon switches and transistors [7, 35, 155], quantum circulators [132], isolators [131], and long-distance quantum state transfer [161, 172]. Understanding few-body physics in systems of strongly interacting photons helps reveal the emergent many-body physics in these systems [114], including quantum phase transitions of light [53, 71].

To characterize the quantum states of light produced in these systems, experiments often probe single-photon transmission and multi-photon statistics. In this chapter, we construct an effective spin model to solve for the single-photon transmission through ensembles of atoms exhibiting cooperative light scattering effects. This spin model is characterized by the presence of single-photon bound states, whose wavefunction is a hybridized single-excitation between light and matter that is localized in space. The bound states correspond directly to zeros in the transmission coefficient and are associated with an analogue of Levinson's theorem [46, 168, 169] for interacting atom-photon systems. In the two-photon transmission, we show that

these zeros in the transmission lead to divergent bunching of the light due to the presence of effective photon-photon interactions in these systems.

Our results and their generalizations can be applied to many systems in which strong interaction between propagating photons is realized. These include photonic-crystal waveguides coupled to atoms [3, 62, 63, 76, 80] and solid-state emitters [75, 103, 139], free-space photons propagating through dense Rydberg atomic clouds [54, 122], optical nanofibers coupled to atoms [39, 61, 131, 132, 140, 141, 144], transmission lines coupled to superconducting qubits [44, 160], and metallic nanowires coupled to NV centers [78] and quantum dots [2]. These systems typically consist of freely propagating photons coupled to a number of emitters that provide the nonlinearity either individually or due to inter-emitter interactions. Recent years have seen significant developments in theoretical methods for such systems [4, 9, 30, 41, 42, 52, 93, 124, 130, 135, 136, 171, 176]. In several of these approaches, the emitters' dynamics are characterized by a spin model $M^{\rm tot}$, which consists of the energy of the atoms and the photon-mediated dipolar interactions $K^{\rm tot}$ between them. $K^{\rm tot}$ contains both a coherent and a dissipative part. For two atoms in vacuum separated by distance r, $K^{\rm tot}$ increases as $1/r^3$ at small r [37]. Photonic observables are then related to $M^{\rm tot}$ in an indirect way via an input-output relation involving emitter degrees of freedom [30, 93, 136, 171]. In contrast, we construct here a spin model M that directly encodes the transmission properties.

We provide a concrete analysis of two-level atoms interacting with linear-dispersion photons, but our approach readily generalizes to other level structures and dispersion relations [166].

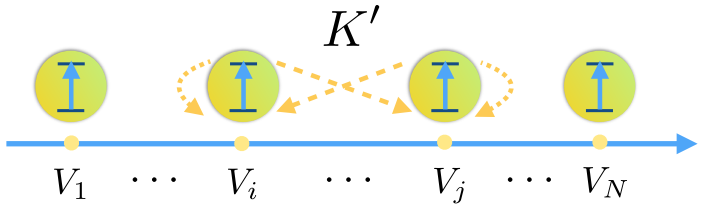

Figure 2.1: An illustration of N atoms coupled to a 1D photon channel, with V_i corresponding to the amplitude of the coupling of the photons to atom i. In addition to this specific photonic channel of interest, the atoms can also interact via additional photonic channels, which results in an effective dipole-dipole interaction K'.

2.2 The system

Figure 2.1 illustrates the system we consider. Photons propagate to the right through a 1D channel and interact with N two-level atoms with energy ω_{eg}. In addition to the 1D channel of interest, the atoms also interact with other photonic modes called the reservoir modes. If we are not interested in scattering into these other modes, their effect can be captured by a dipole-dipole interaction K'_{ij}, which physically describes photon emission and re-absorption via the other modes. Note that if K describes the additional dipole-dipole interactions mediated by the 1D channel, $K^{\text{tot}} = K' + K$. In many nanofiber experiments, photons are sent into the fiber in a particular transverse mode and measured at the output in the same transverse mode. Such systems are well described by our model, where the 1D channel consists of a continuous spectrum of right-propagating photons in the transverse mode of interest, while the reservoir modes include left-propagating photons and photons in other transverse modes.

The 1D system is described by the master equation

$$\dot{\rho} = -i(H\rho - \rho H^\dagger) + i\sum_{i,j=1}^{N}(K'_{ij} - K'^{\dagger}_{ij})b_i\rho b_j^\dagger, \tag{2.1}$$

where the effective Hamiltonian H is non-Hermitian and the recycling term (the last term) comes from the reservoir-induced interaction K'. We treat the two-level atoms as harmonic oscillators with creation operators $b_i^\dagger$ and introduce a hard-core interaction U in H to prevent atoms from being excited more than once. Hence H is given by

$$H = H_0 + V + U, \tag{2.2}$$

$$H_0 = -\int_{-\infty}^{+\infty} dz\ iC^\dagger(z)\partial_z C(z) + \sum_{i=1}^{N} \omega_{eg} b_i^\dagger b_i, \tag{2.3}$$

$$V = \left[\sum_{i=1}^{N} V_i C(z_i) b_i^\dagger + \text{h.c}\right] + \sum_{i,j=1}^{N} K'_{ij} b_i^\dagger b_j, \tag{2.4}$$

$$U = \sum_{i=1}^{N} u b_i^\dagger b_i^\dagger b_i b_i, \qquad u = +\infty, \tag{2.5}$$

where H_0 is the Hamiltonian of the right-propagating free photons with linear dispersion (speed of light $c = 1$) and N noninteracting two-level atoms. $C^\dagger(z)$ creates a photon in the transverse mode of interest at position z in the 1D channel, and V is the quadratic interaction. The first term in V describes the atom-photon interaction whereby atom i is excited through the absorption of a photon at location z_i. The second term describes the dissipative dipole-dipole interaction K' between atoms induced by the Markovian reservoir. Its Hermitian component describes coherent dipolar interactions while the anti-Hermitian component describes collective spontaneous emission. In our definition, K' is dissipative if $-i(K' - K'^\dagger)$ has only non-positive eigenvalues. Since we are interested in scattering amplitudes where the number of output photons in the 1D channel is the same as the number of input photons, it suffices to consider the effective Hamiltonian H in place of the full master equation [67, 122].

2.3 Dissipative bound states

Consider the eigenstates of the effective Hamiltonian H in the single-excitation Hilbert space, whose projected Hamiltonian is denoted as H_1. Note that H_1 also describes the classical problem where coherent states of light interact with classical dipoles. Therefore, all the single-photon results can be applied to this classical problem as well.

Every incoming free photon $|k\rangle$ uniquely labels a scattering state with energy k; therefore, the scattering-state energy spectrum is $(-\infty, +\infty)$. There may also exist bound states in the continuum [58, 77, 162], but their existence requires fine-tuning of parameters. When K' describes coherent interaction, H_1 is Hermitian and its spectrum is real; there are no generic bound states in the system. When K' includes dissipative interactions, H_1 becomes non-Hermitian. In principle, we can have bound states with complex eigenenergies, isolated from the real line occupied by the scattering states.

The non-Hermitian nature of H_1 implies that its left and right eigenvectors can be different and the set of all left (or right) eigenvectors is not guaranteed to form a complete basis. Generically the basis of eigenvectors is complete, in which case the Hamiltonian is diagonalizable and takes the form

$$H_1 = \int_{-\infty}^{+\infty} dk\ k|\psi_k\rangle\langle\pi_k| + \sum_{\alpha=1}^{N_B} E_\alpha|\psi_\alpha\rangle\langle\pi_\alpha|, \tag{2.6}$$

where $|\psi_k\rangle$ and $|\pi_k\rangle$ are, respectively, the right and left scattering eigenvectors with eigenenergy $E_k = k$ and $|\psi_\alpha\rangle$ and $|\pi_\alpha\rangle$ are, respectively, the right and left bound states with complex eigenenergy E_α. N_B is the number of bound states. The orthogonality relations among the eigenstates are $\langle\pi_k|\psi_{k'}\rangle = \delta(k-k'), \langle\pi_\alpha|\psi_\beta\rangle = \delta_{\alpha\beta}, \langle\pi_k|\psi_\alpha\rangle =$

$\langle\pi_\alpha|\psi_k\rangle = 0$. From a mathematical perspective, the bound states are necessary for the completeness of the basis: $\mathbb{1} = \int_{-\infty}^{+\infty} dk|\psi_k\rangle\langle\pi_k| + \sum_{\alpha=1}^{N_B} |\psi_\alpha\rangle\langle\pi_\alpha|$. It is one of our main goals in this chapter to understand the physical significance of these dissipative bound states. The first main result of this chapter is that the bound state eigenenergies E_α can be calculated from an effective spin model M. For a single excitation, M is an $N \times N$ matrix:

$$M_{ij} = \omega_{eg}\delta_{ij} + K'_{ij} + K^\dagger_{ij}, \tag{2.7}$$

where K is the dissipative dipole-dipole interaction induced by the 1D photon modes of interest:

$$K_{ij} = -iV_iV_j^* \exp(i\omega_{eg}(z_i - z_j))\Theta(z_i - z_j), \tag{2.8}$$

and $K^\dagger$ is its Hermitian conjugate. In comparison, $M^{\text{tot}}_{ij} = \omega_{eg}\delta_{ij} + K'_{ij} + K_{ij}$ is the single-excitation effective Hamiltonian matrix for the atoms after all the photon channels are traced out of the system. One can intuitively understand K as describing a process dissipating energy from the atoms to the 1D channel, while $K^\dagger$ describes an energy-absorption process. In this context, the appearance of $K^\dagger$ in M can be directly related to an energy conservation condition in the bound-state eigenvalue equation, as explained later in Sec. 2.7.

Because M^{tot} is dissipative, all its eigenvalues are either on or below the real line. Unlike M^{tot}, the eigenvalues of M can be anywhere with respect to the real axis; the ones below the real axis correspond to the bound state energies. Fig. 2.2 shows schematically the eigenvalues of M and M^{tot} for $N = 7$. In this case, there are $N_B = 3$ bound states illustrated as yellow dots. These bound states have a hybrid

light-matter wavefunction whereby the photonic field of the 1D mode is localized in space (i.e., bound) near the atoms. The bound states constantly leak energy into the reservoir modes without changing shape.

Given a bound-state energy E_α, if its algebraic and geometric multiplicity are different as an eigenvalue of M, both M and H_1 are non-diagonalizable. In this case, Eq. (2.6) and the completeness relation of the eigenstates of H_1 do not hold. However, one can define generalized bound states using so-called "generalized eigenvectors" of M corresponding to E_α. With these generalized bound states, the completeness relation is restored [166].

2.3.1 Derivation of spin model M

In this subsection, we derive M and its relation to bound states. Define the right bound state corresponding to energy E_α:

$$|\psi_\alpha\rangle = \int_{-\infty}^{+\infty} dz \phi_\alpha(z) C^\dagger(z)|0,g\rangle + \sum_{j=1}^{N} e_{j,\alpha} b_j^\dagger |0,g\rangle, \tag{2.9}$$

where $\phi_\alpha(z)$ is the photon wavefunction and $e_{j,\alpha}$ is the excitation amplitude for the j-th atom. The left bound state and its normalization are discussed in Sec. 2.3.2. By definition, $H_1|\psi_\alpha\rangle = E_\alpha|\psi_\alpha\rangle$. We integrate the steady-state equations of motion for photons along z and get

$$\phi_\alpha(z) = \sum_{j=1}^{N} e_{j,\alpha} V_j^* G_{E_\alpha}(z - z_j), \tag{2.10}$$

where the coordinate-space free-photon propagator $G_\omega(z') = -\eta_\omega i\Theta(\eta_\omega z')\exp(i\omega z')$ depends on η_ω, the sign of $\mathrm{Im}[\omega]$. There is no inhomogeneous term in Eq. (2.10) because the bound-state wavefunction vanishes at $z = \pm\infty$.

To solve for $e_{j,\alpha}$, Eq. (2.10) is substituted into the steady-state equations of motion for the atoms. We get

$$E_\alpha e_{i,\alpha} = \sum_{j=1}^{N} (\omega_{eg}\delta_{ij} + K'_{ij} + V_i V_j^* G_{E_\alpha}(z_i - z_j)) e_{j,\alpha}. \tag{2.11}$$

This equation can be reduced to an eigenvector calculation of an $N \times N$ matrix if $G_{E_\alpha}(z_i - z_j)$ is independent of E_α. Let us study when this approximation can be made. When $\mathrm{Im}[E_\alpha] < 0$, $G_{E_\alpha}(z_i - z_j) = G_{\omega_{eg}-i0}(z_i - z_j)\exp(i(E_\alpha - \omega_{eg})(z_i - z_j))$, where $i0$ represents an infinitesimal imaginary number above the real line. Since $E_\alpha - \omega_{eg}$ is on the order of $\Gamma \sim \frac{V_i^2}{2}$, the phase $\exp(i(E_\alpha - \omega_{eg})(z_i - z_j))$ is negligible when the length of the 1D atomic cloud is much smaller than c/Γ. In this case, we can let $G_{E_\alpha}(z_i - z_j) = G_{\omega_{eg}-i0}(z_i - z_j)$, which corresponds to the Markov approximation. Similarly, when $\mathrm{Im}[E_\alpha] > 0$, $G_{E_\alpha}(z_i - z_j) = G_{\omega_{eg}+i0}(z_i - z_j)$ under the Markov approximation.

Note that K_{ij} defined in Eq. (2.8) is equal to $V_i V_j^* G_{\omega_{eg}+i0}(z_i - z_j)$, and $K_{ij}^\dagger$ is equal to $V_i V_j^* G_{\omega_{eg}-i0}(z_i - z_j)$. $G_{\omega_{eg}+i0}(z)$ and $G_{\omega_{eg}-i0}(z)$ are the retarded and advanced Green's functions of the free photons in the 1D channel. When $\mathrm{Im}[E_\alpha] \leq 0$, Eq. (2.11) becomes $E_\alpha e_{i,\alpha} = M_{ij} e_{j,\alpha}$, where M is defined in Eq. (2.7). A self-consistency condition indicates that all the eigenvalues of M below the real line in the complex plane are bound-state eigenvalues. It is easy to verify that the corresponding photon wavefunctions ϕ_α calculated using Eq. (2.10) vanish for large z.

Does there exist a bound-state energy with a positive imaginary component? If the answer is yes, E_α should be the eigenvalues of $M^{\mathrm{tot}} = \omega_{eg} + K' + K$ above the real line. However, as M^{tot} is dissipative, all its eigenvalues are either real or below the real line in the complex plane [See Fig. b]. Hence there is no bound-state energy above the real line.

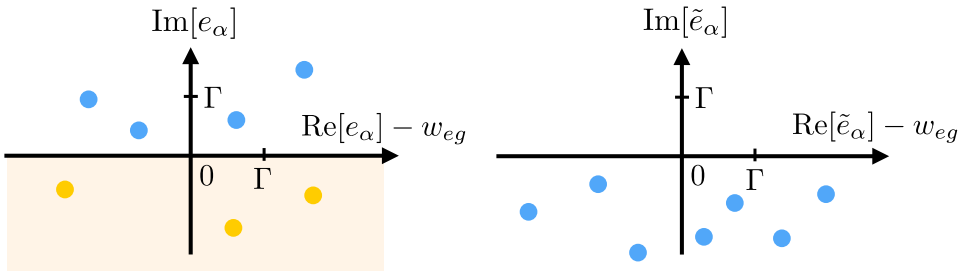

(a) Eigenvalues of M (b) Eigenvalues of M^{tot}

Figure 2.2: (Color online) Schematic of the eigenvalues of (a) M and (b) M^{tot} for $N = 7$. $\Gamma \sim \frac{V_i^2}{2}$ is the scale of the single-atom decay rate to the 1D channel. The eigenvalues of M in the lower half plane (shaded region) give valid bound states (yellow). There is no eigenvalue of M^{tot} above the real line.

2.3.2 Bound states and their wavefunction normalization

For the non-Hermitian single-excitation Hamiltonian H_1, its left and right eigenvectors are different. In Sec. 2.3.1, we only discussed the right bound states. For completeness, let us discuss the left bound state $|\pi_\alpha\rangle$ corresponding to bound-state energy E_α:

$$|\pi_\alpha\rangle = \int_{-\infty}^{+\infty} dz \bar{\phi}_\alpha(z) C^\dagger(z)|0,g\rangle + \sum_{j=1}^{N} \bar{e}_{j,\alpha} b_j^\dagger |0,g\rangle, \tag{2.12}$$

where $\bar{\phi}_\alpha$ is the photon wavefunction and $\bar{e}_{j,\alpha}$ is the excitation amplitude for atom j. $|\pi_\alpha\rangle$ is also the right eigenvector of the Hermitian conjugate of H_1 with eigenenergy E_α^*:

$$H_1^\dagger |\pi_\alpha\rangle = E_\alpha^* |\pi_\alpha\rangle. \tag{2.13}$$

The left bound states can be calculated in a similar method as the right bound states discussed in Sec. 2.3.1. Integrating the steady-state equation of motion along the real

axis, we get

$$\bar{\phi}_\alpha(z) = \sum_{j=1}^{N} \bar{e}_{j,\alpha} V_j^* G_{E_\alpha^*}(z - z_j). \tag{2.14}$$

From Eq. (2.14) and Eq. (2.10), we can see that the bound-state photon wavefunction is localized around each atom with a width given by $1/\mathrm{Im}[E_\alpha]$. Substituting Eq. (2.14) into the steady-state equations of motion for the atomic excitation $\bar{e}_{j,\alpha}$, we get

$$M_{ij}^\dagger \bar{e}_{j,\alpha} = E_\alpha^* \bar{e}_{i,\alpha}. \tag{2.15}$$

This set of eigenvalue equations determines the atomic amplitude $\bar{e}_{i,\alpha}$ up to a normalization constant. We want to choose the normalization of $\bar{e}_{i,\alpha}$ and $e_{i,\alpha}$ such that the orthogonality $\langle \pi_\alpha | \psi_\beta \rangle = \delta_{\alpha\beta}$ is ensured. Let us take a look at the overlap between the left and right bound states:

$$\langle \pi_\alpha | \psi_\beta \rangle = \sum_{j=1}^{N} \bar{e}_{j,\alpha}^* e_{j,\beta} + \int_{-\infty}^{+\infty} dz \bar{\phi}_\alpha^*(z) \phi_\beta(z). \tag{2.16}$$

In this equation, the overlap between the photon wavefunctions is

$$\int_{-\infty}^{+\infty} dz \bar{\phi}_\beta^*(z) \phi_\alpha(z) \sim \sum_{i,j=1}^{N} V_j V_i^* (z_i - z_j) \exp(i E_\beta z_j - i E_\alpha z_i) \sim |V|^2 L, \tag{2.17}$$

where L is the length of the 1D atomic cloud and V is the scale of the interaction strength. Under the Markov approximation, $|V|^2 L \ll 1$, the overlap between the photon wavefunctions is negligible. Therefore, if we choose $e_{i,\alpha}$ ($\bar{e}_{i,\alpha}$) to be the components of the normalized right (left) eigenvectors of M, the orthogonality relation $\langle \pi_\alpha | \psi_\beta \rangle \approx \sum_{j=1}^{N} \bar{e}_{j,\alpha}^* e_{j,\beta} = \delta_{\alpha\beta}$ is ensured.

2.3.3 Single-atom example

In this subsection, we illustrate the dissipative bound states using the well-studied example of a single atom ($N = 1$) at $z_1 = 0$. We set $V_1 = V$, decay rates $K' = -i\Gamma'$ and $K = -iV_1^2/2 \equiv -i\Gamma$ [127, 134]. Physically, Γ and Γ' correspond to the atomic decay rate into the 1D channel and reservoir modes, respectively.

Using Eqs. (2.10) and (2.14), we can compute the normalized right and left bound states $|\psi_B\rangle$ and $|\pi_B\rangle$. The atomic excitation $e_{1,B} = \bar{e}_{1,B} = 1$, and the photon wavefunctions are

$$\phi_B(z) = -iV^* \exp(i\omega_{eg} z + (\Gamma' - \Gamma)z)\Theta(-z), \tag{2.18}$$

$$\bar{\phi}_B(z) = iV^* \exp(i\omega_{eg} z - (\Gamma' - \Gamma)z)\Theta(z). \tag{2.19}$$

The wavefunctions decay exponentially in space with width $1/(\Gamma' - \Gamma)$. When the atom is decoupled from the 1D channel, $V = 0$, then $\phi_B(z) = \bar{\phi}_B(z) = 0$. In this case, the bound state is simply the single atom in its excited state with eigenenergy $E_B = w_{eg} - i\Gamma'$.

When $\Gamma' > \Gamma$, a bound state exists with eigenenergy $E_B = \omega_{eg} - i\Gamma' + i\Gamma$. When $\Gamma' < \Gamma$, no bound state exists. Thus, we see that the decay to the reservoir is the key to the existence of the bound states. At $\Gamma' = \Gamma$, the system is at the critical regime where a new dissipative bound state is on the verge of appearance. At this choice of paramter, the photon wavefunction of the right bound state $\phi_B(z)$ has an extended wavefunction to the right side of the atom, which looks like a scattering state with zero transmission. This behavior is an example of a general principle in dissipative scattering systems: when a dissipative bound state is on the verge of appearance from the continuum at energy E_r, the transmission coefficient of the photon at energy E_r

goes to 0. In the next section, we introduce the transmission coefficient and explain this principal in more detail.

2.4 Transmission coefficient

In this section, we focus on the transmission coefficient t_k of a single photon and provide an important formulae relating it to the spin matrices M and M^{tot}. This formula plays a central role in understanding the relationship between the dissipative bound states and the scattering of photons. In particular, it shows that the appearance of bound states corresponds to zero transmission in the system.

2.4.1 Overview of results

In a dissipative scattering system, the transmission coefficient is defined through the asymptotic behavior of the right scattering eigenstate. The right scattering eigenstate with energy k can be written as

$$|\psi_k\rangle = \int_{-\infty}^{+\infty} dz \phi_k(z) C^\dagger(z)|0,g\rangle + \sum_{j=1}^{N} e_{j,k} b_j^\dagger |0,g\rangle, \tag{2.20}$$

where $\phi_k(z)$ is the photon wavefunction and $e_{j,k}$ is the excitation amplitude for the j-th atom. $|0,g\rangle$ is the ground state with zero excited atoms or photons. Outside the region of atoms, $\phi_k(z)$ is a plane wave satisfying $\lim_{z\to\pm\infty}\phi_k(z) = a_k^\pm \exp(ikz)$. The transmission coefficient $t_k(z) = a_k^+/a_k^-$ is an easily accessible experimental observable. The purpose of this section is to introduce the following formulae that we discover:

$$t_k = \frac{\det(k\mathbb{1} - M)}{\det(k\mathbb{1} - M^{\mathrm{tot}})} = \prod_{\alpha=1}^{N} \frac{k - e_\alpha}{k - \tilde{e}_\alpha}, \tag{2.21}$$

where $\mathbb{1}$ is an $N \times N$ identity matrix, and e_α and $\tilde{e}_\alpha$ are the eigenvalues of M and M^{tot}, respectively. In the literature, the transmission through the 1D channel is usually derived from M^{tot} via an input-output relation [30, 93, 136, 171]. Here, however, we give a concise formula where a different spin model M directly encodes this useful information about photon transport. Before proving Eq. (2.21) in the following subsection, we explain the implications of Eq. (2.21).

The second equality in Eq. (2.21) is applicable when both M and M^{tot} are diagonalizable. It shows that if a real eigenvalue e_α of M is not an eigenvalue of M^{tot}, then the transmission coefficient $t_{k=e_\alpha} = 0$. The corresponding eigenstate is not a bound state—it is a scattering state with zero transmission. When e_α crosses the real line in the complex plane during the continuous tuning of parameters, a bound state appears or disappears. If a real eigenvalue e_α of M is also an eigenvalue of M^{tot}, it corresponds to a bound state in the continuum [166]. In this case, $t_{k=e_\alpha}$ is not necessarily 0.

In Sec. 2.3.3, we discussed the case of a 1D photon channel coupled to a single atom located at $z_1 = 0$. The transmission coefficient in this model is $t_k = \frac{k-(\omega_{eg}-i\Gamma'+i\Gamma)}{k-(\omega_{eg}-i\Gamma'-i\Gamma)}$. At $\Gamma' = \Gamma$, a bound state is on the verge of appearance and $t_{k=\omega_{eg}}$ is equal to 0.

2.4.2 The proof

In this subsection we prove Eq. (2.21) and show that it is valid beyond the Markov approximation. The exact relation we want to prove is

$$t_k = \frac{\det(k\mathbb{1} - M(k))}{\det(k\mathbb{1} - M^{\text{tot}}(k))}, \tag{2.22}$$

where $M(k) = \omega_{eg}\mathbb{1} + K^\dagger(k) + K'$ and $M^{\text{tot}}(k) = \omega_{eg}\mathbb{1} + K(k) + K'$. Here, $K_{ij}(k) = -iV_iV_j^* \exp(ik(z_i - z_j))$ is the frequency-dependent interaction between atoms i and

j induced by the 1D photon channel without making the Markov approximation.

To calculate t_k, we solve for the right scattering-state wavefunction corresponding to energy k. Integrating the steady-state equation of motion at energy k and choosing the boundary condition $\lim_{z\to-\infty}\phi_k(z) = \exp(ikz)$, we get

$$\phi_k(z) = -i\sum_{j=1}^{N} e_{j,k}V_j^* \exp(ik(z-z_j)) + \exp(ikz), \tag{2.23}$$

where $e_{j,k}$ is the atomic excitation defined in Eq. (2.20). This gives the transmission coefficient

$$t_k = 1 - i\sum_{j=1}^{N} e_{j,k}V_j^* \exp(-ikz_j). \tag{2.24}$$

Substituting Eq. (2.23) into the steady-state equation of motion for the atoms, we obtain a set of linear equations for $e_{j,k}$:

$$(k\delta_{ij} - M_{ij}^{\mathrm{tot}}(k))e_{j,k} = V_i \exp(ikz_i). \tag{2.25}$$

To prove Eq. (2.22), we collect the atomic-excitation amplitudes and the interaction amplitudes by defining two N-dimensional vectors:

$$|e_k\rangle \equiv (e_{1,k}, \ldots, e_{N,k})^T, \tag{2.26}$$

$$|v_k\rangle \equiv (V_1 \exp(ikz_1), \ldots, V_N \exp(ikz_N))^T. \tag{2.27}$$

Now, Eq. (2.25) can be rewritten as

$$|e_k\rangle = (k\mathbb{1} - M^{\mathrm{tot}}(k))^{-1}|v_k\rangle. \tag{2.28}$$

And Eq. (2.24) can be rewritten as

$$t_k = 1 - i\langle v_k|(k\mathbb{1} - M^{\text{tot}}(k))^{-1}|v_k\rangle \tag{2.29}$$

$$= 1 - i\text{Tr}[|v_k\rangle\langle v_k|(k\mathbb{1} - M^{\text{tot}}(k))^{-1}]. \tag{2.30}$$

Using the property $K(k) - K^\dagger(k) = -i|v_k\rangle\langle v_k|$, we get $M(k) = M^{\text{tot}}(k) + i|v_k\rangle\langle v_k|$, and Eq. (2.22) can be rewritten as

$$t_k = \frac{\det(k\mathbb{1} - M^{\text{tot}}(k) - i|v_k\rangle\langle v_k|)}{\det(k\mathbb{1} - M^{\text{tot}}(k))}. \tag{2.31}$$

Our goal is to prove that Eq. (2.30) is equivalent to Eq. (2.31). For simplicity of notation, let us define $X = k - M^{\text{tot}}(k)$ and $|v\rangle = |v_k\rangle$. The equality we want to prove is reduced to

$$\frac{\det(X - i|v\rangle\langle v|)}{\det(X)} = 1 - i\text{Tr}(|v\rangle\langle v|X^{-1}). \tag{2.32}$$

Since determinant and trace are basis-independent, we can choose an orthonormal basis such that $|v\rangle$ is parallel to one of its basis vectors. Without loss of generality, we can choose $|v\rangle = |v| \cdot (1, 0, \ldots, 0)^T$, where $|v|$ is a normalization factor. With this choice of basis, there is only one non-zero matrix element in the matrix $-i|v\rangle\langle v|$:

$$-i|v\rangle\langle v| = -i|v|^2 \begin{pmatrix} 1 & 0 & \ldots & 0 \\ 0 & 0 & \ldots & 0 \\ \vdots & & & \end{pmatrix}. \tag{2.33}$$

The simple structure of Eq. (2.33) simplifies the calculation of both sides of Eq. (2.32).

The right-hand side of Eq. (2.32) is

$$1 - i\mathrm{Tr}[|v\rangle\langle v|X^{-1}] = 1 - i|v|^2(X^{-1})_{11}, \tag{2.34}$$

where $(X^{-1})_{11}$ is the $(1,1)$ matrix element of X^{-1}. The left-hand side of Eq. (2.32) is

$$\frac{\mathrm{Det}(X - i|v\rangle\langle v|)}{\mathrm{Det}(X)} = \frac{\mathrm{Det}(X) - i|v|^2 L_{11}}{\mathrm{Det}(X)}, \tag{2.35}$$

where $L_{11} = \mathrm{Det}(X_{\not{1},\not{1}})$, and $X_{\not{1},\not{1}}$ is the minor matrix of X obtained by eliminating the 1^{st} row and 1^{st} column of X. Using the property of the inverse

$$(X^{-1})_{11} = \frac{L_{11}}{\mathrm{Det}(X)}, \tag{2.36}$$

we can see that the right-hand side of Eqs. (2.35) and (2.34) are equal, which concludes the proof.

2.5 Second-order photon-photon correlation function for a weak coherent pulse

Zeros in the transmission coefficient t_k also lead to divergent bunching in the second-order photon-photon correlation function, which is an important signature of strongly-correlated light measured in the experiment. As we will demonstrate soon, for infinitesimally weak coherent-state inputs,

$$g^{(2)}(\tau) = \frac{|\psi^{(2)}(r=\tau)|^2}{|t_k|^4}, \tag{2.37}$$

where $\psi^{(2)}(r)$ is the two-photon steady state at the output and r is the relative coordinate of the two photons. The two-photon delay τ is equal to r in units where the speed of light $c = 1$. When $t_k = 0$, $\psi^{(2)}(r)$ is nonzero due to two-photon interactions mediated by the hard-core atomic interaction U. Therefore, $g^{(2)}(\tau) = \infty$ at all τ.

In the following, we provide more details of the above argument by defining $g^{(2)}(\tau)$ and deriving Eq. (2.37). Consider a long weak coherent pulse of uniform amplitude. Let us define the creation operator $\mathcal{E}^\dagger$ which generates a single photon with duration T and center z_0 at the initial time $t = 0$:

$$\mathcal{E}^\dagger = \frac{1}{\sqrt{cT}} \int_{-\infty}^{+\infty} dz l(z) \exp(ikz) C^\dagger(z), \tag{2.38}$$

$$l(z) = \Theta(z - z_0 + cT/2)\Theta(-z + z_0 + cT/2). \tag{2.39}$$

$\mathcal{E}^\dagger$ and its Hermitian conjugate $\mathcal{E}$ satisfy the commutation relation $[\mathcal{E}, \mathcal{E}^\dagger] = 1$. The coherent-state pulse with average photon number $|\alpha|^2$ is defined as

$$|\alpha\rangle = \exp(-|\alpha|^2/2) \left(\sum_{n=0}^{\infty} \frac{\alpha^n}{\sqrt{n!}} \mathcal{E}^{\dagger n} |0\rangle \right), \tag{2.40}$$

where $|0\rangle$ is the vacuum state and $\exp(-|\alpha|^2/2)$ is the normalization factor. $|\alpha\rangle$ is prepared at time $t = 0$, sent through the atomic cloud, and measured at time t_f after the pulse has completely exited the cloud. Because of the dissipation induced by the reservoir photon modes, the output pulse at t_f is described by a density matrix ρ.

The second-order photon-photon correlation function is defined as

$$g^{(2)}(r_1, r_2) = \frac{\langle C^\dagger(r_1) C^\dagger(r_2) C(r_1) C(r_2) \rangle}{\langle C^\dagger(r_1) C(r_1) \rangle \langle C^\dagger(r_2) C(r_2) \rangle}, \tag{2.41}$$

where the coordinates r_1 and r_2 of the measurements are chosen within the length of

the output pulse away from the edges, and the averages are taken with respect to the density matrix ρ.

$\Gamma \sim V_i^2/2$ is the energy scale of the atom-photon interaction and $\mathcal{R} = |\alpha|^2/T$ is the rate of the incoming photons. When $\mathcal{R}/\Gamma \ll 1$, the probability of having two photons simultaneously interacting with the atoms is much smaller than 1. In the Supplemental Material of Ref. [98], it is shown that, when $\mathcal{R}/\Gamma \ll 1$, the density of photons $\langle C^\dagger(r)C(r)\rangle$ and the two-point correlation function $\langle C^\dagger(r_1)C^\dagger(r_2)C(r_1)C(r_2)\rangle$ evaluated with respect to the output state ρ depend only on the single-photon and two-photon scattering processes, respectively. Specifically, in the limit $\mathcal{R}/\Gamma \to 0$,

$$\langle C^\dagger(r)C(r)\rangle = \mathcal{R}|t_k|^2, \tag{2.42}$$

$$\langle C^\dagger(r_1)C^\dagger(r_2)C(r_1)C(r_2)\rangle = \mathcal{R}^2|\psi^{(2)}(r_1,r_2)|, \tag{2.43}$$

where t_k is the single-photon transmission coefficient. $\psi^{(2)}(r_1,r_2)$ is the coordinate-space wavefunction of $|\psi^{(2)}\rangle$, which is the two-photon output state corresponding to the input state $|k,k\rangle$ of two free photons with frequency k. $|\psi^{(2)}\rangle = S|k,k\rangle$ where S is the two-photon S-matrix. Here, we have assumed that the bandwidth of the pulse satisfies $1/T \ll \Gamma$, so the scattering amplitudes of the different number-state manifolds of the pulse are very close to those of the plane waves.

We define the center of mass coordinate $R = (r_1+r_2)/2$ and the relative coordinate $r = r_1 - r_2$. Due to the exchange symmetry of photons, $\psi^{(2)}(r,R) = \psi^{(2)}(-r,R)$. Except for the edges of the two-photon wavefunction, the output satisfies $\psi^{(2)}(r,R) = \exp(2ikR)\psi^{(2)}(r)$. Therefore, $g^{(2)}(r,R)$ is independent of the center of mass coordinate R and $g^{(2)}(r) = g^{(2)}(-r)$. For speed of light $c = 1$, the two-photon delay τ is equal to r. In the limit $\mathcal{R}/\Gamma \to 0$, Eq. (2.41) becomes Eq. (2.37), which is what we are trying

to derive.

2.5.1 Single atom example

To illustrate that $g^{(2)}(\tau)$ diverges at the emergence of a dissipative bound state, we calculate $g^{(2)}(\tau)$ at the output when a pulse of weak coherent state is scattered by a single atom. To calculate $\psi^{(2)}(r)$ in Eq. (2.37), we refer to Refs. [127, 136] for the expression of the symmetrized two-photon S-matrix when the energies of the two incoming photons are k_1, k_2 and the energies of the output photons are k_1', k_2'. In the center of mass frame, $E = k_1 + k_2$, $q = (k_1 - k_2)/2$, $E' = k_1' + k_2'$, $q' = (k_1' - k_2')/2$. $S(E', q', E, q) \equiv \langle k_1', k_2'|S|k_1, k_2\rangle$ is given by

$$S(E', q', E, q) = t_{E/2+q} t_{E/2-q} (\delta(q - q') + \delta(q + q'))\delta(E - E') - 4\pi i T(E', q', E, q)\delta(E - E'), \tag{2.44}$$

where the T-matrix element $T(E', q', E, q)$ is given by

$$T(E', q', E, q) = -\frac{16\Gamma^2}{\pi^2} \frac{E - 2w_{eg} + 2i\Gamma^{\text{tot}}}{[4q^2 - (E - 2w_{eg} + 2i\Gamma^{\text{tot}})^2][4q'^2 - (E - 2w_{eg} + 2i\Gamma^{\text{tot}})^2]}. \tag{2.45}$$

$\Gamma = V^2/2$ is the decay rate of the atom to the 1D channel and $\Gamma^{\text{tot}} = \Gamma' + \Gamma$ is the total decay rate of the atom. The first term of $S(E', q', E, q)$ is equal to the amplitude of two photons scattering off the atom independently. The second term is the amplitude of scattering processes involving the non-linearity of the atom. $\psi^{(2)}(r, R)$ can be computed from a Fourier transform of $S(E', q', E, q = 0)$ with respect to E', q'. For a weak coherent-state pulse resonant with the two-level atom, the two input photons

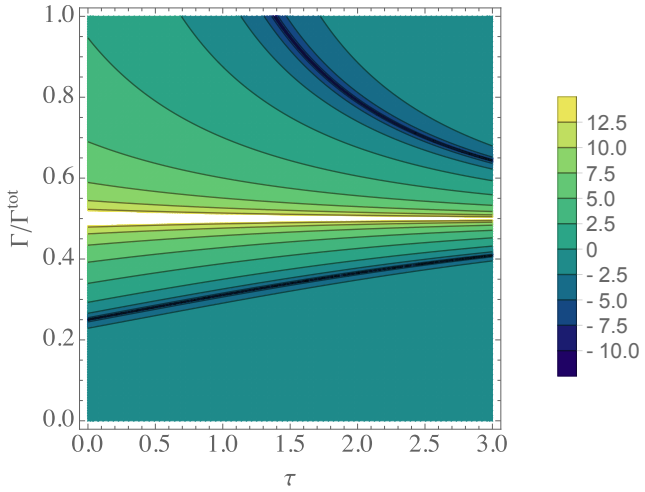

Figure 2.3: (Color online) $\log(g^{(2)}(\tau))$ as a function of the ratio $\Gamma/\Gamma^{\rm tot}$ and $\tau = r$. At $\Gamma/\Gamma^{\rm tot} = 0.5$, $t_{k=w_{eg}} = 0$ and $g^{(2)}(\tau)$ diverges for all τ.

have the same energy $k_1 = k_2 = w_{eg}$, so $\psi^{(2)}(r, R)$ is given by

$$\psi^{(2)}(r,R) = \frac{1}{\sqrt{2\pi}} \int_{-\infty}^{+\infty} dq' dE' \exp(iq'r + iE'R) S(E', q', E = 2w_{eg}, q = 0)$$
$$= \left[\frac{(\Gamma' - \Gamma)^2}{\pi(\Gamma^{\rm tot})^2} \cos(qr) - \frac{4\Gamma^2}{\pi(\Gamma^{tot})^2} \left(\exp(\Gamma^{\rm tot} r)\Theta(-r) + \exp(-\Gamma^{\rm tot} r)\Theta(r) \right) \right] \exp(2iw_{eg}R). \tag{2.46}$$

The transmission coefficient on resonance is $t_{k=w_{eg}} = \frac{\Gamma'-\Gamma}{\Gamma^{\rm tot}}$. Using Eq. (2.37) and Eq. (2.46), we plot $g^{(2)}(\tau)$ for $N = 1$ as a function of $\Gamma/\Gamma^{\rm tot}$. When $\frac{\Gamma}{\Gamma^{\rm tot}} = 0.5$, the single-photon transmission $t_{k=w_{eg}} = 0$ and $g^{(2)}(\tau)$ diverges.

2.6 Levinson's theorem

Since the bound states are orthogonal to the scattering states, they cannot be excited by sending photons into the 1D channel, which raises the the question: How can one probe these bound states in a scattering experiment? We recall Levinson's theorem for the Schrödinger equation, which relates the number of bound states and

the difference of scattering phase shifts at zero and infinite energy [46, 168, 169]. If a similar relation exists in our interacting atom-photon system, then we can measure N_B directly in experiments through a phase measurement of t_k (e.g. by an interferometric technique). We can explore this numerically by plotting t_k as a function of $k \in (-\infty, +\infty)$ in the complex plane. Fig. a shows the trajectory of t_k for the case of $N = 1$ with various parameters $\frac{\Gamma}{\Gamma^{\rm tot}} = 1, 0.5, 0.2$, where $\Gamma^{tot} = \Gamma + \Gamma'$. The trajectories go in the counter-clockwise direction when k increases. The figure implies that t_k encloses the origin when there is no bound state ($\frac{\Gamma}{\Gamma^{\rm tot}} > \frac{1}{2}$) and does not enclose the origin when the bound state exists ($\frac{\Gamma}{\Gamma^{\rm tot}} < \frac{1}{2}$). At the threshold ratio $\frac{\Gamma}{\Gamma^{\rm tot}} = 0.5$, the trajectory passes through 0 at $k = E_B = \omega_{eg}$. The single-atom case shows that the winding number of t_k around the origin is related to N_B. Using Eq. (2.21) and the definition of the winding number, we find

$$\frac{1}{2\pi i}\int_{-\infty}^{+\infty} dk\; t_k^{-1}\frac{dt_k}{dk} = N - N_B, \tag{2.47}$$

where N_B includes the number of bound states inside the continuum.

To further illustrate the significance of Eq. (2.47), we consider a two-atom system with interaction strength $V_1 = V_2$, distance $r_1 - r_2 = \frac{2\pi}{\omega_{eg}}$, and $\Gamma = \frac{V^2}{2}$. The dipole-dipole interaction induced by the 1D channel is $K = \Gamma \begin{pmatrix} -i & -2i \\ 0 & -i \end{pmatrix}$. We consider the scenario when both atoms decay to the reservoir with rate $-i\Gamma'$ and interact coherently with strength $-\Gamma'$. In this case, $K' = \Gamma' \begin{pmatrix} -i & -1 \\ -1 & -i \end{pmatrix}$[1]. The total decay rate of each atom is $\Gamma^{\rm tot} = \Gamma + \Gamma'$. Fig. b shows the trajectory of t_k for

[1]The matrix K for any N-atom system satisfies the property that $K - K^\dagger = -i|v\rangle\langle v|$ is proportional to a projector in the N-dimensional space. In principle, K' can be any $N \times N$ dissipative matrix

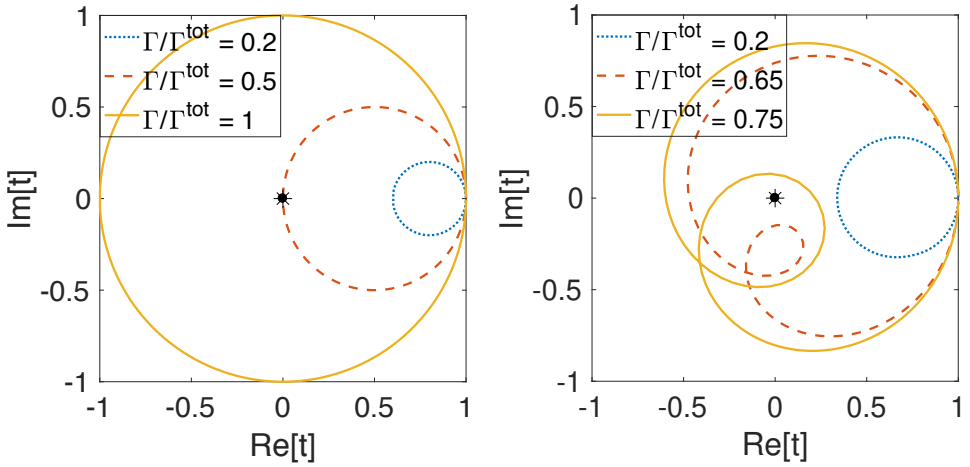

(a) $N = 1$ (b) $N = 2$

Figure 2.4: (Color online) $\mathrm{Im}[t_k]$ vs. $\mathrm{Re}[t_k]$ as k varies from $-\infty$ to $+\infty$ for (a) $N = 1$ and (b) $N = 2$. The trajectories start from $(1, 0)$, go in the counter-clockwise direction, and end at $(1, 0)$. The origins are marked as stars in the center of the figures. The number of times the trajectories enclose $(0, 0)$ is equal to $N - N_B$, where N_B is the number of dissipative bound states.

$\Gamma/\Gamma^{\mathrm{tot}} = 0.2,\ 0.65,\ 0.75$. All three trajectories are asymmetric about the real axis [2]. The corresponding number of bound states $N_B = 2,\ 1,\ 0$ decreases with decreasing dissipation. The corresponding winding number of t_k increases from 0 to 2.

In many experiments, achieving $\Gamma/\Gamma^{\mathrm{tot}}$ above a few percent is difficult. Therefore, it is hard to achieve $N_B \neq N$ in the $N = 1, 2$ examples discussed above. However, we show in Ref. [166] that when N is large, $N_B < N$ can be achieved for realistic values of 1D decay rate Γ.

2.7 Energy exchange processes associated with the spin models

The purpose of this section is to illustrate the energy exchange processes associated with the eigenvectors of M^{tot}, M, and the scattering states. To be specific, we want

[2]The trajectory of t_k is symmetric about the real axis when the eigenvalues of M and M^{tot} are symmetric about the same vertical line $\mathrm{Re}[E] = E^*$ in the complex plane (Re[E],Im[E]) for some real number E^*

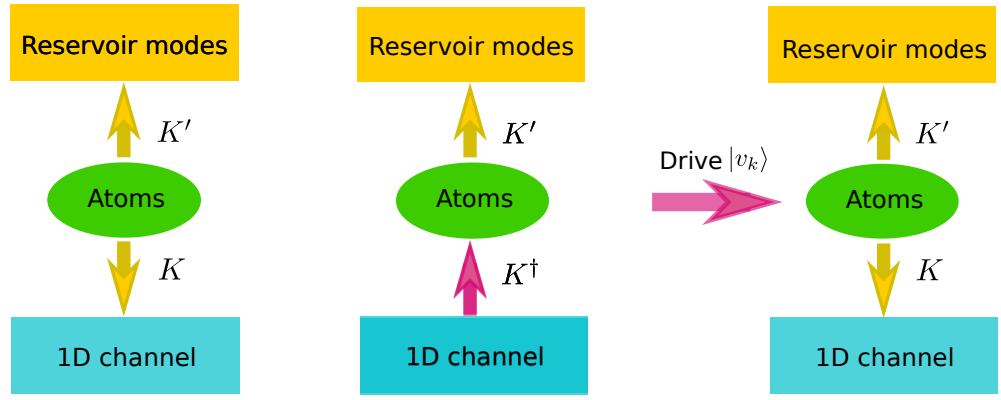

(a) $M^{\text{tot}}|\tilde{e}_\alpha\rangle = \tilde{e}_\alpha|\tilde{e}_\alpha\rangle$ (b) $M|e_\alpha\rangle = e_\alpha|e_\alpha\rangle$ (c) $(k\mathbb{1} - M^{\text{tot}})|e_k\rangle = |v_k\rangle$

Figure 2.5: The energy flow digrams associated with (a) the eigenvectors of M^{tot}, (b) the single-photon bound states and (c) the scattering states. $M^{\text{tot}} = w_{eg}\mathbb{1} + K + K'$ and $M = w_{eg}\mathbb{1} + K^\dagger + K'$.

to compare the following three equations:

$$M^{\text{tot}}|\tilde{e}_\alpha\rangle = \tilde{e}_\alpha|\tilde{e}_\alpha\rangle, \tag{2.48}$$

$$M|e_\alpha\rangle = e_\alpha|e_\alpha\rangle, \tag{2.49}$$

$$(k\mathbb{1} - M^{\text{tot}})|e_k\rangle = |v_k\rangle. \tag{2.50}$$

Eqs. (2.48) and (2.49) are the eigenequations of M^{tot} and M with respective eigenvectors $|\tilde{e}_\alpha\rangle = (\tilde{e}_{1,\alpha}, \ldots, \tilde{e}_{N,\alpha})^T$ and $|e_\alpha\rangle = (e_{1,\alpha}, \ldots, e_{N,\alpha})^T$. Eq. (2.50) is equivalent to Eq. (2.28), which is the linear equation for the calculation of atomic amplitudes for the scattering states. The vectors that represent the atomic amplitudes $|e_k\rangle$ and the drive $|v_k\rangle$ were defined in Eqs. (2.26) and (2.27).

Since M^{tot} is the single-excitation effective Hamiltonian matrix when all photons are traced out of the system, its eigenvector $|\tilde{e}_\alpha\rangle$ corresponds to a state $|\tilde{\psi}_\alpha\rangle = \sum_{i=1}^{N} \tilde{e}_{i,\alpha} b_i^\dagger |0, g\rangle$ that decays to all photon channels during time evolution without changing shape. Fig. a illustrates the direction of the energy flow from the atoms during the time evolution of $|\tilde{\psi}_\alpha\rangle$, where the atoms dissipate energy to the 1D and

reservoir modes through dissipative interactions K and K', respectively. The total energy loss rate of the atoms is given by $\mathrm{Im}[\tilde{e}_\alpha]$.

The eigenvectors $|e_\alpha\rangle$ of M correspond to single-photon bound states $|\psi_\alpha\rangle$ when $\mathrm{Im}(e_\alpha) < 0$. These photon-atom hybrid states dissipate energy to the reservoir modes without changing shape. Fig. b illustrates the direction of energy flow between the atoms and photon channels during the time evolution of $|\psi_\alpha\rangle$. The atoms absorb energy from the 1D channel through interaction $K^\dagger$ and dissipate energy to the reservoir modes through K'. The net rate of energy change for the atoms is $\mathrm{Im}[e_\alpha] < 0$.

For a scattering state $|\psi_k\rangle$ with atomic amplitudes given by the vector elements of $|e_k\rangle$, the direction of energy exchange is illustrated in Fig. c. The atoms absorb energy through the drive (represented by vector $|v_k\rangle$) and dissipate energy to all photon channels through dissipative interaction $K+K'$. The magnitude of the atomic amplitudes is constant during time evolution, as the energy absorption rate from the drive is equal to the energy-dissipation rate to the photon channels.

2.8 Outlook

Many of our findings can be generalized to non-Markovian or multi-channel systems, other level structures, and dispersion relations [166]. Re-examining similar bound states in various dissipative systems may open the door to new insights into well-studied systems. Finally, with the high degree of control available in atomic, molecular, and optical systems, the first experimental study of Levinson's theorem is likely not far away.

Chapter 3: Resonant enhancement of three-body loss between strongly interacting photons

Work in this chapter was published in Ref. [90].

3.1 Introduction

Systems exhibiting strong interactions between single photons are an exciting frontier of quantum optics [36]. They are practically relevant for quantum networks [91] and can give rise to new exotic states of matter [34, 108, 120]. Obtaining better control and understanding of these systems in the quantum few-body limit is central to realizing this potential in near-term experiments. An important step in this direction is the mastery of the three-body problem. Although in general not analytically solvable, the three-body problem has emergent universal properties, such as the existence of Efimov bound states [48]. Moreover, three-body forces can greatly influence the properties of quantum many-body systems as in the case of nuclear systems [27], neutron stars [146], and fractional quantum Hall states [113].

By coupling photons to Rydberg atoms using electromagnetically induced transparency (EIT) [56], strong and tunable pairwise interactions between photons are achievable [31, 38, 47, 54, 65, 66, 86, 97, 99, 111, 123, 133, 143, 145, 147, 154–157]. Recently, it has been demonstrated that three-body forces between Rydberg polaritons can be very strong as well [22, 72, 73, 83, 99], which distinguishes them from

weaker three-body forces engineered with ultracold atoms [59] and molecules [28, 40, 88, 112]. However, those previous studies considered dispersive three-body interactions, whereas dissipative interactions have only begun to be explored [79]. Dissipative forces are of interest as they often lead to exotic nonequilibrium dynamics in driven-dissipative systems [21, 67, 123, 159, 175], while also finding applications in engineering topological phases of matter such as the Pfaffian state [129].

In this chapter, we study the influence of dissipative three-body interactions on the physics of Rydberg cavity polaritons. Pure three-body scattering processes in Rydberg-EIT systems are strong and often comparable to two-body effects [73, 79, 83, 99, 147]. There is also evidence that effective three-body interactions are enhanced in this system [73, 83, 99] due to Rydberg blockade effects [104]. Here, by studying a simplified cavity model that can be treated with a rigorous renormalization group technique, we clearly establish the existence of a universal regime where both dispersive and dissipative three-body forces can be enhanced in a tunable fashion. This enhancement appears due to a near-resonant process when the incoming state can conserve energy and momentum by scattering to a large manifold of intermediate lossy states. Due to the role played by an intermediate resonant channel, this effect has similarities to Feshbach resonances [96]. The interaction can be tuned using the strength and the frequency of the classical control fields. We show how these effects can be probed in current experiments by studying the cavity transmission.

Because of the multi-component nature of the Rydberg polaritons, the theoretical description of the three-body problem is nuanced and complex. To make our analysis analytically tractable, we concentrate on a single-mode cavity, with the extensions to multi-mode cavities presented in our upcoming work [89]. Specifically, based on the microscopic model of photons in a cavity [60, 69, 101, 121, 142, 145] interacting with Rydberg atoms under EIT conditions, we derive analytical formulae for the

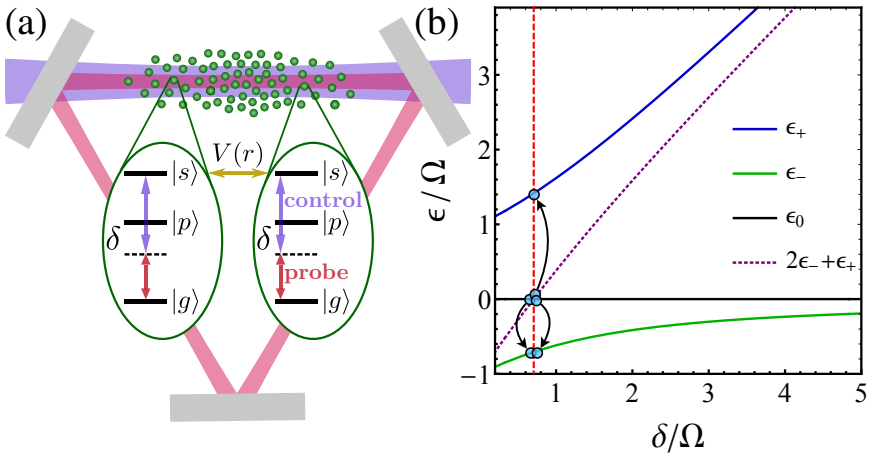

Figure 3.1: (a) Gas of neutral atoms is suspended in an optical cavity. Each atom is a three-level system with the ground state $|g\rangle$, intermediate lossy state $|p\rangle$ with half-width γ, and a high-lying Rydberg state $|s\rangle$, which experiences strong interactions. Classical control field with Rabi frequency Ω and detuning δ couples states $|p\rangle$ and $|s\rangle$. Quantum photon field with collective coupling g drives the $|g\rangle - |p\rangle$ transition and is tuned to the two-photon resonance. (b) Energy of the upper (blue) and lower (green) branches of spin waves as a function of the single-photon detuning. At $\delta = \Omega/\sqrt{2}$ scattering of three DSPs (black) into spin waves (dotted purple) is on resonance.

interaction-induced shifts in energies and decay rates of three dark-state polaritons (DSPs). We show how to gain additional insights into the system by introducing an effective Hamiltonian describing dark state polaritons alone–this approach may be useful in deriving effective descriptions of the free-space system. We solve the three-body problem using a simplified version of the Faddeev equations. Even in these simplified cavity models, it is only with the considerable simplifications afforded by the Faddeev equation formalism that we have been able to rigorously solve for the three-body force in the relevant parameter regimes. The methods introduced here allow one to extend the analysis of Ref. [83] to compute energy shifts for arbitrary multi-mode cavities and improve the accuracy of the extracted three-body force. They may also aid in developing a more systematic and rigorous renormalization group approach for the free-space problem [73].

3.2 System

The medium we consider consists of three-level atoms with ground-state $|g\rangle$, and an intermediate state $|p\rangle$ coupled to Rydberg state $|s\rangle$ by a coherent laser, with Rabi frequency Ω, and a complex detuning $\Delta = \delta - i\gamma$ [see Fig. 3.1(a)], which captures the $|p\rangle$-state's decay rate 2γ. The atomic cloud is suspended in a single-mode running-wave cavity. The quantum photon field, with collective coupling g, is tuned to the EIT resonance with the noninteracting Hamiltonian

$$H_0 = \int dz\, \vec{\psi}^\dagger(z) \begin{pmatrix} 0 & g & 0 \\ g & \Delta & \Omega \\ 0 & \Omega & 0 \end{pmatrix} \vec{\psi}(z), \tag{3.1}$$

where $\vec{\psi}^\dagger(z) = [u_0^*(z)a^\dagger, P^\dagger(z), S^\dagger(z)]$ is a vector of bosonic creation operators for the cavity field a with mode function $u_0(z)$ and atomic states $|p\rangle, |s\rangle$ at position z. We set $\hbar = 1$ throughout. H_0 couples the cavity field to one $|p\rangle$ mode and one $|s\rangle$ mode, both with the same mode function $u_0(z)$. Diagonalizing the resulting 3-by-3 matrix leads to three eigenmodes. The zero-energy mode is the DSP, which has no overlap with the lossy intermediate state. The two "bright-state" polariton modes are energetically separated and do not influence the DSP behavior in the experimentally relevant limit of strong coupling ($g \to \infty$) considered here. The remaining eigenstates of H_0 (spin waves) correspond to the excitations of the atomic cloud, have no photonic component, and couple to the polaritons only via atom-atom interactions. In the presence of Rydberg interactions $H_{\text{int}} = \frac{1}{2}\int dz dz' S^\dagger(z)S^\dagger(z')V(z-z')S(z')S(z)$,

polaritons experience an effective two-body potential [17, 20, 68]

$$U_2(\omega; r) = \frac{V(r)}{1 - \chi(\omega)V(r)}, \tag{3.2}$$

where $\chi(\omega)$ is a function of Δ, Ω, and the total energy ω of the incoming polaritons. The bare interaction $V(r) = C_6/r^6$ is the van der Waals potential between two atoms separated by distance r. The effective potential in Eq. (3.2) saturates to a constant value at short distances and decays as $1/r^6$ for large separations. Intuitively, at large distances, the van der Waals interaction is directly transferred onto the polaritons, while at distances shorter than the blockade radius $r_b = |\chi(0)C_6|^{1/6}$, the interaction shifts the two Rydberg states out of resonance (the so-called Rydberg blockade mechanism) leading to the renormalization of the effective interaction potential.

To gain insight into few-body interactions, we consider a cavity as our setup, since its treatment requires only a finite number of photonic modes. When the photonic modes are near-degenerate (or there is only one relevant photonic mode), there is a natural separation of scale that appears between low-energy polaritons and high-energy atomic excitations (spin waves). We can take advantage of this energy separation to obtain an effective theory for the polaritons–renormalized by the influence of high-energy spin waves. In contrast, in free space, there is a continuum of energies connecting these two regimes, which makes a similar procedure more difficult.

For simplicity, we consider an effectively one-dimensional running-wave cavity with a single, fixed-momentum photonic mode on EIT resonance and a uniform density of atoms filling the entire cavity mode. We present the generalization of our results to nonuniform setups, e.g., as in Fig. 3.1(a), in our upcoming work [89]. We focus on this model because we have found that it captures generic physical features of multi-mode systems, while simplifying certain technical aspects of the calculations.

Independent of the geometry, in such cavity models, the interactions between polaritons most simply appear as shifts in the energies and decay rates of the polariton modes. To calculate these shifts, we use a master equation description of the problem in the weak-driving regime, such that the anti-Hermitian part of the non-Hermitian Hamiltonian is sufficient to account for losses in the system [33]. Complex energy shifts for the two- and three-body problems coincide with the value of poles in the corresponding two- and three-body T-matrix describing correlation functions in this system.

3.2.1 Running-wave cavity Hamiltonian

In this subsection, we introduce more details of the microscopic model used in this chapter.

We consider a running-wave optical cavity in one dimension, supporting a single photonic mode. Moreover, we assume a constant density of the atomic cloud, so that the system is translationally invariant. The cavity mode with the profile $u_0(z)$ is created by the operator $a^\dagger$. While there is only one photonic mode present, the atomic medium can support a broad range of excitations, which are captured by introducing additional mode functions $u_{q\neq 0}(z)$. Together, $\{u_0, u_{q\neq 0}\}$ form an orthonormal basis and can be used to express various field operators

$$E^\dagger(z) = u_0^*(z)a^\dagger, \qquad P_q^\dagger = \int dz\, u_q(z)P^\dagger(z), \qquad S_q^\dagger = \int dz\, u_q(z)e^{ik_c z}S^\dagger(z), \tag{3.3}$$

where $E^\dagger(z)$ creates the cavity photon at position z, while $P^\dagger(z)$ and $S^\dagger(z)$ create an excitation of the medium at position z to the atomic state $|p\rangle$ ans $|s\rangle$, respectively. Thanks to the translational symmetry, we can identify index q with momentum and write the explicit form of these mode functions: $u_q(z) = \frac{1}{\sqrt{L}}e^{iqz}$. This way, the

momentum $q = 0$ corresponds to the cavity photon in the rotating frame. The Hamiltonian for such a system is

$$H_{\text{cav}} = \underbrace{\begin{pmatrix} a \\ P_0 \\ S_0 \end{pmatrix}^\dagger \begin{pmatrix} \delta_r & g & 0 \\ g & \Delta & \Omega \\ 0 & \Omega & -i\gamma_s \end{pmatrix} \begin{pmatrix} a \\ P_0 \\ S_0 \end{pmatrix}}_{\text{Photon mode}} + \underbrace{\sum_{q\neq 0} \begin{pmatrix} P_q \\ S_q \end{pmatrix}^\dagger \begin{pmatrix} \Delta & \Omega \\ \Omega & -i\gamma_s \end{pmatrix} \begin{pmatrix} P_q \\ S_q \end{pmatrix}}_{\text{Spin waves}} + H_{\text{int}}, \tag{3.4}$$

where $\Delta = \delta - i\gamma$ is the complex detuning of the classical field with Rabi frequency Ω, $2\gamma_s$ is the decay rate of the Rydberg state, and δ_r is the (two-photon) detuning from the EIT resonance. Note the difference in form from Eq. (3.1) is that we write Eq. (3.4) in a momentum basis, whereas Eq. (3.1) is in a real-space basis. The real-space representation is convenient for presentation because it naturally generalizes to other cavity geometries. The interaction Hamiltonian H_{int} is

$$\begin{aligned} H_{\text{int}} &= \frac{1}{2}\int dz dz' S^\dagger(z) S^\dagger(z') V(z-z') S(z') S(z') \\ &= \frac{1}{2}\sum_{q_1,q_2} S^\dagger_{q_1} S^\dagger_{-q_1} S_{q_2} S_{-q_2} \int \frac{dr}{L}\, V(r) e^{i(q_1-q_2)r}, \end{aligned} \tag{3.5}$$

where second equality holds for vanishing total momentum $K = 0$, which is the case we consider here (as we will explain in Sec. 3.4.2, only the $K = 0$ solution to the two-body problem will be necessary for our solution to the three-body problem). We assume $\Delta = \delta$ to be real throughout all derivations. Then, we analytically continue the result to the complex case $\Delta = \delta - i\gamma$. Throughout all derivations, we also consider the situation where the photon field is on the EIT resonance ($\delta_r = 0$) and the Rydberg state decay rate is negligible ($\gamma_s = 0$).

Spectral decomposition of the spin-wave part of the Hamiltonian (3.4) gives en-

ergies $\epsilon_\pm$ of the upper/lower spin wave and their respective overlaps $\alpha_\pm$ with the $|s\rangle$ state:

$$\epsilon_\pm = \frac{1}{2}\left(\Delta \pm \sqrt{\Delta^2 + 4\,\Omega^2}\right), \qquad \alpha_\pm = \frac{1}{2}\left(1 \pm \frac{\Delta}{\sqrt{\Delta^2 + 4\,\Omega^2}}\right). \tag{3.6}$$

In the coordinate space, the single-particle propagator ($\hat{g}_s$) is

$$g_s(\omega; x, x') = \underbrace{\sum_{\mu=\pm} \frac{\alpha_\mu}{\omega - \epsilon_\mu + i0^+}}_{\eta(\omega)} \sum_{q\neq 0} e^{iq(x-x')} + \frac{1}{\omega + i0^+}, \tag{3.7}$$

where the first term corresponds to the spin-wave excitation and the second to the dark-state polariton. In the large-coupling limit $g \gg \Omega, |\Delta|$, only the dark branch of polaritons contributes because the energy of bright polaritons is proportional to $g \to \infty$, so their effect can be neglected – see Ref. [17] for a more detailed discussion. The energy-dependent factor $\eta(\omega)$ can be evaluated to

$$\eta(\omega) = \frac{\omega - \Delta}{\omega^2 - (\Omega^2 + \Delta\,\omega)}, \tag{3.8}$$

and one needs to use the full expression with $i0^+$ included if integration occurs.

In the previous work of Refs. [73, 83], the authors considered the limit $\Omega \ll \Delta$, where only one spin-wave branch contributes. However, in our regime of interest $\Omega \sim \Delta$ and we must solve the more general problem that includes all branches. In addition, both Ref. [83] and Ref. [73] made (different) simplifying approximations which led to slight quantitative differences between all three solutions for the effective three-body force: Ref. [83], Ref. [73], and the present work. The current approach is more systematic and can be rigorously derived as an asymptotic perturbative expansion of the solutions to the three-body Schrödinger equation. We present further

extensions of these results to general multi-mode cavities in our upcoming work [89]. Generalizing these cavity solutions to the free-space problem remains an outstanding challenge. An alternative technique, that has been successfully applied in free-space, is to define effective three-body parameters through nonperturbative matching techniques [99]. In this alternative approach, these parameters are tuned in an effective field theory to reproduce low-energy observables (e.g., the dimer-polariton scattering length) obtained from the solution to the microscopic model.

3.2.2 Qualitative picture

Before moving to the main derivations of this chapter, we briefly discuss the physical origin of the enhanced three-body dissipation in our system, which is the main result of this work. This phenomenon has an intuitive explanation: three dark-state polaritons propagating at EIT resonance have zero energy. At the same time, upper and lower branches of spin waves have energies $\epsilon_\pm = \frac{1}{2}(\Delta \pm \sqrt{\Delta^2 + 4\Omega^2})$. Strong losses occur at $\delta = \Omega/\sqrt{2}$ because, at this point, $2\epsilon_- + \epsilon_+ = 0$, which means that three-body scattering into lossy atomic excitations is on energetic resonance [see Fig.3.1(b)].

3.3 Two-body problem

First, we turn to the two-body problem. Consider an incoming state of two polaritons (labeled 1 and 2) initially located at positions $\vec{x} = (x_1, x_2)$ and later measured at positions $\vec{x}'$ after interactions take place. The amplitude for this process can be described within the framework of scattering theory. The multi-component nature of the polariton problem means that the full (bold) two-body T-matrix $\hat{\boldsymbol{T}}_{\boldsymbol{2}}(\omega)$ is a 3×3 operator-valued matrix. However, only the Rydberg ($|s\rangle$) component experiences in-

teractions. Therefore, we can restrict our considerations to the ss-component $\hat{T}_2(\omega)$ of the full two-body T-matrix $\hat{\boldsymbol{T}}_{\boldsymbol{2}}(\omega)$ [17–19]. $\hat{T}_2(\omega)$ is governed by the Lippmann-Schwinger equation, see Fig. 3.2(a). In these cavity problems, one can equivalently study the integrated T-matrix $T_2(\omega) \equiv \int d\vec{x} d\vec{x}' \, T_2(\omega; \vec{x}, \vec{x}')$, where $T_2(\omega; \vec{x}, \vec{x}')$ is the matrix element of $\hat{T}_2$ in coordinate space.

To gain insight into the influence of the additional spin-wave branch, we begin by studying the two-body problem. Description of the two-body processes is contained in the off-shell two-body T-matrix $T_2(\omega)$. In the following, we derive that

$$T_2(\omega) = \frac{\omega \, U_2(\omega)}{\omega - U_2(\omega)[1 - \omega \, \chi(\omega)]}, \tag{3.9}$$

where $U_2 \equiv \int \frac{dr}{L} U_2(\omega; r)$ and L is the mode volume of the DSP. The two-body energy shift is given by the poles of $T_2(\omega)$.

The derivation of Eq. (3.9) starts here. An equation for $T_2(\omega)$ can be written explicitly using a supporting definition $T_2(\omega) = \int \frac{dr}{L} T_2(\omega; r)$, where $T_2(\omega; r) = \int \frac{d\vec{x}'}{L^2} \frac{dR}{L} T_2(\omega; \vec{x}, \vec{x}')$, $\vec{x} = (x_1, x_2)$, $\vec{x}' = (x_1', x_2')$, $r = x_1 - x_2$ is the relative coordinate, and $R = (x_1 + x_2)/2$ is the center of mass coordinate. $T_2(\omega; r)$ is given by

$$T_2(\omega; r) = V(r) + \int \frac{dr'}{L} \, V(r) G_2(\omega; r, r') T_2(\omega; r'), \tag{3.10}$$

where the two-body propagator G_2 can be obtained from the Hamiltonian (3.4) and is given by

$$G_2(\omega; r, r') = (\omega + i0^+)^{-1} + \chi(\omega) \sum_{q \neq 0} e^{iq(r - r')}, \tag{3.11}$$

where the zero-momentum term $(\omega + i0^+)^{-1}$ is the propagator of two dark-state

polaritons. It can be related to our formulation using $\hat{g}_s$ via

$$G_2(\omega; r, r') \stackrel{!}{=} \int \frac{d\omega'}{2\pi i} g_s(\omega'; x_1, x_1') g_s(\omega - \omega'; x_2, x_2'), \tag{3.12}$$

where $\stackrel{!}{=}$ means that it is equal only under the integral in Eq. (3.10) and after enforcing the total-momentum conservation. The coefficient $\chi(\omega)$, in the part of G_2 corresponding to the double excitation of spin waves, is

$$\chi(\omega) = \frac{\Delta - \frac{\omega}{2} - \frac{\Omega^2}{\Delta - \omega}}{\omega\left(\Delta - \frac{\omega}{2}\right) + 2\Omega^2}, \tag{3.13}$$

which coincides with the two-body propagator in free space in the infinite-momentum limit [17]. Equation (3.10) is represented schematically in Fig. 3.2(a). To solve it, we rewrite the propagator from Eq. (3.11) as

$$G_2(r, r') = [(\omega + i0^+)^{-1} - \chi(\omega)] + L\chi(\omega)\,\delta(r - r'), \tag{3.14}$$

and plug it back into Eq. (3.10). After rearrangement and integration of both sides by $\int \frac{dr}{L}$, we obtain the equation for $T_2(\omega)$, which gives

$$T_2(\omega) = U_2(\omega) + U_2(\omega)[(\omega + i0^+)^{-1} - \chi(\omega)]T_2(\omega), \tag{3.15}$$

where $U_2(\omega)$ is a well-known [17] renormalized two-body interaction (for $g \to \infty$) between dark-state polaritons, presented in Eq. (3.2). In the limit of large separation, it reduces to the bare van der Waals potential. Conversely, for small distances, it saturates at a finite value, an effect caused by the so-called Rydberg blockade mechanism.

Solving algebraic equation Eq. (3.15) for $T_2(\omega)$ reproduces Eq. (3.9). Notice that,

to the leading order in r_b/L, Eq. (3.15) describes the scattering of two infinitely heavy particles under the influence of potential $U_2(\omega; r)$. Additional terms encapsulate effects specific to the cavity setup.

3.4 Three-body problem

3.4.1 Main results

After discussing the two-body problem, we are ready to discuss the three-body problem. We first provide an overview in this subsection and provide the details of the calculation in the following subsection.

Three-body problems are complex both in classical and quantum physics. Previous works on the three-body problem for Rydberg polaritons considered the restricted limit $\Omega \ll |\delta|$ [72, 73, 83]; here, we extend the regime of applicability to $\Omega > |\delta|$, which allows for a more general description of the system, including repulsive photons [17] and dissipative behavior.

Although dramatically simplified, the three-body problem cannot, to the best of our knowledge, be solved exactly in the single-mode cavity model considered in this chapter. Instead, we approximate the full result by a power series in the small parameter r_b/L, which is effectively the product of the blockade radius and the density of polaritons in this few-body limit. We stress, that this approach is still nonperturbative in the bare interaction $V(r)$. Our final expression for the three-body energy shift to second order in r_b/L is given by

$$\begin{aligned} \delta E_3 &= \frac{r_b}{L} E_3^{(1)} + \frac{r_b^2}{L^2} E_3^{(2)} + \mathcal{O}(r_b^3/L^3) \\ &= \underbrace{3U_2}_{\mathcal{O}(r_b/L)} + \underbrace{3U_3 + 3U_2\,(3U_2' - \chi\, U_2)}_{\mathcal{O}(r_b^2/L^2)}, \end{aligned} \tag{3.16}$$

where U_3 is a *universal* effective three-body force (see Fig. 3.2) that emerges for Rydberg cavity polaritons and $U_2' \equiv dU_2(\omega)/d\omega|_{\omega=0}$. U_3 has a similar expression to U_2 as an integral over a local three-body potential. The other terms at order r_b^2/L^2 represent additional nonlocal, nonperturbative corrections that are specific to the cavity geometry we consider. The resonant three-body loss process we study is only present in the U_3 term.

In contrast to the two-body problem [17], the three-body Rydberg polariton problem cannot be reduced to a single scalar equation – even in the perturbative expansion in r_b/L. Inspired by the seminal work of Faddeev on three-body quantum systems [51], we take the Faddeev equation approach to solving the Schrödinger equation. An indispensable advantage in the present case is that the Faddeev equations can be expressed entirely in terms of Rydberg spin-wave correlation functions, which simplifies the theoretical treatment of the multi-component nature of DSPs. In this formalism, the three-body problem can be recast as an infinite series of two-body interactions. All scattering processes are grouped depending on which pair of particles interacts first. Crucially, the T-matrix separates into the sum $\hat{T}_3(\omega) = \frac{1}{3}\sum_{i<j}\hat{T}_3^{ij}(\omega, \epsilon_k)$, where $\hat{T}_3^{ij}(\omega, \epsilon_k)$ denotes the T-matrix for scattering where particles i, j interact first and the third particle $k \neq i, j$ has incoming energy ϵ_k. Similarly to the two-body case, we consider just the sss-component $\hat{T}_3$ of the full three-body T-matrix $\hat{\boldsymbol{T}}_{\mathbf{3}}$. The equation for $\hat{T}_3^{12}(\omega, \epsilon)$, when all outgoing states are DSPs, is

$$\begin{aligned}\hat{T}_3^{12}(\omega,\epsilon) &= \hat{T}_2^{12}(\omega-\epsilon)\hat{g}_s(\omega)[\hat{T}_2^{23}(\omega)+\hat{T}_2^{13}(\omega)]+ \\ &\int d\tilde{\epsilon}\,\hat{T}_2^{12}(\omega-\epsilon)\hat{g}_s(\tilde{\epsilon})\hat{g}_s(\omega-\epsilon-\tilde{\epsilon})[\hat{T}_3^{23}(\omega,\tilde{\epsilon})+\hat{T}_3^{13}(\omega,\tilde{\epsilon})],\end{aligned} \tag{3.17}$$

where $\hat{T}_2^{ij}$ describes the two-body scattering of particles labeled i, j. The Rydberg-component propagator $\hat{g}_s$ is a complex object that involves contributions from differ-

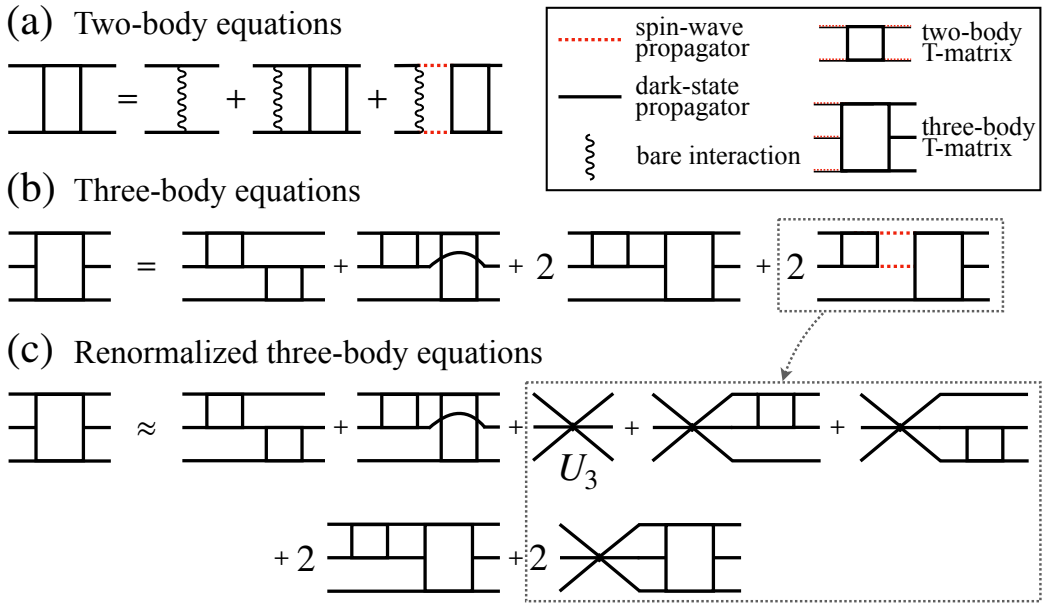

Figure 3.2: (a) Diagrammatic representation (see inset for legend) of the Lippmann-Schwinger equation for the scattering of two dark-state polaritons. Processes with only one spin wave are forbidden by momentum conservation. (b) Schematic representation of Faddeev equations for the three-body T-matrix $T_3^{12}(\omega)$, where particles 1 and 2 interact first. (c) Truncation of the three-body equations (b) to second order in r_b/L allows us to express the spin-wave contribution using an effective three-body potential U_3 between DSPs.

ent spin-wave branches and the DSP mode. Note that the simple form of Eq. (3.17) is thanks to the use of abstract operators. The representation in e.g. a coordinate basis is more involved, as we show in the following subsection.

To derive an effective DSP theory, we separate spin-wave and DSP components in $\hat{g}_s$, which will allow us to perform the expansion in r_b/L. The equation for the T-matrix describing DSP-to-DSP scattering $\hat{T}_3(\omega) \equiv \hat{T}_3^{12}(\omega, 0)$ is represented diagrammatically in Fig. 3.2(b), where we explicitly showed separated spin-wave (red) and DSP (black) propagators. Next, we restrict both sides of Eq. (3.17) to the second order in r_b/L. For this purpose, we keep only those terms where either the sum over a macroscopic number of spin waves is present or the all-dark intermediate state arises. Finally, we rewrite the original Faddeev equations in an approximate form shown in

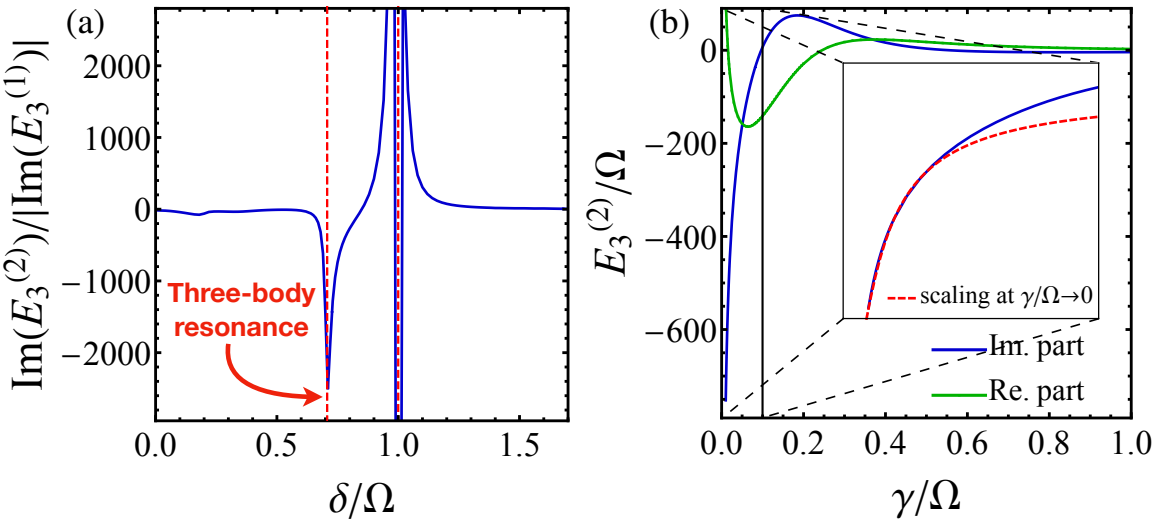

Figure 3.3: (a) Ratio of imaginary parts of $E_3^{(2)}$ and $E_3^{(1)}$ at $\gamma/\Omega = 0.01$. Near $\delta/\Omega = 1/\sqrt{2}$, we observe enhancement caused by a three-body resonance. $\delta = \Omega$ is a singular point where $r_b \to 0$. (b) Real and imaginary parts of $E_3^{(2)}$ as a function of γ/Ω at $\delta/\Omega = 1/\sqrt{2}$. (inset) Our numerical results (blue) agree with analytical scaling arguments (dashed red) suggesting that the ratio $\mathrm{Im}(E_3^{(2)})/\mathrm{Re}(E_3^{(2)})$ diverges as Ω/γ in the limit $\gamma/\Omega \to 0$.

Fig. 3.2(c) – without any spin-wave degrees of freedom. We provide the full set of equations in the following subsection.

In Fig. 3.3(a), we characterize the strength of three-body loss using the ratio of the expansion coefficients $\mathrm{Im}(E_3^{(2)})/\mathrm{Im}(E_3^{(1)})$. The denominator $\mathrm{Im}(E_3^{(1)})$ from Eq. (3.16) contains contributions to three-body loss from disconnected two-body processes only. We see the expected enhancement at the resonance condition $\delta = \Omega/\sqrt{2}$. There is an additional resonant feature at $\delta = \Omega$ that arises because of a two-body interference effect whereby χ vanishes and, therefore, r_b goes to zero. This leads to an overall enhancement of both two and three-body interaction effects. In contrast, for the three-body resonance condition $\delta = \Omega/\sqrt{2}$, there are no resonant features that appear in the two-body problem. Therefore, we interpret the enhancement of the three-body loss observed at this point as a genuinely three-body effect.

In Fig. 3.3(b), we show the dependence of $E_3^{(2)}$ on the decay rate γ at the resonance

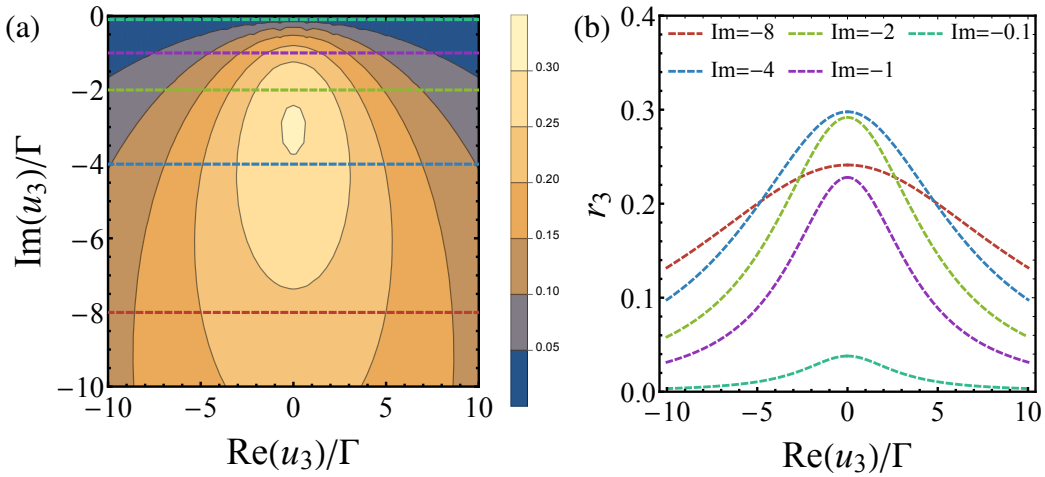

Figure 3.4: (a-b) Three-body loss parameter r_3 in units of Γ^{-2} as a function of real and imaginary part of u_3/Γ for the case of $u_2 = 0$, which corresponds to negligible two-body correlations in the microscopic model. The five curves in (b) correspond to the five values of Im(u_3) indicated by the horizontal lines in (a).

condition $\delta = \Omega/\sqrt{2}$. We find a divergence as $\gamma/\Omega \to 0$ (see inset) indicating that the enhancement factor for three-body loss can be made arbitrarily large. This behavior is in agreement with analytical scaling arguments that predict $\mathrm{Im}(E_3^{(2)}) \sim 1/\gamma$, which stems from the fact that, for finite γ, we have $\mathrm{Im}(2\epsilon_- + \epsilon_+) \sim \gamma$. We note, however, that our calculations only apply when the perturbative expansion in Eq. (3.16) is valid. As a result, we cannot definitively say whether the three-body loss dominates over two-body loss for finite r_b/L because we have not obtained any bounds on higher order terms in the expansion.

This enhancement is independent of the details of the photonic mode geometry [89]; therefore, we interpret it as a universal effect for Rydberg polariton systems that provides a promising path to the realization of physical systems driven by three-body interactions. Recently, we experimentally studied an enhanced three-body loss feature in free-space that occurs in a similar parameter regime $\Omega \sim \delta$, but has a richer physical origin [79].

3.4.2 Details of the three-body calculation

In this section, we provide more details on the calculations of the scattering of three dark-state polaritons. Schematic representation of the key equations is presented in Fig. 3.2(b-c).

As in the two-body case, the influence of the interaction on the physics of the three-body problem is captured by the analytical structure of the T-matrix $\boldsymbol{T_3}$. Specifically, the energy shift corresponds to the pole of the integrated T-matrix $T_3(\omega)$.

To calculate this object, one can in principle employ the Schrödinger equation. However, such a treatment can lead to spurious, nonphysical solutions. In order to avoid this issue, another approach to the quantum three-body problem was developed by Faddeev [51]. In this formulation, all scattering processes are grouped depending on which two particles interact first. This way one introduces a rigorous method for expressing the three-body scattering as a series of two-body processes (a three-body force can also be included). As a consequence, the three-body T-matrix can now be written as a sum of three (sub)T-matrices

$$\hat{T}_3(\omega) = \frac{1}{3}\sum_{i<j} \hat{T}_3^{ij}(\omega, \epsilon_k), \tag{3.18}$$

where $\hat{T}_3^{ij}(\omega; \epsilon_k)$ denotes the T-matrix for the group of processes, where particles labeled i and j interacted first and the third particle $k \neq i, j$ has energy ϵ_k. These $\hat{T}_3^{ij}(\omega, \epsilon_k)$ objects are coupled to each other by the set of equations called Faddeev equations. In our case, the situation is further complicated by the multi-component nature of the polariton system. Let us define $\hat{T}_3^{ij}(\omega) \equiv \hat{T}_3^{ij}(\omega; 0)$ and $\hat{T}_\mu^{ij}(\omega) \equiv \hat{T}_3^{ij}(\omega; \epsilon_{\mu=\pm})$.

Every T-matrix we consider has all three outgoing DSPs. In our system, exact

Faddeev equations [51] describing the off-shell scattering of three zero-momentum DSPs are

$$T_3^{12}(\omega) = T_2(\omega)\frac{2}{\omega + i0^+}T_2(\omega) + T_2(\omega)\frac{1}{\omega + i0^+}\left(T_3^{13}(\omega) + T_3^{23}(\omega)\right) + \sum_{\mu=\pm}\int \frac{dr_{12}}{L}\frac{dr_3}{L}T_2(\omega; r_{12})\,\alpha_\mu\eta_\mu\left(T_\mu^{13}(\omega;\vec{x}) + T_\mu^{23}(\omega;\vec{x})\right) - T_2(\omega)\,\alpha_\mu\eta_\mu\left(T_\mu^{13}(\omega) + T_\mu^{23}(\omega)\right) \tag{3.19}$$

and the two analogous equations for $T_3^{13}(\omega)$ and $T_3^{23}(\omega)$ obtained through permutation of indices. Here $T_\mu^{ij}(\omega;\vec{x}) = \int \frac{d\vec{x}'}{L^3}\frac{dR}{L}T_\mu^{ij}(\omega;\vec{x},\vec{x}')$ is the T-matrix for the process with the third incoming leg being a spin wave belonging to the branch μ. Variable r_{12} denotes the distance between particles labeled 1 and 2, $r_3 = (x_1 + x_2)/2 - x_3$ is the standard third Jacobi coordinate, and $\eta_\mu = \eta(\omega - \epsilon_\mu)$.

Eq. (3.19) is a direct implementation of the operator equation [Eq. (3.17)] from Section 3.4.1. Here, we explicitly separated spin-wave and DSP terms of $\hat{g}_s$ as in Eq. (3.7) and then performed the $\tilde{\epsilon}$ integration with the enforcement of momentum invariance. Note that, in contrast to the two-body problem, here we do not obtain an effective few-body propagator as $\chi(\omega)$, since the three-body T-matrix depends on the energy of the third particle and prevents such grouping.

Now we introduce our main approximation, which allows us to write a self-consistent system of equations to the lowest non-trivial order in r_b/L. For this purpose, we keep only those terms where either the sum over a macroscopic number of spin waves is present or the all-dark intermediate state arises. The sum over a macroscopic number of spin waves introduces a factor of $L\,\delta(x)$, while the all-dark-state propagator contributes $(\omega + i0^+)^{-1}$, which is of order L/r_b because the energy shift satisfies $\omega \sim r_b/L$. In comparison, all other terms are negligible in the limit of vanishing r_b/L, as they are of order ~ 1 or smaller. The key consequence of these

rules is as follows: $\{T_3\} = 1$ and $\{T_\mu\} = 2$, where $\{X\}$ denotes the leading order of X in r_b/L. Finally, the two-body term $\{T_2\} = 1$, which follows directly from Eq. (3.15).

For clarity, we will omit terms that arise from higher-order corrections to the g_s propagator (such as the last term in Eq. (3.19)) as they do not contribute to our lowest-order solution. We note that, in general, the T_2 matrix depends on the total momentum of two particles K, but in all our equations we can either truncate it to U_2, or it arises in a situation (outer T_2 contributions) where $K = 0$.

In order to close the system of equations, we need to calculate T_μ^{ij}, which is described by another set of Faddeev equations expanded to leading order in r_b/L

$$T_\mu^{12}(\omega,\vec{x}) = \sum_{b\neq(12)(3)} \left[U_2^\mu(x_1-x_2)\eta_\mu\, T_2(\omega; x_{b_1}-x_{b_2}) + \sum_{\nu=\pm} \alpha_\nu\, U_2^\mu(x_1-x_2)\eta_{\mu\nu} T_\nu^{b_1 b_2}(\omega;\vec{x}) \right] + \sum_{b\neq(12)(3)} U_2^\mu(x_1-x_2)\eta_\mu\, T_2(\omega; x_{b_1}-x_{b_2}) \frac{1}{\omega+i0^+} \left[2\,T_2(\omega) + \sum_{c\neq(b_1b_2)(b_3)} T_3^{c_1c_2}(\omega) \right], \tag{3.20}$$

where $U_2^\mu(x) \equiv U_2(\omega-\epsilon_\mu; x)$ and $\eta_{\mu\nu} = \eta(\omega-\epsilon_\mu-\epsilon_\nu)$. It is easier to first calculate $\tilde{T}_\mu^{12}$, where the tilde denotes that it is a T-matrix where the intermediate DSPs come only from nonperturbative corrections to T_2. This is given by

$$\tilde{T}_\mu^{12}(\omega,\vec{x}) = \sum_{b\neq(12)(3)} \left[U_2^\mu(x_1-x_2)\eta_\mu\, T_2(x_{b_1}-x_{b_2}) + \sum_{\nu=\pm} \alpha_\nu\, U_2^\mu(x_1-x_2)\eta_{\mu\nu} \tilde{T}_\nu^{b_1 b_2}(\omega;\vec{x}) \right] \tag{3.21}$$

and is related to Eq. (3.20) by

$$T_\mu^{12}(\omega;\vec{x}) = \tilde{T}_\mu^{12}(\omega;\vec{x}) + \tilde{T}_\mu^{12}(\omega;\vec{x}) \frac{1}{\omega+i0^+} \left(T_3^{13}(\omega) + T_3^{23}(\omega) + 2\,T_2(\omega) \right). \tag{3.22}$$

This solution can be verified by inserting Eqs. (3.21) and (3.22) into Eq. (3.20) and

seeing that everything cancels out (we also use $T_3^{ij}(\omega) = T_3^{kl}(\omega)$ for any $i \neq j$, $k \neq l$). The system of algebraic equation in Eq. (3.21) can be solved analytically. Inserting this result into Eq. (3.19) and summing over all pairs i, j gives the renormalized system of equations for the dark-state T-matrix

$$\begin{aligned} T_3(\omega) = T_2(\omega)\frac{2}{\omega + i0^+}T_2(\omega) + T_2(\omega)\frac{2}{\omega + i0^+}T_3(\omega) + \Phi^2\, U_3(\omega) \\ + \Phi^2\, U_3(\omega)\frac{2}{\omega + i0^+}\left[T_3(\omega) + T_2(\omega)\right] + \mathcal{O}(r_b^3/L^3), \end{aligned} \tag{3.23}$$

where $\Phi = T_2(\omega)/U_2(\omega)$ is the non-perturbative correction. The effective three-body potential $U_3(\omega)$ can be concisely written as

$$U_3(\omega) = \int \frac{dx}{L}\frac{dy}{L} \sum_{\mu=\pm} 2\, U_2(\omega; x-y)\, \eta_\mu \alpha_\mu\, \widehat{T}_\mu^{12}(\omega; x, y), \tag{3.24}$$

which was possible due to symmetries with respect to the relabeling of particles and coordinates. Variables $x = x_1 - x_2$ and $y = x_3 - x_2$ describe relative distances of pairs of particles and $\widehat{T}_\mu^{12}(\omega; x, y) = \tilde{T}_\mu^{12}(\omega; x, y)/\Phi$ is governed by Eq. (3.21) with $T_2 \to U_2$. The function $U_3(\omega)$ can be intuitively understood as an effective three-body potential, with direct analogy to $U_2(\omega)$ in the two-body scenario.

Solving Eq. (3.23) for $T_3(\omega)$, we get

$$T_3(\omega) = \frac{2T_2(\omega)^2 + (\omega + 2T_2(\omega))\, U_3/(1 - U_2[1 - \chi(\omega)\,\omega])^2}{\omega - 2\left(T_2(\omega) + U_3(\omega)/(1 - U_2(\omega)[1 - \chi(\omega)\,\omega])^2\right)}, \tag{3.25}$$

Its pole gives the equation for the three-body energy shift:

$$\delta E_3 = 3U_2(\delta E_3) + 3U_3(\delta E_3) - \chi(0) U_2(\delta E_3)\, \delta E_3 + \mathcal{O}(r_b^3/L^3). \tag{3.26}$$

To obtain a self-consistent solution, we must expand both sides to the appropriate

order in r_b/L. For this purpose, we analyze the order of each constituent:

$$\{\delta E_3\} = 1, \qquad \{U_2\} = 1, \qquad \{U_3\} = 2, \qquad \{\chi(0)\} = 0. \tag{3.27}$$

This allows us to write the final solution

$$\delta E_3 = \underbrace{3U_2}_{\mathcal{O}(r_b/L)} + \underbrace{3U_3 + 3U_2\,(3U_2' - \chi\,U_2)}_{\mathcal{O}(r_b^2/L^2)} + \mathcal{O}(r_b^3/L^3), \tag{3.28}$$

where $U_2' = dU_2/d\omega$ and all functions are evaluated at $\omega = 0$. Notice that the multi-branch character of the problem is contained in U_3 and in the more complicated form of χ compared to the regime $\Omega \ll |\delta|$.

3.5 Experimental probing

In order to relate our microscopic description to experimentally measurable quantities, we now study the transmission through our cavity system. We use a low-energy model for the transmission where the only excitations in the cavity coupled to the waveguide are the DSPs. The effective Hamiltonian for the cavity-DSPs is

$$H = -i(\Gamma + \kappa)b^\dagger b + u_2(b^\dagger)^2 b^2 + u_3(b^\dagger)^3 b^3, \tag{3.29}$$

where $b^\dagger$ is a bosonic creation operator for the DSPs, 2Γ is the decay rate of DSPs from the cavity into the waveguide, 2κ is the decay rate to other modes, and the coefficients u_2, u_3 are related to energy shifts $\delta E_2,\ \delta E_3$, calculated as described above from the full microscopic theory, through $u_2 = \delta E_2$ and $u_3 = \delta E_3 - 3\,\delta E_2$. For simplicity, we focus on the limit where three-body effects dominate over two-body phenomena by taking $u_2 = 0$ in Eq. (3.29). We use a measure of three-body loss that is appropriate

when all decay is into the waveguide ($\kappa = 0$) and when two-body interactions u_2 are zero or negligibly small $r_3 = \int d\tau_1 d\tau_2 \, [1 - g^{(3)}(\tau_1, \tau_2)]$, where $g^{(3)}(\tau_1, \tau_2)$ is the three-photon correlation function at the output of the waveguide and where $\tau_{1,2}$ are relative coordinates. The r_3 parameter measures the probability that three-photons are lost from the pulse due to the interactions. We can analytically compute r_3 for this transmission problem as detailed in the following subsection. We have also extended these calculations to account for arbitrary κ, u_2, and u_3 [166]. In Fig. 3.4(a), we show a contour plot of r_3 as a function of the real and imaginary parts of the three-body interaction u_3. Interestingly, r_3 does not increase arbitrarily as the three-body loss rate is increased, but instead has a maximum value at $\mathrm{Im}(u_3) \sim \Gamma$ [see Fig. 3.4(b)]. The appearance of a maximum in r_3 is attributable to a type of quantum Zeno effect, whereby too large a value of three-body loss blocks the photons from entering the cavity, reducing the overall amount of loss in the system.

3.5.1 Transmission calculations

In the following, we present the model describing the transmission of photons in a chiral waveguide coupled to a single-mode cavity described by Eq. (3.29). We analytically calculate the three-body loss parameter r_3 in the case when $u_2 = \kappa = 0$, which corresponds to the situation where three-body effects dominate. The results presented in this section are used to obtain Fig. 3.4(a-b).

The whole system is described by the transmission Hamiltonian

$$H_{\mathrm{tr}} = \int_{-\infty}^{+\infty} dk \, k \, C^\dagger(k) C(k) + \int_{-\infty}^{+\infty} dk \, \sqrt{2\pi} g \left(b^\dagger C(k) + C^\dagger(k) b \right) + u_3 \, (b^\dagger)^3 b^3,$$

where the first term describes the Hamiltonian of the photons in the chiral waveguide. $C^\dagger(k)$ and $C(k)$ are creation and annihilation operators of chiral photons at momen-

tum k, respectively. Speed of light is set to unity ($c = 1$). The second term describes the quadratic coupling between photons in the waveguide and the cavity, where $b^\dagger$ (b) creates (destroys) a cavity photon. The last term describes the three-body nonlinear interactions of cavity photons.

To compute few-photon scattering, it is convenient to partition the Hamiltonian into the quadratic part H_0 and the nonlinear interactions:

$$\begin{aligned} H_{\rm tr} &\equiv H_0 + U, \\ H_0 &= \int_{-\infty}^{+\infty} dk\, k\, C^\dagger(k) C(k) + \int_{-\infty}^{+\infty} dk\, \sqrt{2\pi} g \left(b^\dagger C(k) + C^\dagger(k) b \right), \\ U &= u_3\, (b^\dagger)^3 (b)^3. \end{aligned}$$

The quadratic part H_0 of the Hamiltonian $H_{\rm tr}$ can be diagonalized into the scattering eigenstates:

$$\begin{aligned} H_0 &= \int_{-\infty}^{+\infty} dk\, k \psi_k^\dagger \psi_k, \\ \psi_k^\dagger &= e_k b^\dagger + \int_{-\infty}^{+\infty} dk'\, \psi_k(k') C^\dagger(k), \end{aligned}$$

where $e_k = \frac{1}{\sqrt{2\pi}} \frac{g}{k + i\kappa + i\Gamma}$ and $[\psi_k, \psi_{k'}^\dagger] = \delta(k - k')$. $\{\psi_k^\dagger | k \in (-\infty, +\infty)\}$ form a complete basis of the Hilbert space, which we refer to as the dressed-photon basis. Let $\psi_k(z)$ be the Fourier transform of $\psi_k(k')$ in the coordinate space. The asymptotic behavior of $\psi_k(z)$ gives the single-photon transmission coefficient

$$t_k = \frac{\lim_{z \to +\infty} \psi_k(z)}{\lim_{z \to -\infty} \psi_k(z)} = \frac{k - i\Gamma}{k + i\Gamma}. \tag{3.30}$$

The nonlinear interaction U can also be expressed in the dressed photon basis:

$$U = \int d\vec{k} d\vec{k'}\ U(\vec{k}, \vec{k'}) \psi^\dagger_{k'_1} \psi^\dagger_{k'_2} \psi^\dagger_{k'_3} \psi_{k_1} \psi_{k_2} \psi_{k_3}, \tag{3.31}$$

$$U(\vec{k}, \vec{k'}) = e^*_{\vec{k'}} e_{\vec{k}} u_3, \tag{3.32}$$

where we have used the definitions $\vec{k} = (k_1, k_2, k_3)$ and $e_{\vec{k}} = e_{k_1} e_{k_2} e_{k_3}$. Note that, in the dressed-photon basis, $U(\vec{k}, \vec{k'})$ is expressed as the product of separable functions of the incoming and outgoing momenta. We will use this feature to introduce a simple ansatz for the three-body dressed-photon T-matrix, which is a solution to the Lippmann-Schwinger equation:

$$T^{(3)}(\omega, \vec{k}, \vec{k'}) = U(\vec{k}, \vec{k'}) + \int_{-\infty}^{+\infty} d\vec{k''} \frac{U(\vec{k}, \vec{k''})}{\omega - k} T^{(3)}(\omega, \vec{k}, \vec{k''}). \tag{3.33}$$

Proposing an ansatz $T^{(3)}(\omega, \vec{k}, \vec{k'}) = \bar{T}(\omega) e^*_{\vec{k'}} e_{\vec{k}}$ and inserting it into Eq. (3.33), we find

$$\bar{T}(\omega) = \frac{1}{\frac{1}{u_3} - \frac{1}{\omega + 3i\Gamma}}, \tag{3.34}$$

where we have assumed that $\mathrm{Im}[\omega] > 0$.

Hence we obtain the three-photon S-matrix for the dressed photons:

$$S^{(3)}(\vec{k}, \vec{k'}) = \delta(\vec{k} - \vec{k'}) - 2\pi i \delta(K - K') T^{(3)}(K + i0, \vec{k}, \vec{k'}), \tag{3.35}$$

which represents the transmission amplitude of incoming dressed photons with energy $\vec{k} = (k_1, k_2, k_3)$ scattered into outgoing dressed photons with energy $\vec{k'} = (k'_1, k'_2, k'_3)$. K and K' are the total momenta/energies of the incoming and outgoing photons: $K = k_1 + k_2 + k_3$, $K' = k'_1 + k'_2 + k'_3$. Note that the S-matrix $S^{(3)}_0$ for free photons (as opposed to dressed photons) is more relevant for direct experimental measurements and can

be obtained from the dressed-photon S-matrix $S^{(3)}$ using single-photon transmission coefficients: $S_0^{(3)}(\vec{k},\vec{k'}) = t_{k'_1} t_{k'_2} t_{k'_3} S^{(3)}(\vec{k},\vec{k'})$.

Next, we calculate r_3. It represents a good measure of three-body loss in the case of zero one- and two-body losses:

$$r_3 = \int_{-\infty}^{+\infty} d\tau_1 d\tau_2 \, [1 - g^{(3)}(\tau_1, \tau_2)]. \tag{3.36}$$

$g^{(3)}(\tau_1, \tau_2)$ is the three-photon correlation function at the output of the waveguide, where $\tau_1 = t_2 - t_3, \tau_2 = t_1 - t_3$ are the time differences between the photon number measurements at times $t_{1,2,3}$. For a weak and continuous coherent-state input with photon momentum k, $g^{(3)}(\tau_1, \tau_2)$ is related to the output three-photon wavefunction $\psi^{(3)}(z_1 = t_1, z_2 = t_2, z_3 = t_3)$ in the dressed-photon basis, which is the Fourier transform of $S^{(3)}(\vec{k} = (k,k,k), \vec{k'})$ with respect to the output momenta $\vec{k'}$.

Defining $R = (z_1 + z_2 + z_3)/3$ as the center of mass coordinate, we have

$$\psi^{(3)}(z_1, z_2, R) = \exp(3ikR)(1 - \phi^{(3)}(z_1, z_2)), \tag{3.37}$$

where $\phi^{(3)}(z_1, z_2)$ is the Fourier transform of $y(k'_1, k'_2) = 2\pi i T^{(3)}(3k + i0, \vec{k}, k'_1, k'_2, k'_3 = 3k - k'_1 - k'_2)$ with respect to k'_1, k'_2. $g^{(3)}(\tau_1, \tau_2)$ is then given by

$$g^{(3)}(\tau_1, \tau_2) = |\psi^{(3)}(z_1, z_2, R)|^2 = |1 - \phi^{(3)}(z_1, z_2)|^2, \tag{3.38}$$

where $z_1 = -\frac{1}{3}\tau_1 + \frac{2}{3}\tau_2$, $z_2 = \frac{2}{3}\tau_1 - \frac{1}{3}\tau_2$. Hence r_3 defined in Eq. (3.36) can be

calculated as follows:

$$r_3 = \int_{-\infty}^{+\infty} dz_1 dz_2 \; [1 - |1 - \phi^{(3)}(z_1, z_2)|^2] \tag{3.39}$$

$$= \int_{-\infty}^{+\infty} dz_1 dz_2 \; 2\mathrm{Re}[\phi^{(3)}(z_1, z_2)] - |\phi^{(3)}(z_1, z_2)|^2 \tag{3.40}$$

$$= 2\mathrm{Re}[y(k_1' = k, k_2' = k)] - \int_{-\infty}^{+\infty} dk_1' dk_2' |y(k_1', k_2')|^2 \tag{3.41}$$

$$= 4\pi \left(\frac{\Gamma}{\pi} \frac{1}{k^2 + \Gamma^2} \right)^3 \frac{\mathrm{Im}[-\frac{1}{u_3^*}]}{\left| \frac{1}{u_3} - \frac{1}{3k + 3i\Gamma} \right|^2} \geq 0. \tag{3.42}$$

We comment that the calculation of r_3 presented here for $\kappa = u_2 = 0$ is a special case of a general calculation applicable to arbitrary values of κ, u_2 and presented in an upcoming work on cavity transmission [166].

3.6 Outlook

In this chapter, we showed the existence of a parameter regime for Rydberg polaritons where three-body loss can be resonantly enhanced. We focused on dissipative dynamics because, for currently accessible experimental parameters [38, 86, 133, 143], the dissipative interactions can be strongly enhanced by working close to the resonance. Through further experimental improvements and by tuning slightly away from the resonance, one could also operate in a regime of enhanced dispersive three-body interactions. We would like to stress that although our results are based on a perturbative expansion, this does not mean the interactions are weak. On the contrary, the asymptotic expansion in r_b/L means that our results hold for arbitrary optical depths and can give rise to strong effects on the correlations between a few photons [115]. To efficiently study the many-body regime in quasi-1D geometries, one can apply matrix-product-state methods [21, 110]. The extension of the presented work to free

space is another important direction to explore. Our work demonstrates the possibilities offered by Rydberg-EIT to tune the properties of multi-body interactions. This motivates further exploration of possible interactions, which might give rise to different exotic phases of matter [22, 70].

Chapter 4: Universal scattering with general dispersion relations

Work in this chapter was published in Ref. [167].

4.1 Introduction

The quantum mechanical scattering of few-body systems remains a challenging theoretical problem. Even at low incoming energies, nonperturbative effects render a general solution out of reach. A common workaround is based on effective field theory whereby low-energy scattering is described in terms of a few parameters such as the scattering length a and the effective range r_0 [15, 24, 25]. When $a \gg r_0$, the system is in the unitarity limit where the universal physics of Efimov states [24, 25, 49] and unitary Fermi gases [116, 117, 153] can emerge. Another approach where general results can be obtained is by studying the analytic structure of the S-matrix at low energies. One striking result in this context is the simple effect of dimensionality on scattering theory.

Two particles with short-range interactions perfectly reflect off each other at the threshold in one dimension (1D), while they transmit without seeing each other in higher dimensions. This effect arises because the density of states diverges at the threshold as $1/\sqrt{E}$ in 1D, but stays finite in higher dimensions.

Recent experimental progress in synthetic quantum matter allows for broad control of dispersion relations. One class of such systems consists of tunable periodic

structures, including photonic crystal waveguides [62, 63, 76, 80, 87, 103, 170], twisted bilayer graphene [32, 151], superconducting qubit arrays [44, 149, 160], atomic arrays [11, 50, 107], and trapped-ion spin chains [43, 126]. Another class is polaritonic [8, 92] or spin-orbit coupled [29, 100] systems, where the dispersion relation can be tuned *in situ* by external fields [54, 55, 109, 122]. In principle, the density of states at the scattering threshold can be tuned to diverge faster than it does for quadratic dispersion relations. This opens up the door to studying the implications of a more general density of states without changing the dimension of the system. Recently, there is a growing interest in the study of general dispersion relations in condensed matter systems, where divergent electronic density of states is referred to as a high-order Van Hove singularity [82, 173, 174]. In particular, power-law-divergent density of states near the Fermi level leads to nontrivial metallic states termed supermetals [174].

In this chapter, we explore the physics of divergent density of states from the perspective of scattering theory. We illustrate that, when a particle has a divergent density of states at a certain energy, its scattering matrix has a nontrivial universal limit that depends on the rate of the divergence. In particular, we study single-particle scattering of many WQED systems in 1D with a dispersion relation $\epsilon(k) = \pm|d|k^m$, where $m \geq 2$ is an integer. Notably, these WQED models describe the low-energy scattering in many synthetic quantum matter experiments with tunable dispersion relations. We discover that the S-matrix can take different universal limits $\lim_{E\to 0} S(E)$ for different values of m. The total reflection at the threshold for a quadratic dispersion relation is an example of such universal behavior corresponding to $m = 2$. In general, there may be multiple classes of universal behaviors in the S-matrix corresponding to each m, depending on the properties of interactions at $k = 0$. In this chapter, we consider a physically natural class of interactions and characterize the universal behavior for each m. We also extend a key index theorem

in scattering theory known as Levinson's theorem—which relates the scattering phases to the number of bound states [6, 12, 45, 46, 81, 84, 95, 105, 106, 125, 169]—to the class of models considered in this chapter with these more general dispersion relations. Although we focus on photon-emitter interactions in 1D, we expect our methodology to readily generalize to higher dimensions and other types of interactions, e.g. two-body interacting systems or spin-boson models.

4.2 Emitter scattering

In many synthetic quantum systems, particles propagating in a 1D channel are scattered by emitters such as atoms, quantum dots, or superconducting qubits. The emitters are often coupled to the environment, which adds dissipation to the system composed of the emitters and the 1D channel. Since we are interested in the scattering processes with a single photon coming in and a single photon going out, it suffices to use a non-Hermitian effective quadratic Hamiltonian

$$H = H_0 + V, \tag{4.1}$$

$$H_0 = \int_{-\infty}^{+\infty} dk\ \epsilon(k) C^\dagger(k) C(k) + \sum_{i,j=1}^{N} K_{ij}^R b_i^\dagger b_j, \tag{4.2}$$

$$V = \int_{-\infty}^{+\infty} dk \left[\sum_{i=1}^{N} V_i(k) C(k) b_i^\dagger + \text{h.c} \right], \tag{4.3}$$

where the bare Hamiltonian H_0 consists of the freely propagating particles, while the interacting emitters are indexed by $i = 1, 2, \ldots N$. V describes the quadratic interaction between the particles and the emitters. Since we are discussing single-particle scattering with bounded-strength interactions, only local spectral properties of the dispersion relation matter, and our results are insensitive to the detailed behavior

of the dispersion far away from the threshold energy. In this chapter, we focus on the dispersion relation $\epsilon(k) = \sigma|d|k^m$, where $\sigma = \pm 1$, $|d|$ is a positive constant, and $m \geq 2$ is an integer. When $\sigma = \pm 1$ and m is even, $\epsilon(k)$ can be understood as the lowest-order approximation of a dispersion relation around its local minima/maxima, after a change of reference points for both energy and momentum. Depending on whether we are considering bosons scattered by bosonic emitters or fermions scattered by fermionic emitters, we have either commutation or anti-commutation relations: $[C(k), C^\dagger(k')]_\pm = \delta(k - k'), [b_i, b_j^\dagger]_\pm = \delta_{ij}$. K_{ij}^R represents the matrix element of the $N \times N$ matrix $\boldsymbol{K}^R$; $\boldsymbol{K}^R$ is the only non-Hermitian term in the Hamiltonian: the Hermitian $\boldsymbol{A}$ and anti-Hermitian $i\boldsymbol{B}$ components of $\boldsymbol{K}^R = \boldsymbol{A} + i\boldsymbol{B}$ represent, respectively, the coherent and incoherent interactions among the emitters. $\boldsymbol{K}^R$ is dissipative when $\boldsymbol{B}$ is non-positive and nonzero.

For convenience, we introduce a vector function $|v_k\rangle = [V_1(k), \ldots, V_N(k)]^T$, with corresponding basis states given by the emitter excitations $\{b_1^\dagger |0, g\rangle, \ldots, b_N^\dagger |0, g\rangle\}$, where $|0, g\rangle$ is the ground state with zero excitation. In the most generic scenario, $V_i(k)$ for different emitters are independent of each other. Here, we consider the case where $|v_k\rangle$ can be written as $|v_k\rangle = V(k)|u\rangle$. We further assume $V(k)$ is continuous at 0 and $V(0) \neq 0$. Under this constraint, the only relevant vector around $k = 0$ is $|u\rangle$, and effectively, there is only a single relevant "degree of freedom" in the emitter vector space at $k = 0$. We then show that the zero-energy scattering behavior for multiple emitters can be reduced to the behavior for $N = 1$. As a result, we are able to obtain a complete classification of the universal low-energy scattering behavior in these models.

4.3 Universal scattering

4.3.1 Overview of results

We start with a discussion that applies to the case of general $|v_k\rangle$. The S-matrix for a single particle is defined through the incoming and outgoing scattering eigenstates $|\psi_k^{\pm}\rangle$, where the superscript $\pm$ specifies the boundary conditions of the scattering states. The S-matrix element from one single-particle scattering state k to another k' is $\mathcal{S}(k,k') = \langle\psi_{k'}^{-}|\psi_k^{+}\rangle$. To explain the universal behavior of the S-matrix, it is useful to write down its relation to the on-shell T-matrix:

$$\mathcal{S}(k,k') = \delta(k-k') - 2\pi i\delta(\epsilon(k)-\epsilon(k'))T(E+i0^+,k,k'), \tag{4.4}$$

where $0^+/0^-$ represents an infinitesimal positive/negative real number and $E=\epsilon(k)$. For dispersion relation $\epsilon(k)=\sigma|d|k^m$ with even m, there are two degenerate momenta $k_1(E), k_2(E)$ corresponding to any energy $E>0$ ($E<0$) for $\sigma=+1$ ($\sigma=-1$). We can define a 2×2 matrix $\boldsymbol{S}(E)$ by picking out the scattering amplitudes between degenerate momenta:

$$S_{\alpha\beta}(E) = \delta_{\alpha\beta} - 2\pi i\,\frac{T[E+i0^+,k_\alpha(E),k_\beta(E)]}{\sqrt{|\epsilon'(k_\alpha(E))\epsilon'(k_\beta(E))|}}, \tag{4.5}$$

where $\alpha,\beta\in\{1,2\}$ and the prefactor $|\epsilon'(k_\alpha(E))\epsilon'(k_\beta(E))|^{-1/2}$ comes from $\delta(\epsilon(k)-\epsilon(k'))$ in Eq. (4.4). When m is odd, we can define $\boldsymbol{S}(E)=S(E)$ as a single complex number, given by Eq. (4.5) when $k_\alpha(E)=k_\beta(E)=k(E)$ is the momentum corresponding to energy E. If the Hamiltonian is Hermitian, $S(E)$ is unitary.

In 1D scattering, the matrix $\boldsymbol{S}(E)$ directly describes the transmission and reflection between degenerate momenta and is often used instead of the function $\mathcal{S}(k,k')$

with divergences. When $E \to 0$, $|\epsilon'(k_\alpha(E))\epsilon'(k_\beta(E))|^{-1/2}$ diverges. Since $|S_{\alpha\beta}(E)| \leq 1$, $T(E+i0, k_\alpha, k_\beta)$ in Eq. (4.5) must approach zero to cancel the divergence, which is the key behind the universal behavior of $\boldsymbol{S}(E)$.

To proceed further, we note that the Lippmann-Schwinger equations for this emitter scattering model have a simple analytic structure. As a result, we can write down the single-particle T-matrix $T(\omega, k, k')$ in terms of the Green's function of the emitters $\boldsymbol{G}(\omega)$, which is a finite-dimensional matrix [148]:

$$T(\omega, k, k') = \langle v_{k'}|\boldsymbol{G}(\omega)|v_k\rangle, \tag{4.6}$$

$$\boldsymbol{G}(\omega) = \frac{1}{\omega \mathbb{1}_N - \boldsymbol{K}^R - \boldsymbol{K}(\omega)}, \tag{4.7}$$

$$\boldsymbol{K}(\omega) = \int_{-\infty}^{+\infty} dk \frac{|v_k\rangle\langle v_k|}{\omega - \epsilon(k)}, \tag{4.8}$$

where $\mathbb{1}_N$ is an $N \times N$ identity matrix. Equations (4.6)-(4.8) hold for general photon-emitter couplings where $V_i(k)$ are independent functions for different emitters. There are two mathematical conditions on $V_i(k)$ that are necessary for the integral in Eq. (4.8) to be well-defined at any complex $\omega \neq 0$ outside the continuum spectrum [1].

First, we require that $V_i(k)$ is a locally square-integrable complex function on the real line. Second, to ensure that no ultraviolet divergences are present in the model, we impose a restriction on the large-k behavior of $V_i(k)$: when $k \to \pm\infty$, there exist $\gamma > 1$ such that $|V_i(k)|^2 = o(|k|^{m-\gamma})$. Each element of the $N \times N$ matrix $\boldsymbol{K}(\omega)$ is an analytic function on the complex plane with a branch cut along the continuum spectrum. $\boldsymbol{K}(\omega = E + i0^+)$ can be understood as describing effective interactions between emitters induced by the 1D channel.

To understand the properties of $T(E+i0)$ close to $E = 0$, we need to understand

[1] In WQED it is natural to define the continuum spectrum for odd m to be $(-\infty, 0) \cup (0, +\infty)$; for even m to be $(0, +\infty)$ when $\boldsymbol{s} = +1$ and $(-\infty, 0)$ when $\boldsymbol{s} = -1$.

the behavior of $\boldsymbol{K}(\omega)$ around $\omega = 0$. We can show that the value of $\boldsymbol{K}(\omega)$ around $\omega = 0$ is decided by the dispersion relation and $V(0)\,|u\rangle$. Define $L(\omega)$ as the integral over the free-particle propagator:

$$L(\omega) = \int_{-\infty}^{+\infty} dk \frac{1}{\omega - \epsilon(k)}. \tag{4.9}$$

We see that, when $\omega \to 0$, $L(\omega)^{-1}\frac{1}{\omega-\epsilon(k)}$ as a function of k diverges at $k = 0$ and vanishes everywhere else. In addition, $\int_{-\infty}^{+\infty} dk\; L(\omega)^{-1}\frac{1}{\omega-\epsilon(k)} = 1$ by definition of $L(\omega)$. Hence it follows from a standard result in functional analysis attributed to Toeplitz [94] that $\lim_{\omega\to 0} L(\omega)^{-1}\frac{1}{\omega-\epsilon(k)} = \delta(k)$. Using the condition that $|v_k\rangle = V(k)\,|u\rangle$ is continuous at $k = 0$ and the definition of $\boldsymbol{K}(\omega)$ in Eq. (4.8), we have

$$\lim_{\omega\to 0} L^{-1}(\omega)\boldsymbol{K}(\omega) = |V(0)|^2\,|u\rangle\,\langle u|\,. \tag{4.10}$$

When the emitter region consists of a single site, $\boldsymbol{K}^R = K^R$ is a complex number and Eq. (4.10) becomes $\lim_{\omega\to 0} L^{-1}(\omega)\boldsymbol{K}(\omega) = |V(0)|^2$. Using Eqs. (4.6) and (4.7), we then have

$$\lim_{\omega\to 0} L(\omega)T(\omega, k, k') = -\frac{V^*(k')V(k)}{|V(0)|^2}, \tag{4.11}$$

which is no longer dependent on K^R because $\lim_{\omega\to 0} L^{-1}(\omega)K^R = 0$. Although Eq. (4.11) is derived for the case of $N = 1$, we show through a rigorous mathematical analysis in Sec. 4.3.4 that Eq. (4.11) holds as long as the Hamiltonian does not support a "bright" zero-energy eigenstate, defined as a zero-energy eigenstate that has a non-zero emitter and photonic amplitude. In Sec. 4.3.3, we give a introduction to these bright states and explain that they are distinguished from "dark" states that have only a nonzero photonic amplitude and rather generically arise at zero-energy

in these models. The proof of Eq. (4.11) for $N > 1$ is the main technical result of this chapter as it underlies both the universal scattering results and our proof of Levinson's theorem.

When we evaluate the S-matrix in the limit $E \to 0$ using Eq. (4.5), $k_\alpha(E), k_\beta(E)$ in the T-matrix are both sent to 0. Using Eq. (4.11) and the condition that $V(k)$ is continuous at $k = 0$, we have

$$\lim_{E\to 0} L(E + i0^+)T(E + i0^+, k_\alpha(E), k_\beta(E)) = -1, \tag{4.12}$$

which shows that the on-shell T-matrix in the zero-energy limit is independent of the details of the interaction and fully determined by the dispersion relation; this is the reason behind the universal limit of the S-matrix when $E \to 0$. In Sec. 4.3.2, we evaluate Eq. (4.9) and obtain the m-dependent value of $L(\omega)$:

$$L(\omega) = -2\pi i \kappa_m \rho(|\omega|) \exp\left(-i\theta \frac{m-1}{m}\right), \tag{4.13}$$

where the complex frequency ω is parameterized in polar coordinates as $\omega = \sigma \exp(i\theta)|\omega|$, and $\rho(|\omega|) = \frac{1}{m|d|^{1/m}}|\omega|^{-1+1/m}$ corresponds to the density of states at energy $E = |\omega|$.

For even m, $\kappa_m = \frac{2}{1-a^2}$ with $a = \exp(i\pi/m)$, while $L(\omega)$ has a branch cut along the continuum spectrum $(0, +\infty)$ for $\sigma = +1$ or $(-\infty, 0)$ for $\sigma = -1$. For odd m, $\kappa_m = -\frac{1}{a-1}$ for $\theta \in (0, \pi)$ and $\kappa_m = -\frac{1}{a(a-1)}$ for $\theta \in (\pi, 2\pi)$, while $L(\omega)$ has a branch cut along the real line. For both even and odd m, $L(\omega)$ diverges at the rate of density of states $\rho(|\omega|)$ when ω approaches 0.

Now, we are ready to evaluate the limit of the S-matrix at zero energy. When m is odd, energy E can approach 0 from both above and below: $E \to 0^\pm$. When m is even, E can only approach 0 from one side: $E \to 0^+$ when $\sigma = +1$ or $E \to 0^-$ when

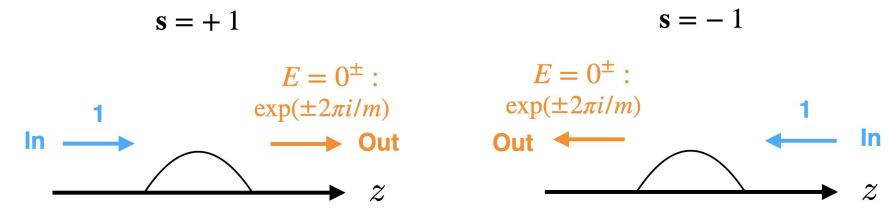

(a) odd m

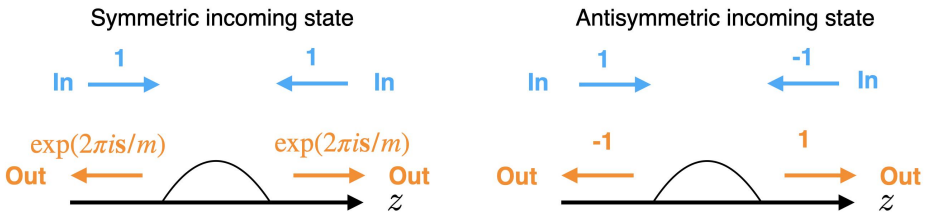

(b) even m

Figure 4.1: Illustration of 1D scattering (z is a spatial coordinate) near zero energy for dispersion relation $\epsilon(E) = \sigma|d|k^m$ with $\sigma = \pm 1$. Panel (a) is for odd m, where the scattering matrix is a single transmission coefficient dependent on m and the sign of energy is $E = 0^{\pm}$. Panel (b) is for even m, where the scattering matrix is a 2×2 matrix. The eigenstates of the scattering matrix are the symmetric and antisymmetric incoming states, with eigenphases $\exp(2\pi i\sigma/m)$ and 1, respectively.

$\sigma = -1$. Taking the limit $E \to 0^{\pm}$ in Eq. (4.5) for the respective cases properly, we have

$$\lim_{E\to 0^{\pm}} S_{\alpha\beta}(E) = \delta_{\alpha\beta} + \lim_{E\to 0^{\pm}} 2\pi i\rho(|E|)L^{-1}(E + i0^{+}), \tag{4.14}$$

where we have used Eq. (4.12) and the observation that $\lim_{E\to 0} |\epsilon'(k_\alpha(E))\epsilon'(k_\beta(E))|^{1/2}\rho(E) = 1$. Using Eqs. (4.13) and (4.14), we have,

$$\lim_{E\to 0^{\pm}} S(E) = \exp(\pm\pi i/m), \tag{4.15}$$

as illustrated in Fig. a. And for even m, the S-matrix

$$\lim_{E\to\sigma 0^{+}} \boldsymbol{S}(E) = \exp(\sigma i\pi/m) \begin{bmatrix} \cos(\pi/m) & \sigma i \sin(\pi/m) \\ \sigma i \sin(\pi/m) & \cos(\pi/m) \end{bmatrix} \tag{4.16}$$

is symmetric in the basis of degenerate momenta $\{|k_1 = 0^{+}\rangle, |k_2 = 0^{-}\rangle\}$. The symmetric eigenstate $|\psi_{\rm s}\rangle = \frac{1}{\sqrt{2}}(1, 1)^T$ has an eigenphase $\exp(i\pi\sigma/m)$, while the antisymmetric eigenstate $|\psi_{\rm a}\rangle = \frac{1}{\sqrt{2}}(1, -1)^T$ has a trivial eigenphase 1. The scattering of the symmetric and antisymmetric incoming states near zero energy is illustrated in Fig. b. For quadratic dispersion $\epsilon(k) = |d|k^2$, we recover the well-known total reflection:

$$\lim_{E\to 0^{+}} \boldsymbol{S}(E) = \begin{bmatrix} 0 & -1 \\ -1 & 0 \end{bmatrix}. \tag{4.17}$$

In the remaining subsections of Sec. 4.3, we fill in the details omitted in the derivation of Eq. (4.11), which is a vital relation that leads to our main results, Eqs. (4.15) and (4.16).

4.3.2 Calculation of $L(\omega)$

In this subsection, we derive the value of $L(\omega)$, given in Eq. (4.13) in Sec. 4.3.1. We start with the definition of $L(\omega)$ in Eq. (4.9):

$$L(\omega) = \int_{-\infty}^{+\infty} dk \frac{1}{\omega - \epsilon(k)}. \tag{4.18}$$

The dispersion relation is given by $\epsilon(k) = \sigma|d|k^m$, where $\sigma = \pm 1$ and $m \geq 2$ is a positive integer. To compute the integral, we close the integration contour in the upper half [2] of the complex plane and apply the residue theorem:

$$L(\omega) = -2\pi i \sum_{\mathrm{Im}[y_j]>0} \epsilon'(y_j)^{-1}, \tag{4.19}$$

where the complex numbers y_i satisfy $\epsilon(y_j) = \sigma|d|y_i^m = \omega$ and $\mathrm{Im}[y_j] > 0$. Given the parametrization of ω in polar coordinates as $\omega = \sigma \exp(i\theta)|d|p^m$, we have $y_j = \exp(i\theta/m)p\mu^{2j}$, where $\mu = \exp(i\pi/m)$ and $j \in \{0, 1, \ldots, m-1\}$. Define A as the set of j for which y_j is above the real line. Equation (4.19) can then be expressed as

$$L(\omega) = -2\pi i \sum_{j\in A} \frac{1}{m|d|y_j^{m-1}}, \tag{4.20}$$

$$= -2\pi i \frac{1}{m|d|p^{m-1}} \exp\left(-i\theta\frac{m-1}{m}\right) \sum_{j\in A} (-\mu)^{2j}, \tag{4.21}$$

where the set A and the value of $\kappa_m \equiv \sum_{j\in A}(-\mu)^{2j}$ are given in Table 4.1 for both odd and even m. Note that the prefactor $\frac{1}{m|d|p^{m-1}}$ in Eq. (4.21) is equal to the density of states $\rho(|\omega|) = \frac{1}{m|d|^{1/m}}|\omega|^{-1+1/m}$. Hence, we have proved that $L(\omega)$ is given by Eq. (4.13).

[2] Closing the contour in the lower half of the complex plane would give the same answer

As we have mentioned in Sec. 4.3.1, if there exists no bright zero-energy eigenstate, Eq. (4.11) holds for the class of models where $|v_k\rangle = V(k)\,|u\rangle$, even when $N \geq 2$. In the following subsection, we give the definition of bright zero-energy eigenstates and provide a physical explanation as to why our universality results require their absence.

4.3.3 Bright zero-energy eigenstates

Due to the multi-component nature of our emitter scattering problems, we find it necessary to categorize all eigenstates of the Hamiltonian into bright, dark, and emitter eigenstates. Bright eigenstates have a nonzero photon and emitter wavefunction, while dark eigenstates have only a nonzero photonic amplitude, and emitter eigenstates have only a nonzero emitter amplitude. With this terminology established, we now give an overview of the properties of the different types of eigenstates at zero energy. The zero-energy emitter states correspond to the null vectors of $\boldsymbol{K}^R$ that are orthogonal to $|v_k\rangle = V(k)\,|u\rangle$. They are decoupled from the photon channel, hence their existence has no impact on the universal behavior of the S-matrix. For $V(k)$ with nonzero derivatives at $k = 0$, there generally exist uncountably many zero-energy dark states independent of $\boldsymbol{K}^R$, which are polynomial functions with degree less than $m - 1$. Bright states at zero-energy are fine-tuned and have a constant photon wavefunction in space. As we show below, these states come into existence precisely when the universal scattering behavior fails.

Table 4.1: The set A and the value of $\kappa_m = \sum_{j\in A}(-\mu)^{2j}$ for both odd and even m.

		A	$\kappa_m \equiv \sum_{j\in A}(-\mu)^{2j}$
Odd m	$\theta \in (0,\pi)$	$(0,1,2,\ldots\frac{m-1}{2})$	$-\frac{1}{\mu-1}$
	$\theta \in (\pi,2\pi)$	$(0,1,2,\ldots\frac{m-3}{2})$	$-\frac{1}{(\mu-1)\mu}$
Even m	$\theta \in (0,2\pi)$	$(0,1,2,\ldots\frac{m-2}{2})$	$\frac{2}{1-\mu^2}$

To give a heuristic explanation for why universal scattering at zero energy fails at these fine-tuned parameters, we consider the classic model of 1D potential scattering with quadratic dispersion relation ($m = 2$), i.e., a 1D quantum mechanical problem described by the Schrödinger equation

$$-\frac{d^2\psi(z)}{dz^2} + V(z)\psi(z) = E\psi(z), \tag{4.22}$$

where we set the mass equal to 1/2. A particle being scattered off a generic, short-range potential $V(z)$ would experience a total reflection in the limit $E \to 0$, similarly to what happens in our 1D emitter scattering models. Another feature of these 1D potential scattering problems is that there exists a fine-tuned, critical regime when the scattering in the limit $E \to 0$ becomes total transmission instead of total reflection. This occurs when there is a zero-energy eigenstate and there is no energy scale to compare with when the limit $E \to 0$ is taken. The zero-energy eigenstate can be understood as the effective "transition state" when a new bound state emerges or disappears upon the continuous tuning of parameters.

Similarly, in our emitter scattering models, the universal scattering behavior that takes place for generic parameters would fail at certain fine-tuned parameters. An important difference to note is that, unlike in potential scattering, not all zero-energy eigenstates in emitter scattering are associated with the critical regime where the universal scattering behavior fails. For the particular type of interactions $|v_k\rangle$ being considered in this chapter, we discover that the critical regime can be associated with the existence of a particular type of eigenstates at zero energy, which we call bright zero-energy states (defined above).

4.3.4 The proof

After explaining the physical meaning of the conditions when the universal results would fail, we are ready to delve into the proof. In order to state our goal more explicitly, we rewrite the Hamiltonian given by Eq. (4.3) in the single-excitation manifold:

$$H^{(1)} = \int_{-\infty}^{+\infty} dk\ \epsilon(k) C^\dagger(k) C(k) + \int_{-\infty}^{+\infty} dk\ \left[C^\dagger(k) V^*(k) \left\langle u \right| + C(k) V(k) \left| u \right\rangle \right] + \boldsymbol{K}^R, \tag{4.23}$$

where we have used the matrix representation $\boldsymbol{K}^R$ to replace $\sum_{i,j=1}^N K_{ij}^R b_i^\dagger b_j$ and the vector $|v_k\rangle = V(k)\,|u\rangle$ to replace the emitter creation operators $\sum_{i=1}^N V_i(k) b_i^\dagger$.

Our goal in this subsection is to prove the following theorem:

Theorem 1. *Suppose $V(k)$ is a locally square-integrable function continuous at $k = 0$ and $V(k = 0) \neq 0$. When $k \to \pm\infty$, $|V(k)|^2 = o(k^{m-\gamma})$ for some $\gamma > 1$. Consider the class of emitter interactions $|v_k\rangle = V(k)\,|u\rangle$, where $|u\rangle$ is a unit vector. The single-particle T-matrix given by Eqs.* (4.6)- (4.8) *reads:*

$$T(\omega, k, k') = V^*(k') V(k) \langle u | \frac{1}{\omega \mathbb{1}_N - \boldsymbol{K}^R - \boldsymbol{K}(\omega)} | u \rangle, \tag{4.24}$$

$$\boldsymbol{K}(\omega) = |u\rangle\langle u| K(\omega), \quad K(\omega) \equiv \int_{-\infty}^{+\infty} \frac{|V(k)|^2}{\omega - \epsilon(k)}. \tag{4.25}$$

When $H^{(1)}$ in Eq. (4.23) *has no bright zero-energy eigenstates, Eq. 4.3.1 holds, namely,*

$$\lim_{\omega \to 0} L(\omega) T(\omega, k, k') = -\frac{V^*(k') V(k)}{|V(0)|^2}. \tag{4.26}$$

Note that $T(\omega, k, k')$ and $\boldsymbol{K}(\omega)$ are defined for ω outside the continuum spectrum, hence the limit $\omega \to 0$ is taken in any direction except from within the continuum spectrum.

Proof. Our proof consists of two lemmas linked by a condition on $\boldsymbol{K}^R$. The idea of the proof is that the absence of bright zero-energy eigenstates can be translated into a condition on $\boldsymbol{K}^R$, which turns out to be necessary for the proof of Eq. (4.26).

Choose an orthonormal basis $\{|u_1\rangle, |u_2\rangle, \ldots |u_N\rangle\}$ for the single-emitter Hilbert space, where $|u_1\rangle \equiv |u\rangle$ is the first vector in this new basis. The link between the two lemmas is the submatrix $\boldsymbol{K}^R_{\not 1}$ constructed from deleting the first row and first column of $\boldsymbol{K}^R$; $\boldsymbol{K}^R_{\not 1}$ can be considered as an operator on the emitter-excitation subspace $\{|u_2\rangle, \ldots |u_N\rangle\}$ orthogonal to $|u\rangle$. In Lemma 2, we prove that Eq. (4.26) holds if any null vector of $\boldsymbol{K}^R_{\not 1}$ also corresponds to the null vector of $\boldsymbol{K}^R$. In Lemma 3, we prove that the condition Lemma 2 relies on is guaranteed by the absence of bright zero-energy eigenstates. Combining the two lemmas completes the proof of Theorem 1.

Lemma 2. *If any null vector of $\boldsymbol{K}^R_{\not 1}$ also corresponds to the null vector of $\boldsymbol{K}^R$, Eq.* (4.26) *follows.*

Proof. Using Eq. (4.24), the l.h.s of Eq. (4.26) can be written as

$$\lim_{\omega\to 0} L(\omega) T(\omega, k, k') = V^*(k') V(k) \lim_{\omega\to 0} L(\omega) \langle u| \boldsymbol{H}(\omega)^{-1} |u\rangle , \tag{4.27}$$

where $\boldsymbol{H}(\omega) \equiv \omega \mathbb{1}_N - \boldsymbol{K}^R - \boldsymbol{K}(\omega)$. Hence, our goal, Eq. (4.26), is equivalent to

$$\lim_{\omega\to 0} L(\omega) \langle u| \boldsymbol{H}(\omega)^{-1} |u\rangle = -\frac{1}{|V(0)|^2}. \tag{4.28}$$

In the new basis where $|u_1\rangle = |u\rangle$ is the first basis vector, $\langle u| \boldsymbol{H}(\omega)^{-1} |u\rangle$ is the $(1,1)$ matrix element of the inverse of $\boldsymbol{H}(\omega)$, and can be computed from the $(N-1)\times(N-1)$ submatrix $\boldsymbol{H}_{\not{1}\not{1}}(\omega)$ constructed from deleting the first row and first column of $\boldsymbol{H}(\omega)$:

$$\langle u| \boldsymbol{H}(\omega)^{-1} |u\rangle = \frac{\det(\boldsymbol{H}_{\not{1}\not{1}}(\omega))}{\det(\boldsymbol{H}(\omega))}. \tag{4.29}$$

Using $\boldsymbol{K}(\omega) = |u\rangle\langle u|K(\omega)$, we have

$$\det(\boldsymbol{H}_{\not{1}\not{1}}(\omega)) = \det(\omega \mathbb{1}_{N-1} - \boldsymbol{K}^R_{\not{1}\not{1}}), \tag{4.30}$$

$$\det(\boldsymbol{H}(\omega)) = -K(\omega)\det(\omega \mathbb{1}_{N-1} - \boldsymbol{K}^R_{\not{1}\not{1}}) + \det(\omega \mathbb{1}_N - \boldsymbol{K}^R). \tag{4.31}$$

Combining Eqs. (4.29), (4.30) and (4.31), the l.h.s of Eq. (4.28) becomes

$$\lim_{\omega\to 0} L(\omega)\,\langle u| \boldsymbol{H}(\omega)^{-1} |u\rangle = \lim_{\omega\to 0} L(\omega)\left(-K(\omega) + \frac{\det(\omega \mathbb{1}_N - \boldsymbol{K}^R)}{\det(\omega \mathbb{1}_{N-1} - \boldsymbol{K}^R_{\not{1}\not{1}})}\right)^{-1}. \tag{4.32}$$

Let us label the N roots of the characteristic polynomial of $\boldsymbol{K}^R$ by E_i for $i = 1, \ldots N$, and the $N-1$ roots of the characteristic polynomial of $\boldsymbol{K}^R_{\not{1}\not{1}}$ by $\bar{E}_i$ for $i = 1, \ldots N-1$. E_i and $\bar{E}_i$ correspond to the eigenvalues of $\boldsymbol{K}^R$ and $\boldsymbol{K}^R_{\not{1}\not{1}}$, respectively, where any eigenvalue with multiplicity $n \geq 2$ is assigned to n different indices. We have

$$\lim_{\omega\to 0} \frac{\det(\omega \mathbb{1}_N - \boldsymbol{K}^R)}{\det(\omega \mathbb{1}_{N-1} - \boldsymbol{K}^R_{\not{1}\not{1}})} = \lim_{\omega\to 0} \frac{\prod_{i=1}^{N}(\omega - E_i)}{\prod_{i=1}^{N-1}(\omega - \bar{E}_i)}. \tag{4.33}$$

Since any null vector of $\boldsymbol{K}^R_{\not{1}\not{1}}$ corresponds to a null vector of $\boldsymbol{K}^R$ by the assumption of the Lemma, if $\boldsymbol{K}^R$ has null vectors, its zero-eigenvalue multiplicity must be greater or equal to that of $\boldsymbol{K}_{\not{1}\not{1}}$. Hence, the limit in Eq. (4.33) is finite.

In Sec, we have introduced the identity $\lim_{\omega\to 0} L^{-1}(\omega)\frac{1}{\omega-\epsilon(k)} = \delta(k)$; hence $\lim_{\omega\to 0} L^{-1}(\omega)K(\omega) =$

$|V(0)|^2 \neq 0$ and Eq. (4.32) leads to Eq. (4.28). The proof of Lemma 2 is complete.

□

If we can prove that the absence of bright zero-energy eigenstates of Eq. (4.23) guarantees that any null vector of $\boldsymbol{K}^R_{\not H}$ also corresponds to the null vector of $\boldsymbol{K}^R$, Eq. (4.26) would immediately follow from Lemma 2. To do this, we prove the contrapositive statement in the following lemma:

Lemma 3. *When there exists a vector* $|e_0\rangle = \sum_{i=2}^{N} e_i |u_i\rangle$ *orthogonal to* $|u\rangle$*, such that* $\boldsymbol{K}^R |e_0\rangle \neq 0$ *and* $\boldsymbol{K}^R_{\not H}|e_0\rangle = 0$*, then there exists a bright zero-energy eigenstate of the Hamiltonian in Eq.* (4.23)*.*

Proof. We plan to write down an ansatz with a nonzero photon and emitter wavefunction and verify that it is a zero-energy eigenstate of the Hamiltonian in Eq. (4.23). The ansatz we propose is the following:

$$|\psi_0\rangle = \int_{-\infty}^{+\infty} dz\ \psi_0(z) C^\dagger(z) |0, g\rangle + |e_0\rangle\,, \tag{4.34}$$

$$\psi_0(z) = -V(0)^{-1} \langle u|\boldsymbol{K}^R|e_0\rangle\,, \tag{4.35}$$

where the photon wavefunction $\psi_0(z)$ in the coordinate space is a constant function. By definition, $|e_0\rangle$ is orthogonal to $|u\rangle$. Because $\boldsymbol{K}^R |e_0\rangle \neq 0$ and $\boldsymbol{K}^R_{\not H}|e_0\rangle = 0$, $\boldsymbol{K}^R |e_0\rangle$ is a nonzero vector proportional to $|u\rangle$. Hence, $\psi_0(z) \neq 0$.

Our goal is to prove that the ansatz given by Eqs. (4.34) and (4.35) is the zero-energy eigenstate of the Hamiltonian in Eq. (4.23). Applying $H^{(1)}$ in Eq. (4.23) to

the Fourier transform of the ansatz in Eq. (4.34), we get

$$H^{(1)}\left|\psi_0\right\rangle = \int_{-\infty}^{+\infty} dk\ \epsilon(k)\psi_0(k)C^\dagger(k)\left|0,g\right\rangle + V^*(k)\left\langle u|e_0\right\rangle C^\dagger(k)\left|0,g\right\rangle + \psi_0(k)V(k)\left|u\right\rangle + \boldsymbol{K}^R\left|e_0\right\rangle, \tag{4.36}$$

where the momentum-space photon wavefunction $\psi_0(k) = -V(0)^{-1}\left\langle u|\boldsymbol{K}^R|e_0\right\rangle\delta(k)$ is the Fourier transform of Eq. (4.35). Since the dispersion relation satisfies $\epsilon(0) = 0$, the first term on the r.h.s of Eq. (4.36) is zero: $\int_{-\infty}^{+\infty} dk\ \epsilon(k)\psi_0(k)C^\dagger(k)\left|0,g\right\rangle = 0$. Because $\langle u|e_0\rangle = 0$, the second term on the r.h.s of Eq. (4.36) is also equal to 0. The third term

$$\int_{-\infty}^{+\infty} dk\ \psi_0(k)V(k)\left|u\right\rangle = -\left|u\right\rangle\left\langle u\right|\boldsymbol{K}^R\left|e_0\right\rangle \tag{4.37}$$

cancels with the fourth term $\boldsymbol{K}^R\left|e_0\right\rangle$ on the r.h.s of Eq. (4.36) because $\boldsymbol{K}^R\left|e_0\right\rangle$ is proportional to $\left|u\right\rangle$. Therefore, $H^{(1)}\left|\psi_0\right\rangle = 0$, and this is the end of the proof for Lemma 3.

□

Combining Lemmas 2 and 3, we can obtain Theorem 1.

□

4.4 Levinson's theorem

4.4.1 Overview of results

Levinson's theorem relates the quantized scattering phase to the number of bound states in the system. In the literature, the theorem has been discussed in various Hermitian systems and various dimensions [6, 12, 45, 46, 81, 84, 95, 105, 106, 125, 169],

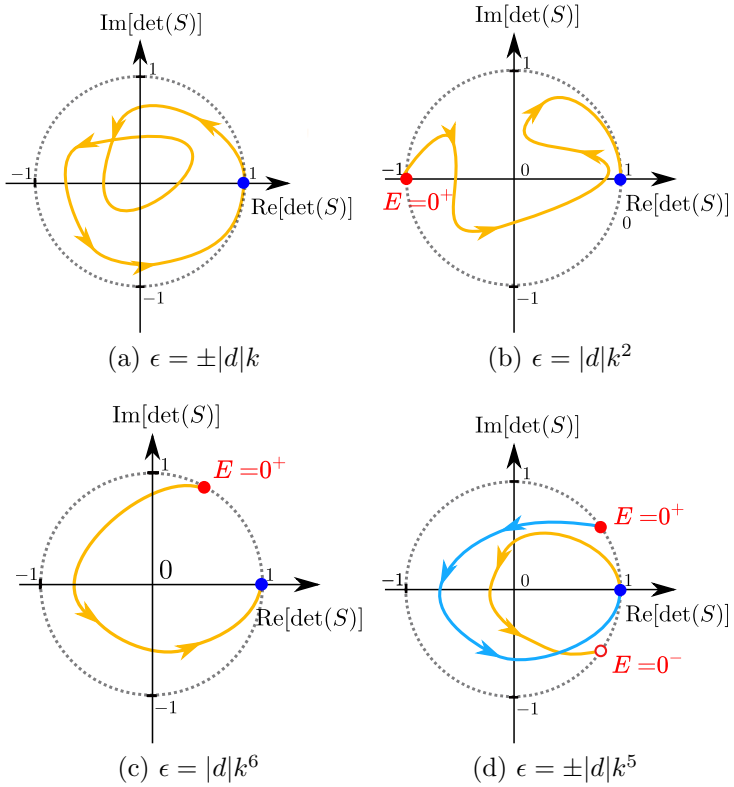

Figure 4.2: Illustrations of the trajectories of $\det[\boldsymbol{S}(E)]$ of a dissipative system in the complex plane when E is increased from E_{min} to E_{max} for (a) $\epsilon(k) = \pm|d|k$, where the trajectory starts and ends at 1. (b) $\epsilon = |d|k^2$, where the trajectory starts at -1 and ends at 1. (c) $\epsilon = |d|k^6$, where the trajectory starts at $\exp(i\pi/3)$ and ends at 1. (d) $\epsilon = \pm|d|k^5$, where the trajectory for $E \in (-\infty, 0)$ (solid yellow) starts at 1 and ends at $S(0^-) = \exp(i\pi/5)$, while the trajectory for $E \in (0, +\infty)$ (solid blue) starts at $S(0^+) = \exp(i\pi/5)$ and ends at 1.

where the dispersion relation close to the scattering threshold is always quadratic. In Chapter 2, we generalized Levinson's theorem to 1D emitter scattering, where dissipation is present and the dispersion relation is linear at all k. In that case, there is no well-defined scattering threshold. When we consider dispersion relations $\epsilon(k) = \sigma|d|k^m$ with the class of photon-emitter couplings $|v_k\rangle = V(k)\,|u\rangle$, the S-matrix can take different universal limits at zero energy, dependent on the value of the integer $m \geq 2$ [see Eqs. (4.15) and (4.16)]. This leads to a modification to Levinson's theorem, as we illustrate in the remainder of this chapter.

For simplicity, we assume that there are no bright zero-energy eigenstates and no bound states in the continuum in the system. Before discussing general m, we summarize the theorem for quadratic ($m = 2$) and linear ($m = 1$) dispersion relations. When energy E is increased from the lower end of the continuum spectrum E_{min} (which can be $-\infty$) to the upper end E_{max} (which can be $+\infty$), $\det[\boldsymbol{S}(E)]$ traces a trajectory in the complex plane. In the case of $\epsilon(k) = k$, the S-matrix is an identity matrix at both ends of the continuum spectrum. The trajectory of $\det[\boldsymbol{S}(E)]$ in these cases forms a closed loop starting and ending at 1, as illustrated in Fig. a. For illustration purposes, we assume that the system is dissipative, so the trajectory is not confined to the unit circle. Levinson's theorem states that the winding number of this loop around the origin is equal to the decrease in the number of bound states ΔN_B after the interaction is turned on [6, 81]. For emitter scattering, the number of bound states for the bare Hamiltonian H_0 is equal to the number of emitters N; hence, $\Delta N_B = N - N_B$, where N_B is the number of bound states for the full Hamiltonian [165]. If we define the scattering phase $\delta(E)$ of $\det[\boldsymbol{S}(E)] \equiv |\det[\boldsymbol{S}(E)]| \exp(2i\delta(E))$ as a continuous function of E [3], the theorem can be stated as $\Delta\delta \equiv \delta(E_{max}) - \delta(E_{min}) = \pi\Delta N_B$. For a quadratic dispersion relation $\epsilon(k) = k^2$, the trajectory of $\det[\boldsymbol{S}(E)]$ starts at $\lim_{E\to 0} \det[\boldsymbol{S}(E)] = -1$ and ends at $\lim_{E\to+\infty} \det[\boldsymbol{S}(E)] = 1$, as illustrated in Fig. b. As compared to the closed-loop case of Fig. a, Levinson's theorem is modified to $\Delta\delta = \pi\Delta N_B + \pi/2$ [4] .

Next, we give our results on Levinson's theorem for emitter scattering with dispersion relation $\epsilon(k) = \sigma|d|k^m$ with $\sigma = \pm 1$ and photon-emitter couplings $|v_k\rangle = V(k)\,|u\rangle$. First, consider the case of even m. When $\sigma = +1$, the trajectory of

[3] For dissipative systems, we assume that $\det[\boldsymbol{S}(E)] \neq 0$ for any E within the continuum spectrum

[4] For potential scattering, see Levinson's theorem for quadratic dispersion relation in 1D in Ref. [46]. For emitter scattering, Levinson's theorem for quadratic dispersion relation is, to our knowledge, first presented by our recent paper [167] corresponding to this chapter.

$\det[\boldsymbol{S}(E)]$ starts at $\lim_{E\to 0^+}\det[\boldsymbol{S}(E)] = \exp(2\pi i/m)$ [see Eq. (4.16)] and ends at $\lim_{E\to+\infty}\det[\boldsymbol{S}(E)] = 1$, as illustrated in Fig. c for $m = 6$. When $\sigma = -1$, the trajectory of $\det[\boldsymbol{S}(E)]$ starts at $\lim_{E\to-\infty}\det[\boldsymbol{S}(E)] = 1$ and ends at $\lim_{E\to 0^-}\det[\boldsymbol{S}(E)] = \exp(-2\pi i/m)$. In the following subsection, we prove that, for both cases,

$$\Delta\delta = \pi(N - N_B) + \pi\frac{m-1}{m}. \tag{4.38}$$

When m is odd, the continuum spectrum is $(-\infty, 0)\cup(0, +\infty)$, and the trajectory of $S(E)$ is discontinuous across 0, as illustrated in Fig. d. When E increases from $-\infty$ to 0, the trajectory starts from 1 and ends at $\exp(-i\pi/m)$ [see Eq. (4.15)]. When E increases from 0 to $+\infty$, the trajectory starts at $\exp(+i\pi/m)$ and ends at 1. If we define $\Delta\delta$ as the sum of the winding phases of the two continuous trajectories, $\Delta\delta$ satisfies Eq. (4.38), as we show in the following subsection.

4.4.2 The proof

In this subsection, we prove Levinson's theorem for the class of emitter scattering models with $|v_k\rangle = V(k)\,|u\rangle$, i.e. Eq. (4.38). Let us restate the objective of our proof in the following theorem:

Theorem 4. *Denote the continuum spectrum by $\mathcal{R}_c$. We assume that there are no bound states in the continuum or bright zero-energy eigenstates in the system. For dissipative systems, we assume that $\det[\boldsymbol{S}(E)] \neq 0$ for $E \in \mathcal{R}_c$. The winding phase $\Delta\delta$ of $\det[\boldsymbol{S}(E)]$ around the origin is defined as*

$$2\Delta\delta = -i\int_{\mathcal{R}_c} dE\frac{\partial_E\det[\boldsymbol{S}(E)]}{\det[\boldsymbol{S}(E)]}. \tag{4.39}$$

Suppose $|v_k\rangle = V(k)\,|u\rangle$ satisfies the properties listed in Theorem 1 and the dis-

persion relation is given by $\epsilon(k) = \sigma|d|k^m$*, where* $\sigma = \pm 1$ *and* $m \geq 2$ *is an integer. We have*

$$\Delta\delta = \pi(N - N_B) + \pi\frac{m-1}{m}, \tag{4.40}$$

where N *is the number of emitters and* N_B *is the number of bound states.*

The main idea of the proof is to define an analytic continuation of $\det[\boldsymbol{S}(E)]$ to the complex plane and observe the fact that the bound state energies are the poles of this function. The proof is similar to Sec. 2.6 in Chapter 2, where we proved Levinson's theorem for photon-emitter models with linear dispersion relations.

In preparation for the proof of Theorem 4, we introduce Theorem 5, where we propose an analytic function $s(\omega)$ that is equal to the analytic continuation of $\det[\boldsymbol{S}(E)]$ to the complex plane. Though introduced here as a tool for proving Theorem 4, Theorem 5 provides a quick method to compute $\det[\boldsymbol{S}(E)]$ using $\boldsymbol{K}^R$ and $\boldsymbol{K}(E+i0^{\pm})$ and is an important theorem itself. We comment that the range of application of Theorem 5 is well beyond the class of photon-emitter models discussed in this chapter: it can be applied to general photon-emitter interactions $|v_k\rangle$ and other dispersion relations beyond $\epsilon(k) = \pm|d|k^m$.

Theorem 5. *Define* $J(\omega) = \det[\omega\mathbb{1}_N - \boldsymbol{K}^R - \boldsymbol{K}(\omega)]$ *as a function on the complement of the continuum spectrum* $\mathcal{R}_c$ *in the complex plane. For the values of* ω *s.t.* $J(\omega) \neq 0$*, we can define* $s(\omega) = \frac{J(\omega^*)}{J(\omega)}$*. When* E *is not equal to the energy of a bound state in the continuum,*

$$s(E + i0^+) = \det[\boldsymbol{S}(E)]. \tag{4.41}$$

We comment that the bound state energies E_B correspond to the poles of the

emitter propagator $\boldsymbol{G}(\omega) = [\omega \mathbb{1}_N - \boldsymbol{K}^R - \boldsymbol{K}(\omega)]^{-1}$, hence they satisfy $J(E_B) = 0$.

Proof. Let $n(E)$ denote the momentum degeneracy at energy E and $k_1, \ldots k_{n(E)}$ the degenerate momenta at energy E. When $\epsilon(k) = \pm|d|k^m$ and $E \in \mathcal{R}_c$, $n(E) = 1$ for odd m and $n(E) = 2$ for even m. According to Eqs. (4.5)-(4.8), the S-matrix $\boldsymbol{S}(E)$ is a $n(E) \times n(E)$ matrix, whose matrix elements are given by

$$S_{\alpha\beta}(E) = \delta_{\alpha\beta} - \frac{2\pi i}{\sqrt{|\epsilon'(k_\alpha(E))\epsilon'(k_\beta(E))|}} \langle v_{k_\beta(E)}|\boldsymbol{G}(E + i0^+)|v_{k_\alpha(E)}\rangle \,, \tag{4.42}$$

where $\alpha, \beta \in (1, 2, \ldots, n(E))$.

Note that in writing down Eq. (4.42), we have implicitly assumed that the limit $\boldsymbol{G}(E + i0^+) \equiv \lim_{\eta\to 0^+} \boldsymbol{G}(E + i\eta)$ exists. However, if $E_c\mathbb{1}_N - \boldsymbol{K}^R - \boldsymbol{K}(E_c + i0^+)$ has a zero eigenvalue for some energy $E_c \in \mathcal{R}_c$, $\boldsymbol{G}(E_c + i\eta)$ does not have a limit when $\eta \to 0^+$ and E_c corresponds to the energy of a bound state in the continuum. This is why the theorem only applies to $E \neq E_c$.

Construct $\boldsymbol{A}$ as a $N \times n(E)$ matrix and $\boldsymbol{A}^\dagger$ its Hermitian conjugate:

$$\boldsymbol{A} = \left(\tfrac{1}{\sqrt{|\epsilon'(k_1)|}}|v_{k_1}\rangle, \ldots \tfrac{1}{\sqrt{|\epsilon'(k_{n(E)})|}}|v_{k_{n(E)}}\rangle \right), \tag{4.43}$$

then the $n(E) \times n(E)$ matrix $\boldsymbol{S}(E)$ for $E \neq E_c$ can be written as

$$\boldsymbol{S}(E) = \mathbb{1}_{n(E)} - 2\pi i \boldsymbol{A}^\dagger \boldsymbol{G}(E + i0^+)\boldsymbol{A}, \tag{4.44}$$

where $\mathbb{1}_{n(E)}$ is an identity matrix of dimension $n(E)$.

Using the definitions of $s(\omega), J(\omega)$ and the properties of determinant, we have,

$$s(E + i0^+) = \det(\mathbb{1}_N + (\boldsymbol{K}(E + i0^+) - \boldsymbol{K}(E + i0^-))\boldsymbol{G}(E + i0^+)), \tag{4.45}$$

where $\boldsymbol{K}(E+i0^+) - \boldsymbol{K}(E+i0^-)$ can be re-written as

$$\begin{aligned}\boldsymbol{K}(E+i0^+) - \boldsymbol{K}(E+i0^-) &= \int_{-\infty}^{+\infty} dk\ |v_k\rangle\langle v_k| \left(\frac{1}{E+i0^+-\epsilon(k)} - \frac{1}{E+i0^--\epsilon(k)}\right), \\ &= -\int_{-\infty}^{+\infty} dk\ |v_k\rangle\langle v_k| 2\pi i\delta(E-\epsilon(k)), \\ &= -2\pi i \sum_{\alpha=1}^{n(E)} \frac{1}{|\epsilon'(k_\alpha)|} |v_{k_\alpha}\rangle\langle v_{k_\alpha}| = -2\pi i \boldsymbol{A}\boldsymbol{A}^\dagger. \end{aligned} \tag{4.46}$$

Inserting Eq. (4.46) into Eq. (4.45), we get

$$s(E+i0^+) = \det\left(\mathbb{1}_N - 2\pi i \boldsymbol{A}\boldsymbol{A}^\dagger \boldsymbol{G}(E+i0^+)\right). \tag{4.47}$$

According to a standard result in linear algebra known as the extension of the matrix determinant lemma, given an invertible $N\times N$ matrix $-2\pi i\boldsymbol{G}(E+i0)$ and a $N\times n(E)$ matrix $\boldsymbol{A}$,

$$\det(\mathbb{1}_N - 2\pi i \boldsymbol{A}\boldsymbol{A}^\dagger \boldsymbol{G}(E+i0^+) = \det(\mathbb{1}_{n(E)} - 2\pi i \boldsymbol{A}^\dagger \boldsymbol{G}(E+i0^+)\boldsymbol{A}). \tag{4.48}$$

Using Eqs. (4.44) and (4.47), we see that the l.h.s and r.h.s of Eq. (4.48) are equal to $s(E+i0^+)$ and $\det[\boldsymbol{S}(E)]$, respectively. This is the end of the proof for Theorem 5.

□

We proceed to prove Theorem 4 with the help of Theorem 5.

Proof. (Theorem 4)

First consider $\epsilon(k) = |d|k^m$ with odd m, in which case the continuum spectrum is $\mathcal{R}_c = (-\infty, 0)\cup(0,+\infty)$. Since we have assumed that there is no bound state in the continuum, using Theorem 5, we can replace $\det[\boldsymbol{S}(E)]$ by $\frac{J(E+i0^-)}{J(E+i0^+)}$ for $E\in\mathcal{R}_c$ and

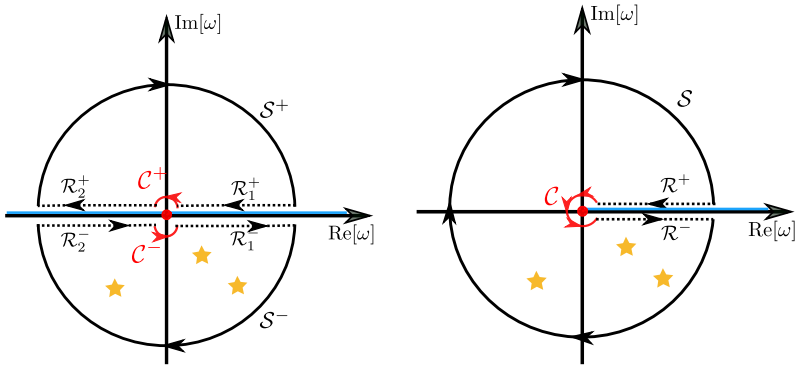

(a) $\epsilon(k) = |d|k^m$, odd m (b) $\epsilon(k) = |d|k^m$, even m

Figure 4.3: Illustration of the integration contours for the calculation of the winding phase of $\det[\boldsymbol{S}(E)]$. (a) Contours for a dispersion relation $\epsilon(k) = |d|k^m$ with odd m. (b) Contours for a dispersion relation $\epsilon(k) = |d|k^m$ with even m. The density of states diverges at the origin $E = 0$, marked by the red dot. The blue lines represent the continuum spectrum, while the yellow stars represent bound-state energies. The dashed lines with arrows are the integration paths for the evaluation of the winding number of $\det[\boldsymbol{S}(E)]$. The semicircles (circles) are added to form closed integration contours so that the residue theorem can be invoked. The red semicircles (circle) go around the origin with an infinitesimal radius, while the black semicircles (circle) have an infinite radius.

rewrite Eq. (4.39) in terms of a contour integral in the complex plane:

$$2\Delta\delta = -i\int_{\mathcal{R}_c} dE\left[\frac{\partial_E J(E+i0^-)}{J(E+i0^-)} - \frac{\partial_E J(E+i0^+)}{J(E+i0^+)}\right] = -i\int_{\mathcal{R}_1^+ + \mathcal{R}_1^- + \mathcal{R}_2^+ + \mathcal{R}_2^-} d\omega \frac{\partial_\omega J(\omega)}{J(\omega)}, \tag{4.49}$$

where E is a real coordinate, ω is a complex coordinate, and the integration contours $\mathcal{R}_1^\pm$ and $\mathcal{R}_2^\pm$ are illustrated by the dashed lines in Fig. 4.3a.

$\mathcal{R}_2^\pm$ and $\mathcal{R}_1^\pm$ represent the contours just above/below the real line for $E < 0$ and $E > 0$, respectively. We can obtain two closed integration contours by adding a pair of semicircles $\mathcal{C}^\pm$ with an infinitesimal radius around 0 and a pair of semicircles $\mathcal{S}^\pm$ with radius $|\omega| \to \infty$. Equation (4.49) can then be rewritten as

$$2\Delta\delta = -i\oint d\omega \frac{\partial_\omega J(\omega)}{J(\omega)} + i\int_{\mathcal{S}^+ + \mathcal{S}^-} d\omega \frac{\partial_\omega J(\omega)}{J(\omega)} + i\int_{\mathcal{C}^+ + \mathcal{C}^-} d\omega \frac{\partial_\omega J(\omega)}{J(\omega)}, \tag{4.50}$$

where $\oint$ represents the sum of integrals over the two closed contours. For odd m, $J(\omega)$ is analytic in the complement of the real line in the complex plane. The poles of $J^{-1}(\omega)$ correspond to the bound state energies; they can only be located below the real line given our assumption that there is no bound state in the continuum. This also implies that when $\boldsymbol{K}^R$ is Hermitian, $N_B = 0$. Applying the residue theorem, the closed contours in the upper and lower half planes yield 0 and $-2\pi i N_B$, respectively. Hence,

$$-i \oint d\omega \frac{\partial_\omega J(\omega)}{J(\omega)} = -2\pi N_B. \tag{4.51}$$

Next, we evaluate the integrals along the small semicircles. $J(\omega)$ is equal to $\det[\boldsymbol{H}(\omega)]$ in Eq. (4.31), which shows that $J(\omega) \sim K(\omega) \sim L(\omega)$ when $\omega \to 0$. Intuitively, the winding phases of $J(\omega)$ along $\mathcal{C}^\pm$ are equal to the winding phases of $L(\omega)$ along $\mathcal{C}^\pm$, which contribute to the term $\pi\frac{m-1}{m}$ in Eq. (4.40). To demonstrate it rigorously, we write $J(\omega)$ as the product of $L(\omega)$ and another function $g(\omega)$:

$$\begin{aligned} &J(\omega) = L(\omega)g(\omega), \\ &g(\omega) \equiv -L^{-1}(\omega)K(\omega)\det(\omega \mathbb{1}_{N-1} - \boldsymbol{K}^R_{\not 1}) + L^{-1}(\omega)\det(\omega \mathbb{1}_N - \boldsymbol{K}^R). \end{aligned} \tag{4.52}$$

This way the winding phases of $J(\omega)$ along $\mathcal{C}^\pm$ can be evaluated as the sum of the winding phases of $g(\omega)$ and $L(\omega)$:

$$i\int_{\mathcal{C}^\pm} d\omega \frac{\partial_\omega J(\omega)}{J(\omega)} = i\int_{\mathcal{C}^\pm} d\omega \frac{\partial_\omega L(\omega)}{L(\omega)} + i\int_{\mathcal{C}^\pm} d\omega \frac{\partial_\omega g(\omega)}{g(\omega)}. \tag{4.53}$$

Using Eqs. (4.21), the winding number of $L(\omega)$ can be evaluated explicitly in polar

coordinates:

$$
\begin{aligned}
i\int_{\mathcal{C}^+} d\omega \frac{\partial_\omega L(\omega)}{L(\omega)} &= i\lim_{r\to 0}\int_{0^+}^{\pi^-} d\theta\ \frac{\partial_\theta L(r,\theta)}{L(r,\theta)}, \\
&= i\lim_{r\to 0}\int_{0^+}^{\pi^-} d\theta\ -i(m-1)/m, \\
&= \pi(m-1)/m, \qquad (4.54)
\end{aligned}
$$

where $\int_{0^+}^{\pi^-} d\theta \equiv \lim_{\theta_1\to 0^+,\theta_2\to\pi^-}\int_{\theta_1}^{\theta_2} d\theta$. The integral along $\mathcal{C}^-$ can be evaluated similarly; and it has the same value as the integral along $\mathcal{C}^+$.

Next, we argue that the winding phases of $g(\omega)$ along $\mathcal{C}^\pm$ are equal to 0. Note that the contour $\mathcal{C}^+/\mathcal{C}^-$ is defined through two limiting processes taken consecutively on an arc centered at the origin of the complex plane. In the first limit, we fix the radius of the arc and send both endpoints of the arc to infinitesimal distances above/below the real line, so the arc almost becomes a semicircle. In the second limit, the radius of the arc is sent to 0. Because of this, we need to first examine $g(E+i\eta)$ when $\eta\to 0^\pm$, and then send $E\to 0$.

Using Eq. (4.52), we see that $g(\omega)$ is an analytic function in the complement of the real line on the complex plane for odd m. Since $\lim_{\eta\to 0^\pm} L^{-1}(E+i\eta)K(E+i\eta)$ and $\lim_{\eta\to 0^\pm} L^{-1}(E+i\eta)$ exist for E anywhere on the real line $\mathcal{R}$, $\lim_{\eta\to 0^\pm} g(E+i\eta)\equiv g(E+i0^\pm)$ exist for $E\in\mathcal{R}$. Furthermore, since $\lim_{\omega\to 0} L^{-1}(\omega)K(\omega) = |V(0)|^2$, $g(E+i0^\pm)$ as functions of $E\in\mathcal{R}$ are continuous at $E=0$.

The winding phase of $g(\omega)$ along $\mathcal{C}^+$ is equal to the phase difference between $g(-|E|+i0^+)$ and $g(|E|+i0^+)$ in the limit $E\to 0$. Similarly, the winding phase of $g(\omega)$ along $\mathcal{C}^-$ is equal to the phase difference between $g(|E|+i0^-)$ and $g(-|E|+i0^-)$ in the limit $E\to 0$. Because of the continuity of $g(E+i0^\pm)$ at $E=0$, $i\int_{\mathcal{C}^++\mathcal{C}^-} d\omega\frac{\partial_\omega g(\omega)}{g(\omega)} = 0$.

Therefore,

$$i\int_{\mathcal{C}^+ + \mathcal{C}^-} d\omega \frac{\partial_\omega J(\omega)}{J(\omega)} = i\int_{\mathcal{C}^+ + \mathcal{C}^-} d\omega \frac{\partial_\omega L(\omega)}{L(\omega)} = 2\pi(m-1)/m. \tag{4.55}$$

At last, we evaluate the integral along the large semicircles, which can be written in polar coordinates as

$$i\int_{\mathcal{S}^+ + \mathcal{S}^-} d\omega \frac{\partial_\omega J(\omega)}{J(\omega)} = i\lim_{r\to\infty}\left(\int_{\pi^-}^{0^+} d\theta \frac{\partial_\theta J(r,\theta)}{J(r,\theta)} + \int_{2\pi^-}^{\pi^+} d\theta \frac{\partial_\theta J(r,\theta)}{J(r,\theta)}\right). \tag{4.56}$$

Using Eq. (4.31), $J(\omega)$ can be written as

$$J(\omega) = -K(\omega)P_{N-1}(\omega) + P_N(\omega), \tag{4.57}$$

where $P_{N-1}(\omega) \equiv \det(\omega \mathbb{1}_{N-1} - \boldsymbol{K}^R_{\not M})$ and $P_N(\omega) \equiv \det(\omega \mathbb{1}_N - \boldsymbol{K}^R)$ are polynomial functions of ω with degrees $N-1$ and N, respectively. From the definition of $K(\omega)$ in Eq. (4.25), we can see that $\lim_{|\omega|\to\infty} K(\omega) = 0$, hence $J(\omega) \sim P_N(\omega) \sim \omega^N$ when $|\omega| \to \infty$; and we expect that the sum of the winding phases of $J(\omega)$ around the large semicircles is equal to $2\pi N$. In the following, we provide a careful mathematical analysis to verify this intuitive result.

Taking the derivative of Eq. (4.57) w.r.t θ, we have

$$\partial_\theta J(r,\theta) = i\omega\partial_\omega J(\omega) = -i\omega\partial_\omega K(\omega)P_{N-1}(\omega) - i\omega K(\omega)\partial_\omega P_{N-1}(\omega) + i\omega\partial_\omega P_N(\omega). \tag{4.58}$$

We can observe from Eq. (4.25) that $\lim_{|\omega|\to\infty} \partial_\omega K(\omega) = \lim_{|\omega|\to\infty} K(\omega) = 0$. In

addition, $\lim_{|\omega|\to\infty} \frac{P_{N-1}(\omega)}{P_N(\omega)} = \lim_{|\omega|\to\infty} \frac{\partial_\omega P_{N-1}(\omega)}{P_N(\omega)} = 0$, hence

$$\lim_{r\to\infty} \frac{\partial_\theta J(r,\theta)}{J(r,\theta)} = \lim_{|\omega|\to\infty} \frac{i\omega\partial_\omega P_N(\omega)}{P_N(\omega)} = iN \tag{4.59}$$

uniformly in $\theta \in (0,\pi) \cup (\pi, 2\pi)$. Applying the dominated convergence theorem, we can evaluate the $r \to \infty$ limit of the following definite integral as a function of the integration end points $\theta_1, \theta_2 \in (0,\pi)$ (or $\theta_1, \theta_2 \in (\pi, 2\pi)$):

$$i \lim_{r\to\infty} \int_{\theta_1}^{\theta_2} d\theta \; \frac{\partial_\theta J(r,\theta)}{J(r,\theta)} = (\theta_1 - \theta_2)N. \tag{4.60}$$

The limit in Eq. (4.60) is uniform in θ_1, θ_2 because the limit in Eq. (4.59) is uniform in θ. This implies that, when we evaluate Eq. (4.56), we can exchange the limit in r and the limits in the integration end points:

$$\begin{aligned} i \int_{\mathcal{S}^+} d\omega \frac{\partial_\omega J(\omega)}{J(\omega)} &\equiv i \lim_{r\to 0} \lim_{\theta_1\to\pi^-} \lim_{\theta_2\to 0^+} \int_{\theta_1}^{\theta_2} d\theta \; \frac{\partial_\theta J(r,\theta)}{J(r,\theta)} \\ &= i \lim_{\theta_1\to\pi^-} \lim_{\theta_2\to 0^+} \lim_{r\to 0} \int_{\theta_1}^{\theta_2} d\theta \; \frac{\partial_\theta J(r,\theta)}{J(r,\theta)} = \pi N, \end{aligned} \tag{4.61}$$

where we have used Eq. (4.60) in evaluating Eq. (4.61). The integration along $\mathcal{S}^-$ can be evaluated similarly, and it has the same value as Eq. (4.61); hence we get

$$i \int_{\mathcal{S}^+ + \mathcal{S}^-} d\omega \frac{\partial_\omega J(\omega)}{J(\omega)} = 2\pi N. \tag{4.62}$$

Combining Eqs. (4.50), (4.51), (4.55) and (4.62), we obtain Eq. (4.40) for the dispersion relation $\epsilon(k) = |d|k^m$ with odd m. The case of $\epsilon(k) = -|d|k^m$ with odd m can be proved identically once we replace E with $-E$.

Next, we discuss the case of $\epsilon(k) = |d|k^m$ with even m. Similarly as in the case of

odd m, the winding phase of $\det[\boldsymbol{S}(E)]$ can be evaluated as

$$2\Delta\delta = \int_{0^+}^{\infty} dE \left[\frac{\partial_\omega J(E - i0)}{J(E - i0)} - \frac{\partial_\omega J(E + i0)}{J(E + i0)} \right] = \int_{\mathcal{R}^+ + \mathcal{R}^-} d\omega \frac{\partial_\omega J(\omega)}{J(\omega)}$$
$$= \oint d\omega \frac{\partial_\omega J(\omega)}{J(\omega)} - \int_{\mathcal{S}} d\omega \frac{\partial_\omega J(\omega)}{J(\omega)} - \int_{\mathcal{C}} d\omega \frac{\partial_\omega J(\omega)}{J(\omega)}, \tag{4.63}$$

where the integration contours are illustrated in Fig. 4.3b. $\mathcal{R}^{\pm}$ represent the contours just above and below the real line along the continuum spectrum. $\oint$ represents the integration over the closed contour. Following a procedure similar to the case of odd m, it is easy to show that the result of this integral is also given by Eq. (4.40). The case of $\epsilon(k) = -|d|k^m$ with even m can be proved similarly.

This is the end of the proof for Theorem 4. □

4.5 Outlook

In this chapter, we have illustrated how a divergent density of states results in a wide variety of universal scattering behavior in photon-emitter models. Our results open up several areas of research in the study of scattering properties of synthetic quantum matter. It would be interesting to extend our results to more general analytic dispersion relations and more than one incoming photon. Another important next step is to see if it is possible to generalize the universal emitter scattering results to scattering off arbitrary, short-range potentials, such as occurs in translationally-invariant two-particle scattering. It would also be interesting to study the universal behavior of the S-matrix in different dimensions when the density of states diverges. An outstanding challenge is to describe emitter scattering when both dissipation and coherent driving are present.

More generally, our work shows how changing the single-particle dispersion rela-

tion modifies the universal properties of the S-matrix in scattering theory. Although our results rigorously apply only in the zero-energy limit, our work establishes the foundation for the development of a universal low-energy theory for unusual dispersion relations. Similar to the case of quadratic dispersion relations, we expect the scattering to be primarily determined by the scattering length when the de Broglie wavelengths of the particles are large compared to the range of the interaction. It will be interesting to explore how other well-studied problems for massive particles—such as Efimov physics [24, 25, 49], renormalization for the effective field theory [1, 14], and the N-body scale [13]—are modified in the presence of these more general dispersion relations. It would also be interesting to understand the implication of our results in the many-body context, e.g. in dilute Bose gases with spin-orbit coupling [29, 64, 100] or in twisted bilayer graphene near a magic angle [82, 173, 174]. The high level of control offered by synthetic quantum systems opens up the prospect that these effects may be realizable in near-term experiments.

Bibliography

[1] Sadhan K Adhikari, T Frederico, and ID Goldman. Perturbative renormalization in quantum few-body problems. *Phys. Rev. Lett.*, 74(4):487, 1995.

[2] A V Akimov, A Mukherjee, C L Yu, D E Chang, A S Zibrov, P R Hemmer, H Park, and M D Lukin. Generation of single optical plasmons in metallic nanowires coupled to quantum dots. *Nature*, 450(7168):402–406, 2007.

[3] Gerasimos Angelatos and Stephen Hughes. Polariton waveguides from a quantum dot chain in a photonic crystal waveguide: an architecture for waveguide quantum electrodynamics. *Optica*, 3(4):370–376, April 2016.

[4] A. Asenjo-Garcia, J. D. Hood, D. E. Chang, and H. J. Kimble. Atom-light interactions in quasi-one-dimensional nanostructures: A Green's-function perspective. *Phys. Rev. A*, 95(3):033818, March 2017.

[5] Alain Aspect, Philippe Grangier, and Gérard Roger. Experimental tests of realistic local theories via bell's theorem. *Phys. Rev. Lett.*, 47(7):460, 1981.

[6] D Atkinson and D Morgan. Levinson's theorem for s-matrix theory with inelasticity. *II Nuovo Cimento A (1971-1996)*, 41(4):559–575, 1966.

[7] M Bajcsy, S Hofferberth, V Balic, T Peyronel, M Hafezi, A S Zibrov, V Vuletic, and M D Lukin. Efficient all-optical switching using slow light within a hollow fiber. *Phys. Rev. Lett.*, 102(20):203902, jan 2009.

[8] Yehuda B Band. *Light and matter: electromagnetism, optics, spectroscopy and lasers*, volume 1. John Wiley & Sons, 2006.

[9] Ben Q Baragiola. *Open systems dynamics for propagating quantum fields*. PhD thesis, University of New Mexico, 2014.

[10] Vania E Barlette, Marcelo M Leite, and Sadhan K Adhikari. Quantum scattering in one dimension. *European Journal of Physics*, 21(5):435, 2000.

[11] Daniel Barredo, Sylvain De Léséleuc, Vincent Lienhard, Thierry Lahaye, and Antoine Browaeys. An atom-by-atom assembler of defect-free arbitrary two-dimensional atomic arrays. *Science*, 354(6315):1021–1023, 2016.

[12] G Barton. Levinson's theorem in one dimension: heuristics. *J. Phys. A Math. Gener.*, 18(3):479, 1985.

[13] Betzalel Bazak, Johannes Kirscher, Sebastian König, M. Pavón Valderrama, Nir Barnea, and Ubirajara Van Kolck. Four-body scale in universal few-boson systems. *Phys. Rev. Lett.*, 122(14):143001, 2019.

[14] Paulo F Bedaque, H-W Hammer, and Ubirajara Van Kolck. Renormalization of the three-body system with short-range interactions. *Phys. Rev. Lett.*, 82(3):463, 1999.

[15] HA Bethe. Theory of the effective range in nuclear scattering. *Phys. Rev.*, 76(1):38, 1949.

[16] Alexios Beveratos, Rosa Brouri, Thierry Gacoin, André Villing, Jean-Philippe Poizat, and Philippe Grangier. Single photon quantum cryptography. *Phys. Rev. Lett.*, 89(18):187901, 2002.

[17] P. Bienias, S. Choi, O. Firstenberg, M. F. Maghrebi, M. Gullans, M. D. Lukin, A. V. Gorshkov, and H. P. Büchler. Scattering resonances and bound states for strongly interacting Rydberg polaritons. *Phys. Rev. A*, 90(5):053804, 2014.

[18] Przemyslaw Bienias. Few-body quantum physics with strongly interacting Rydberg polaritons. *Eur. Phys. J. Spec. Top.*, 225(15-16):2957–2976, 2016.

[19] Przemyslaw Bienias and Hans Peter Büchler. Quantum theory of Kerr nonlinearity with Rydberg slow light polaritons. *New J. Phys.*, 18(12):123026, 2016.

[20] Przemyslaw Bienias and Hans Peter Büchler. Two photon conditional phase gate based on Rydberg slow light polaritons. *J. Phys. B At. Mol. Opt. Phys.*, 53(5):54003, February 2020.

[21] Przemyslaw Bienias, James Douglas, Asaf Paris-Mandoki, Paraj Titum, Ivan Mirgorodskiy, Christoph Tresp, Emil Zeuthen, Michael J. Gullans, Marco Manzoni, Sebastian Hofferberth, Darrick Chang, and Alexey V. Gorshkov. Photon propagation through dissipative Rydberg media at large input rates. *Phys. Rev. Res.*, 2:033049, 2020.

[22] Przemyslaw Bienias, Michael J. Gullans, Marcin Kalinowski, Alexander N. Craddock, Dalia P. Ornelas-Huerta, S. L. Rolston, J. V. Porto, and Alexey V. Gorshkov. Exotic photonic molecules via lennard-jones-like potentials. *Phys. Rev. Lett.*, 125:093601, August 2020.

[23] Dik Bouwmeester, Jian-Wei Pan, Klaus Mattle, Manfred Eibl, Harald Weinfurter, and Anton Zeilinger. Experimental quantum teleportation. *Nature*, 390(6660):575–579, 1997.

[24] Eric Braaten and H-W Hammer. Three-body recombination into deep bound states in a bose gas with large scattering length. *Phys. Rev. Lett.*, 87(16):160407, 2001.

[25] Eric Braaten and H-W Hammer. Universality in few-body systems with large scattering length. *Phys. Rep.*, 428(5-6):259–390, 2006.

[26] Hans J Briegel, David E Browne, Wolfgang Dür, Robert Raussendorf, and Maarten Van den Nest. Measurement-based quantum computation. *Nat. Phys.*, 5(1):19–26, 2009.

[27] G.E. Brown and A.M. Green. Three-body forces in nuclear matter. *Nucl. Phys. A*, 137(1):1 – 19, 1969.

[28] H. P. Büchler, A. Micheli, and P. Zoller. Three-body interactions with cold polar molecules. *Nat. Phys.*, 3(10):726–731, 2007.

[29] Daniel L Campbell, Gediminas Juzeliūnas, and Ian B Spielman. Realistic rashba and dresselhaus spin-orbit coupling for neutral atoms. *Phys. Rev. A*, 84(2):025602, 2011.

[30] Tommaso Caneva, Marco T Manzoni, Tao Shi, James S Douglas, J Ignacio Cirac, and Darrick E Chang. Quantum dynamics of propagating photons with strong interactions: a generalized input–output formalism. *New J. Phys.*, 17(11):113001, October 2015.

[31] Sergio H. Cantu, Aditya V. Venkatramani, Wenchao Xu, Leo Zhou, Brana Jelenković, Mikhail D. Lukin, and Vladan Vuletić. Repulsive photons in a quantum nonlinear medium. *Nat. Phys.*, 16(9):921–925, September 2020.

[32] Yuan Cao, Valla Fatemi, Shiang Fang, Kenji Watanabe, Takashi Taniguchi, Efthimios Kaxiras, and Pablo Jarillo-Herrero. Unconventional superconductivity in magic-angle graphene superlattices. *Nature*, 556(7699):43–50, 2018.

[33] Howard Carmichael. *An open systems approach to quantum optics: lectures presented at the Université libre de Bruxelles, October 28 to November 4, 1991.* Springer-Verlag, 1993.

[34] Iacopo Carusotto and Cristiano Ciuti. Quantum fluids of light. *Rev. Mod. Phys.*, 85(1):299–366, 2013.

[35] Darrick E Chang, Anders S. Sørensen, Eugene A Demler, and Mikhail D Lukin. A single-photon transistor using nanoscale surface plasmons. *Nat. Phys.*, 3(11):807–812, 2007.

[36] Darrick E. Chang, Vladan Vuletić, and Mikhail D. Lukin. Quantum nonlinear optics - Photon by photon. *Nat. Photonics*, 8(9):685–694, August 2014.

[37] L Chomaz, L Corman, T Yefsah, R Desbuquois, and J Dalibard. Absorption imaging of a quasi-two-dimensional gas: a multiple scattering analysis. *New J. Phys.*, 14(5):055001, 2012.

[38] Logan W. Clark, Ningyuan Jia, Nathan Schine, Claire Baum, Alexandros Georgakopoulos, and Jonathan Simon. Interacting Floquet polaritons. *Nature*, 532:571, 2019.

[39] Neil V. Corzo, Baptiste Gouraud, Aveek Chandra, Akihisa Goban, Alexandra S. Sheremet, Dmitriy V. Kupriyanov, and Julien Laurat. Large Bragg Reflection from One-Dimensional Chains of Trapped Atoms Near a Nanoscale Waveguide. *Phys. Rev. Lett.*, 117(13):133603, 2016.

[40] A. J. Daley, J. M. Taylor, S. Diehl, M. Baranov, and P. Zoller. Atomic three-body loss as a dynamical three-body interaction. *Phys. Rev. Lett.*, 102(4):040402, 2009.

[41] Sumanta Das, Vincent E. Elfving, Florentin Reiter, and Anders S. Sørensen. Photon scattering from a system of multilevel quantum emitters. i. formalism. *Phys. Rev. A*, 97:043837, April 2018.

[42] Sumanta Das, Vincent E. Elfving, Florentin Reiter, and Anders S. Sørensen. Photon scattering from a system of multilevel quantum emitters. ii. application to emitters coupled to a one-dimensional waveguide. *Phys. Rev. A*, 97:043838, April 2018.

[43] S Debnath, NM Linke, S-T Wang, C Figgatt, KA Landsman, L-M Duan, and C Monroe. Observation of hopping and blockade of bosons in a trapped ion spin chain. *Phys. Rev. Lett.*, 120(7):073001, 2018.

[44] M H Devoret and R J Schoelkopf. Superconducting circuits for quantum information: an outlook. *Science*, 339(6124):1169–74, March 2013.

[45] Shi-Hai Dong, Xi-Wen Hou, and Zhong-Qi Ma. Relativistic levinson theorem in two dimensions. *Phys. Rev. A*, 58(3):2160, 1998.

[46] Shi-Hai Dong and Zhong-Qi Ma. Levinson's theorem for the schrödinger equation in one dimension. *Int. J. of Theor. Phys.*, 39(2):469–481, 2000.

[47] Y. O. Dudin and A. Kuzmich. Strongly interacting Rydberg excitations of a cold atomic gas. *Science*, 336(6083):887–889, May 2012.

[48] V. Efimov. Energy levels arising from resonant two-body forces in a three-body system. *Phys. Lett. B*, 33(8):563 – 564, 1970.

[49] V Efimov. Energy levels of three resonantly interacting particles. *Nucl. Phys. A*, 210(1):157–188, 1973.

[50] Manuel Endres, Hannes Bernien, Alexander Keesling, Harry Levine, Eric R Anschuetz, Alexandre Krajenbrink, Crystal Senko, Vladan Vuletic, Markus Greiner, and Mikhail D Lukin. Atom-by-atom assembly of defect-free one-dimensional cold atom arrays. *Science*, 354(6315):1024–1027, 2016.

[51] L D Faddeev. Scattering theory for a three-particle system. *Sov. Phys. JETP*, 12(5):1014–1019, 1961.

[52] Shanhui Fan, Şükrü Ekin Kocabaş, and Jung Tsung Shen. Input-output formalism for few-photon transport in one-dimensional nanophotonic waveguides coupled to a qubit. *Phys. Rev. A*, 82(6):063821, 2010.

[53] J. M. Fink, A. Dombi, A. Vukics, A. Wallraff, and P. Domokos. Observation of the photon-blockade breakdown phase transition. *Phys. Rev. X*, 7(1):011012, 2017.

[54] Ofer Firstenberg, Thibault Peyronel, Qi-Yu Liang, Alexey V Gorshkov, Mikhail D Lukin, and Vladan Vuletić. Attractive photons in a quantum nonlinear medium. *Nature*, 502(7469):71–5, 2013.

[55] M. Fleischhauer and M. D. Lukin. Dark-state polaritons in electromagnetically induced transparency. *Phys. Rev. Lett.*, 84:5094–5097, May 2000.

[56] Michael Fleischhauer, Atac Imamoglu, and Jonathan P. Marangos. Electromagnetically induced transparency: Optics in coherent media. *Rev. Mod. Phys.*, 77(2):633–673, July 2005.

[57] Stuart J Freedman and John F Clauser. Experimental test of local hidden-variable theories. *Phys. Rev. Lett.*, 28(14):938, 1972.

[58] H Friedrich and D Wintgen. Interfering resonances and bound states in the continuum. *Phys. Rev. A.*, 32(6):3231, 1985.

[59] F. M. Gambetta, W. Li, F. Schmidt-Kaler, and I. Lesanovsky. Engineering NonBinary Rydberg Interactions via Phonons in an Optical Lattice. *Phys. Rev. Lett.*, 124(4):043402, 2020.

[60] Alexandros Georgakopoulos, Ariel Sommer, and Jonathan Simon. Theory of interacting cavity Rydberg polaritons. *Quantum Sci. Technol.*, 4(1):014005, October 2018.

[61] A. Goban, K. S. Choi, D. J. Alton, D. Ding, C. Lacroûte, M. Pototschnig, T. Thiele, N. P. Stern, and H. J. Kimble. Demonstration of a state-insensitive, compensated nanofiber trap. *Phys. Rev. Lett.*, 109(3):033603, 2012.

[62] A. Goban, C. L. Hung, J. D. Hood, S. P. Yu, J. A. Muniz, O. Painter, and H. J. Kimble. Superradiance for Atoms Trapped along a Photonic Crystal Waveguide. *Phys. Rev. Lett.*, 115(6):063601, 2015.

[63] A. Goban, C. L. Hung, S. P. Yu, J. D. Hood, J. A. Muniz, J. H. Lee, M. J. Martin, A. C. McClung, K. S. Choi, D. E. Chang, O. Painter, and H. J. Kimble. Atom-light interactions in photonic crystals. *Nat. Commun.*, 5:3808, May 2014.

[64] Sarang Gopalakrishnan, Austen Lamacraft, and Paul M Goldbart. Universal phase structure of dilute bose gases with rashba spin-orbit coupling. *Phys. Rev. A*, 84(6):061604, 2011.

[65] H. Gorniaczyk, C. Tresp, P. Bienias, A. Paris-Mandoki, W. Li, I. Mirgorodskiy, H. P. Büchler, I. Lesanovsky, and S. Hofferberth. Enhancement of Rydberg-mediated single-photon nonlinearities by electrically tuned Förster resonances. *Nat. Commun.*, 7:12480, August 2016.

[66] H. Gorniaczyk, C. Tresp, J. Schmidt, H. Fedder, and S. Hofferberth. Single-photon transistor mediated by interstate Rydberg interactions. *Phys. Rev. Lett.*, 113(5):053601, July 2014.

[67] Alexey V. Gorshkov, Rejish Nath, and Thomas Pohl. Dissipative many-body quantum optics in rydberg media. *Phys. Rev. Lett.*, 110:153601, April 2013.

[68] Alexey V. Gorshkov, Johannes Otterbach, Michael Fleischhauer, Thomas Pohl, and Mikhail D. Lukin. Photon-photon interactions via Rydberg blockade. *Phys. Rev. Lett.*, 107(13):133602, September 2011.

[69] A. Grankin, E. Brion, E. Bimbard, R. Boddeda, I. Usmani, A. Ourjoumtsev, and P. Grangier. Quantum statistics of light transmitted through an intracavity Rydberg medium. *New J. Phys.*, 16(4):043020, 2014.

[70] Tobias Grass, Przemyslaw Bienias, Michael J Gullans, Rex Lundgren, Joseph Maciejko, and Alexey V Gorshkov. Fractional quantum Hall phases of bosons with tunable interactions: From the Laughlin liquid to a fractional Wigner crystal. *Phys. Rev. Lett.*, 121(25):253403, 2018.

[71] Andrew D. Greentree, Charles Tahan, Jared H. Cole, and Lloyd C. L. Hollenberg. Quantum phase transitions of light. *Nat. Phys.*, 2(12):856–861, December 2006.

[72] M. J. Gullans, S. Diehl, S. T. Rittenhouse, B. P. Ruzic, J. P. D'Incao, P. Julienne, A. V. Gorshkov, and J. M. Taylor. Efimov States of Strongly Interacting Photons. *Phys. Rev. Lett.*, 119(23):233601, 2017.

[73] M. J. Gullans, J. D. Thompson, Y. Wang, Q. Y. Liang, V. Vuletić, M. D. Lukin, and A. V. Gorshkov. Effective Field Theory for Rydberg Polaritons. *Phys. Rev. Lett.*, 117(11):113601, September 2016.

[74] HW Hammer. Few-body physics in effective field theory. *J. Phys. G. Nucl. Part. Phys.*, 31(8):S1253, 2005.

[75] Birgit J. M. Hausmann, Brendan Shields, Qimin Quan, Patrick Maletinsky, Murray McCutcheon, Jennifer T. Choy, Tom M. Babinec, Alexander Kubanek, Amir Yacoby, Mikhail D. Lukin, and Marko Lončar. Integrated diamond networks for quantum nanophotonics. *Nano Lett.*, 12(3):1578–1582, March 2012.

[76] Jonathan D Hood, Akihisa Goban, Ana Asenjo-Garcia, Mingwu Lu, S. P. Yu, Darrick E Chang, and H J Kimble. Atom-atom interactions around the band edge of a photonic crystal waveguide. *Proc. Natl. Acad. Sci. U. S. A.*, 113(38):10507–12, September 2016.

[77] Chia Wei Hsu, Bo Zhen, A. Douglas Stone, John D. Joannopoulos, and Marin Soljačić. Bound states in the continuum. *Nat. Rev. Mater.*, 1(9):16048, July 2016.

[78] Alexander Huck, Shailesh Kumar, Abdul Shakoor, and Ulrik L. Andersen. Controlled coupling of a single nitrogen-vacancy center to a silver nanowire. *Phys. Rev. Lett.*, 106(9):096801, February 2011.

[79] Dalia P. Ornelas Huerta, Przemyslaw Bienias, Alexander N. Craddock, Michael J. Gullans, Andrew J. Hachtel, Marcin Kalinowski, Mary E. Lyon, Alexey V. Gorshkov, Steven L. Rolston, and J. V. Porto. Tunable three-body loss in a nonlinear Rydberg medium. *arXiv:2009.13599*, 2020.

[80] C. L. Hung, S M Meenehan, D E Chang, O Painter, and H J Kimble. Trapped atoms in one-dimensional photonic crystals. *New J. Phys.*, 15(8):083026, August 2013.

[81] Masakuni Ida. On the relation between the phase shift and the number of bound states. *Prog. of Theor. Phys.*, 21(4):625–639, 1959.

[82] Hiroki Isobe and Liang Fu. Supermetal. *Phys. Rev. Res.*, 1(3):033206, 2019.

[83] Krzysztof Jachymski, Przemysław Bienias, and Hans Peter Büchler. Three-body interactions of slow light Rydberg polaritons. *Phys. Rev. Lett.*, 117:053601, April 2016.

[84] J. M. Jauch. On the relation between scattering phase and bound states. *Helv. Phys. Acta*, 30, 1957.

[85] Thomas Jennewein, Christoph Simon, Gregor Weihs, Harald Weinfurter, and Anton Zeilinger. Quantum cryptography with entangled photons. *Phy. Rev. Lett.*, 84(20):4729, 2000.

[86] Ningyuan Jia, Nathan Schine, Alexandros Georgakopoulos, Albert Ryou, Logan W. Clark, Ariel Sommer, and Jonathan Simon. A strongly interacting polaritonic quantum dot. *Nat. Phys.*, 14:550, 2018.

[87] John D. Joannopoulos, Steven G. Johnson, Joshua N. Winn, and Robert D. Meade. *Photonic Crystals: Molding the Flow of Light*. Princeton University Press, 2 edition, 2008.

[88] P R Johnson, E Tiesinga, J V Porto, and C J Williams. Effective three-body interactions of neutral bosons in optical lattices. *New J. Phys.*, 11(9):093022, September 2009.

[89] Marcin Kalinowski et al. *(in preparation)*, 2021.

[90] Marcin Kalinowski, Yidan Wang, Przemyslaw Bienias, Michael J Gullans, Dalia P Ornelas-Huerta, Alexander N Craddock, Steven L Rolston, JV Porto, Hans Peter Büchler, and Alexey V Gorshkov. Resonant enhancement of three-body loss between strongly interacting photons. *arXiv preprint arXiv:2010.09772*, 2020.

[91] H. J. Kimble. The quantum internet. *Nature*, 453(7198):1023–1030, June 2008.

[92] Charles Kittel. *Introduction to solid state physics*, volume 8. Wiley New York, 1976.

[93] Kevin Lalumière, Barry C. Sanders, A. F. van Loo, A. Fedorov, A. Wallraff, and A. Blais. Input-output theory for waveguide QED with an ensemble of inhomogeneous atoms. *Phys. Rev. A*, 88(4):043806, October 2013.

[94] Peter D Lax. *Functional Analysis*. Wiley, 2002.

[95] N Levinson. On the uniqueness of the potential in a schrodinger equation for a given asymptotic phase. *K. Danske Vidensk. Selsk. K. Mat.-Fys. Medd.*, 25(9), 1949.

[96] Maciej Lewenstein, Anna Sanpera, Veronica Ahufinger, Bogdan Damski, Aditi Sen, and Ujjwal Sen. Ultracold atomic gases in optical lattices: Mimicking condensed matter physics and beyond. *Adv. Phys.*, 56(2):243–379, 2007.

[97] Li Li, John C. Snyder, Isabelle M. Pelaschier, Jessica Huang, Uma Naresh Niranjan, Paul Duncan, Matthias Rupp, Klaus Robert Müller, and Kieron Burke. Understanding machine-learned density functionals. *Int. J. Quantum Chem.*, 116(11):819–833, 2016.

[98] Qi-Yu Liang, Aditya V Venkatramani, Sergio H Cantu, Travis L Nicholson, Michael J Gullans, Alexey V Gorshkov, Jeff D Thompson, Cheng Chin, Mikhail D Lukin, and Vladan Vuletić. Observation of three-photon bound states in a quantum nonlinear medium. *Science*, 359(6377):783–786, 2018.

[99] Qi-Yu Liang, Aditya V. Venkatramani, Sergio H. Cantu, Travis L. Nicholson, Michael J. Gullans, Alexey V. Gorshkov, Jeff D. Thompson, Cheng Chin, Mikhail D. Lukin, and Vladan Vuletić. Observation of three-photon bound states in a quantum nonlinear medium. *Science*, 359(6377):783–786, February 2018.

[100] Y-J Lin, K Jiménez-García, and Ian B Spielman. Spin–orbit-coupled bose–einstein condensates. *Nature*, 471(7336):83–86, 2011.

[101] Marina Litinskaya, Edoardo Tignone, and Guido Pupillo. Cavity polaritons with Rydberg blockade and long-range interactions. *J. Phys. B*, 49(16):164006, August 2016.

[102] Peter Lodahl. Quantum-dot based photonic quantum networks. *Quantum Sci. Technol.*, 3(1):013001, jan 2017.

[103] Peter Lodahl, Sahand Mahmoodian, and Søren Stobbe. Interfacing single photons and single quantum dots with photonic nanostructures. *Rev. Mod. Phys.*, 87(2):347–400, May 2015.

[104] M. D. Lukin, M. Fleischhauer, R. Cote, L. M. Duan, D. Jaksch, J. I. Cirac, and P. Zoller. Dipole blockade and quantum information processing in mesoscopic atomic ensembles. *Phys. Rev. Lett.*, 87:037901, June 2001.

[105] Zhong-Qi Ma. The levinson theorem. *J. of Phys. A: Math. Gener.*, 39(48):R625, 2006.

[106] Zhong-Qi Ma and Guang-Jiong Ni. Levinson theorem for dirac particles. *Phys. Rev. D*, 31(6):1482, 1985.

[107] Ivaylo S Madjarov, Alexandre Cooper, Adam L Shaw, Jacob P Covey, Vladimir Schkolnik, Tai Hyun Yoon, Jason R Williams, and Manuel Endres. An atomic-array optical clock with single-atom readout. *Phys. Rev. X*, 9(4):041052, 2019.

[108] Mohammad F. Maghrebi, Norman Y. Yao, Mohammad Hafezi, Thomas Pohl, Ofer Firstenberg, and Alexey V. Gorshkov. Fractional quantum Hall states of Rydberg polaritons. *Phys. Rev. A*, 91(3):033838, 2015.

[109] Gerald D Mahan. *Many-particle physics*. Springer Science & Business Media, 2013.

[110] Marco T. Manzoni, Darrick E. Chang, and James S. Douglas. Simulating quantum light propagation through atomic ensembles using matrix product states. *Nat. Commun.*, 8(1):1743, December 2017.

[111] D. Maxwell, D. J. Szwer, D. Paredes-Barato, H. Busche, J. D. Pritchard, A. Gauguet, K. J. Weatherill, M. P A Jones, and C. S. Adams. Storage and control of optical photons using Rydberg polaritons. *Phys. Rev. Lett.*, 110(10):103001, March 2013.

[112] L. Mazza, M. Rizzi, M. Lewenstein, and J. I. Cirac. Emerging bosons with three-body interactions from spin-1 atoms in optical lattices. *Phys. Rev. A*, 82(4):043629, 2010.

[113] Gregory Moore and Nicholas Read. Nonabelions in the fractional quantum hall effect. *Nucl. Phys. B*, 360(2):362 – 396, 1991.

[114] Matthias Moos, Michael Höning, Razmik Unanyan, and Michael Fleischhauer. Many-body physics of Rydberg dark-state polaritons in the strongly interacting regime. *Phys. Rev. A*, 92(5):053846, 2015.

[115] Callum Murray and Thomas Pohl. Quantum and nonlinear optics in strongly interacting atomic ensembles. *Adv. At. Mol. Opt. Phys.*, 65:321–372, 2016.

[116] Sylvain Nascimbène, Nir Navon, KJ Jiang, Frédéric Chevy, and Christophe Salomon. Exploring the thermodynamics of a universal fermi gas. *Nature*, 463(7284):1057–1060, 2010.

[117] Yusuke Nishida and Shina Tan. Universal fermi gases in mixed dimensions. *Phys. Rev. Lett.*, 101(17):170401, 2008.

[118] Jeremy L O'brien. Optical quantum computing. *Science*, 318(5856):1567–1570, 2007.

[119] Jeremy L O'brien, Akira Furusawa, and Jelena Vučković. Photonic quantum technologies. *Nat. Photonics*, 3(12):687–695, 2009.

[120] Johannes Otterbach, Matthias Moos, Dominik Muth, and Michael Fleischhauer. Wigner crystallization of single photons in cold Rydberg ensembles. *Phys. Rev. Lett.*, 111(11):113001, September 2013.

[121] Valentina Parigi, Erwan Bimbard, Jovica Stanojevic, Andrew J. Hilliard, Florence Nogrette, Rosa Tualle-Brouri, Alexei Ourjoumtsev, and Philippe Grangier. Observation and measurement of "giant" dispersive optical non-linearities in an ensemble of cold Rydberg atoms. *Phys. Rev. Lett*, 109(2012):233602, December 2012.

[122] Thibault Peyronel, Ofer Firstenberg, Qi Yu Liang, Sebastian Hofferberth, Alexey V. Gorshkov, Thomas Pohl, Mikhail D. Lukin, and Vladan Vuletić. Quantum nonlinear optics with single photons enabled by strongly interacting atoms. *Nature*, 488(7409):57–60, July 2012.

[123] Thibault Peyronel, Ofer Firstenberg, Qi Yu Liang, Sebastian Hofferberth, Alexey V. Gorshkov, Thomas Pohl, Mikhail D. Lukin, and Vladan Vuletić. Quantum nonlinear optics with single photons enabled by strongly interacting atoms. *Nature*, 488(7409):57–60, August 2012.

[124] Mikhail Pletyukhov and Vladimir Gritsev. Scattering of massless particles in one-dimensional chiral channel. *New J. Phys.*, 14(9):095028, September 2012.

[125] Nathan Poliatzky. Levinson's theorem for the Dirac equation. *Phys. Rev. Lett.*, 70(17):2507–2510, 1993.

[126] Diego Porras and J Ignacio Cirac. Effective quantum spin systems with trapped ions. *Phys. Rev. Lett.*, 92(20):207901, 2004.

[127] Eden Rephaeli and Shanhui Fan. Dissipation in few-photon waveguide transport. *Photonics Res.*, 1(3):110, 2013.

[128] Stephan Ritter, Christian Nölleke, Carolin Hahn, Andreas Reiserer, Andreas Neuzner, Manuel Uphoff, Martin Mücke, Eden Figueroa, Joerg Bochmann, and Gerhard Rempe. An elementary quantum network of single atoms in optical cavities. *Nature*, 484(7393):195–200, 2012.

[129] M. Roncaglia, M. Rizzi, and J. I. Cirac. Pfaffian state generation by strong three-body dissipation. *Phys. Rev. Lett.*, 104(9):096803, 2010.

[130] Dibyendu Roy, C. M. Wilson, and Ofer Firstenberg. Colloquium: Strongly interacting photons in one-dimensional continuum. *Rev. Mod. Phys.*, 89(2):021001, May 2017.

[131] Clément Sayrin, Christian Junge, Rudolf Mitsch, Bernhard Albrecht, Danny O'Shea, Philipp Schneeweiss, Jürgen Volz, and Arno Rauschenbeutel. Nanophotonic optical isolator controlled by the internal state of cold atoms. *Phys. Rev. X*, 5(4):041036, 2015.

[132] Michael Scheucher, Adèle Hilico, Elisa Will, Jürgen Volz, and Arno Rauschenbeutel. Quantum optical circulator controlled by a single chirally coupled atom. *Science*, 354(6319):1577–1580, December 2016.

[133] Nathan Schine, Albert Ryou, Andrey Gromov, Ariel Sommer, and Jonathan Simon. Synthetic Landau levels for photons. *Nature*, 534(16):671, June 2016.

[134] Jung Tsung Shen and Shanhui Fan. Strongly correlated two-photon transport in a one-dimensional waveguide coupled to a two-level system. *Phys. Rev. Lett.*, 98(15):153003, 2007.

[135] T Shi and C P Sun. Lehmann-Symanzik-Zimmermann reduction approach to multiphoton scattering in coupled-resonator arrays. *Phys. Rev. B*, 79(20):205111, May 2009.

[136] Tao Shi, Darrick E. Chang, and J. Ignacio Cirac. Multiphoton-scattering theory and generalized master equations. *Phys. Rev. A*, 92(5):053834, 2015.

[137] Peter W Shor. Polynomial-time algorithms for prime factorization and discrete logarithms on a quantum computer. *SIAM Rev.*, 41(2):303–332, 1999.

[138] Christoph Simon. Towards a global quantum network. *Nat. Photonics*, 11(11):678–680, 2017.

[139] A Sipahigil, R E Evans, D D Sukachev, M J Burek, J Borregaard, M K Bhaskar, C T Nguyen, J L Pacheco, H A Atikian, C Meuwly, R M Camacho, F Jelezko, E Bielejec, H Park, M Loncar, and M D Lukin. An integrated diamond nanophotonics platform for quantum-optical networks. *Science*, 354(6314):847–850, November 2016.

[140] P. Solano, P. Barberis-Blostein, F. K. Fatemi, L. A. Orozco, and S. L. Rolston. Super-radiance reveals infinite-range dipole interactions through a nanofiber. *Nat. Commun.*, 8(1):1857, 2017.

[141] Pablo Solano, Jeffrey A. Grover, Jonathan E. Hoffman, Sylvain Ravets, Fredrik K. Fatemi, Luis A. Orozco, and Steven L. Rolston. Optical Nanofibers: A New Platform for Quantum Optics. *Adv. At. Mol. Opt. Phys.*, 66:439–505, jan 2017.

[142] Ariel Sommer, Hans Peter Büchler, and Jonathan Simon. Quantum crystals and Laughlin droplets of cavity Rydberg polaritons. *arXiv:1506.00341*, 2015.

[143] Ariel Sommer and Jonathan Simon. Engineering photonic Floquet Hamiltonians through Fabry-Pérot resonators. *New J. Phys.*, 18(3):35008, 2016.

[144] H. L. Sørensen, J. B. Béguin, K. W. Kluge, I. Iakoupov, A. S. Sørensen, J. H. Müller, E. S. Polzik, and J. Appel. Coherent Backscattering of Light off One-Dimensional Atomic Strings. *Phys. Rev. Lett.*, 117(13):133604, 2016.

[145] Jovica Stanojevic, Valentina Parigi, Erwan Bimbard, Alexei Ourjoumtsev, and Philippe Grangier. Dispersive optical nonlinearities in a Rydberg electromagnetically-induced-transparency medium. *Phys. Rev. A*, 88(5):053845, November 2013.

[146] A W Steiner and S Gandolfi. Connecting neutron star observations to three-body forces in neutron matter and to the nuclear symmetry energy. *Phys. Rev. Lett.*, 108(8):081102, 2012.

[147] Nina Stiesdal, Jan Kumlin, Kevin Kleinbeck, Philipp Lunt, Christoph Braun, Asaf Paris-Mandoki, Christoph Tresp, Hans Peter Büchler, and Sebastian Hofferberth. Observation of Three-Body Correlations for Photons Coupled to a Rydberg Superatom. *Phys. Rev. Lett.*, 121(10):103601, 2018.

[148] H Suhl. Dispersion theory of the kondo effect. *Phys. Rev.*, 138(2A):A515, 1965.

[149] Neereja M Sundaresan, Rex Lundgren, Guanyu Zhu, Alexey V Gorshkov, and Andrew A Houck. Interacting qubit-photon bound states with superconducting circuits. *Phy. Rev. X*, 9(1):011021, 2019.

[150] S Takeda and A Furusawa. Toward large-scale fault-tolerant universal photonic quantum computing. *APL Photonics*, 4(6):060902, 2019.

[151] Grigory Tarnopolsky, Alex Jura Kruchkov, and Ashvin Vishwanath. Origin of magic angles in twisted bilayer graphene. *Phy. Rev. Lett.*, 122(10):106405, 2019.

[152] John R Taylor. *Scattering theory: the quantum theory of nonrelativistic collisions*. Courier Corporation, 2006.

[153] JE Thomas, J Kinast, and A Turlapov. Virial theorem and universality in a unitary fermi gas. *Phys. Rev. Lett.*, 95(12):120402, 2005.

[154] Jeff D. Thompson, Travis L. Nicholson, Qi Yu Liang, Sergio H. Cantu, Aditya V. Venkatramani, Soonwon Choi, Ilya A. Fedorov, Daniel Viscor, Thomas Pohl, Mikhail D. Lukin, and Vladan Vuletic. Symmetry-protected collisions between strongly interacting photons. *Nature*, 542(7640):206–209, 2017.

[155] Daniel Tiarks, Simon Baur, Katharina Schneider, Stephan Duerr, and Gerhard Rempe. Single-photon transistor using a Forster resonance. *Phys. Rev. Lett.*, 113(5):053602, 2014.

[156] Daniel Tiarks, Steffen Schmidt, Gerhard Rempe, and Stephan Dürr. Optical π phase shift created with a single-photon pulse. *Sci. Adv.*, 2(4):e1600036–e1600036, 2016.

[157] Daniel Tiarks, Steffen Schmidt-Eberle, Thomas Stolz, Gerhard Rempe, and Stephan Dürr. A photon-photon quantum gate based on Rydberg interactions. *Nat. Phys.*, 15(2):124–126, 2019.

[158] Wolfgang Tittel, Jürgen Brendel, Hugo Zbinden, and Nicolas Gisin. Quantum cryptography using entangled photons in energy-time bell states. *Phys. Rev. Lett.*, 84(20):4737, 2000.

[159] C. Tresp, P. Bienias, S. Weber, H. Gorniaczyk, I. Mirgorodskiy, H. P. Büchler, and S. Hofferberth. Dipolar dephasing of Rydberg d-state polaritons. *Phys. Rev. Lett.*, 115(8):083602, 2015.

[160] A. F. van Loo, A. Fedorov, K. Lalumiere, B. C. Sanders, A. Blais, and A. Wallraff. Photon-Mediated Interactions Between Distant Artificial Atoms. *Science*, 342(6165):1494–1496, 2013.

[161] B. Vermersch, P. O. Guimond, H. Pichler, and P. Zoller. Quantum State Transfer via Noisy Photonic and Phononic Waveguides. *Phys. Rev. Lett.*, 118(13):133601, March 2017.

[162] J. von Neumann and E. Wigner. Über merkwürdige diskrete eigenwerte. *Phys. Z.*, 30(6):465, 1929.

[163] Edo Waks, Kyo Inoue, Charles Santori, David Fattal, Jelena Vuckovic, Glenn S Solomon, and Yoshihisa Yamamoto. Quantum cryptography with a photon turnstile. *Nature*, 420(6917):762–762, 2002.

[164] Xi-Lin Wang, Xin-Dong Cai, Zu-En Su, Ming-Cheng Chen, Dian Wu, Li Li, Nai-Le Liu, Chao-Yang Lu, and Jian-Wei Pan. Quantum teleportation of multiple degrees of freedom of a single photon. *Nature*, 518(7540):516–519, 2015.

[165] Yidan Wang, Michael J Gullans, Antoine Browaeys, JV Porto, Darrick E Chang, and Alexey V Gorshkov. Single-photon bound states in atomic ensembles. *arXiv:1809.01147*, 2018.

[166] Yidan Wang, Michael J. Gullans, and Alexey V. Gorshkov. *(in preparation)*, 2021.

[167] Yidan Wang, Michael J Gullans, Xuesen Na, and Alexey V Gorshkov. Universality in one-dimensional scattering with general dispersion relations. *arXiv preprint arXiv:2103.09830*, 2021.

[168] Marcel Wellner. Levinson's Theorem (an Elementary Derivation). *Am. J. Phys.*, 32(10):787–789, October 1964.

[169] Jon Alan Wright. Generalization of levinson's theorem to three-body systems. *Phys. Rev.*, 139(1B):B137, 1965.

[170] Lin Xiong, Carlos Forsythe, M Jung, AS McLeod, SS Sunku, YM Shao, GX Ni, AJ Sternbach, S Liu, JH Edgar, et al. Photonic crystal for graphene plasmons. *Nat. Commun.*, 10(1):1–6, 2019.

[171] Shanshan Xu and Shanhui Fan. Input-output formalism for few-photon transport: A systematic treatment beyond two photons. *Phys. Rev. A*, 91:043845, 2015.

[172] Ming Jay Yang, Han Ying Peng, Neil Na, and Yu Shu Wu. Quantum state transfer between valley and photon qubits. *Phys. Rev. B*, 95(7):075407, February 2017.

[173] Noah FQ Yuan and Liang Fu. Classification of critical points in energy bands based on topology, scaling, and symmetry. *Phys. Rev. B*, 101(12):125120, 2020.

[174] Noah FQ Yuan, Hiroki Isobe, and Liang Fu. Magic of high-order van hove singularity. *Nat. Commun.*, 10(1):1–7, 2019.

[175] Emil Zeuthen, Michael J. Gullans, Mohammad F. Maghrebi, and Alexey V. Gorshkov. Correlated photon dynamics in dissipative Rydberg media. *Phys. Rev. Lett.*, 119(043602):043602, 2017.

[176] Huaixiu Zheng, Daniel J. Gauthier, and Harold U. Baranger. Strongly correlated photons generated by coupling a three- or four-level system to a waveguide. *Phys. Rev. A*, 85(4):043832, April 2012.